Estimating Rate Constants of Chemical Reactions using Spectroscopy

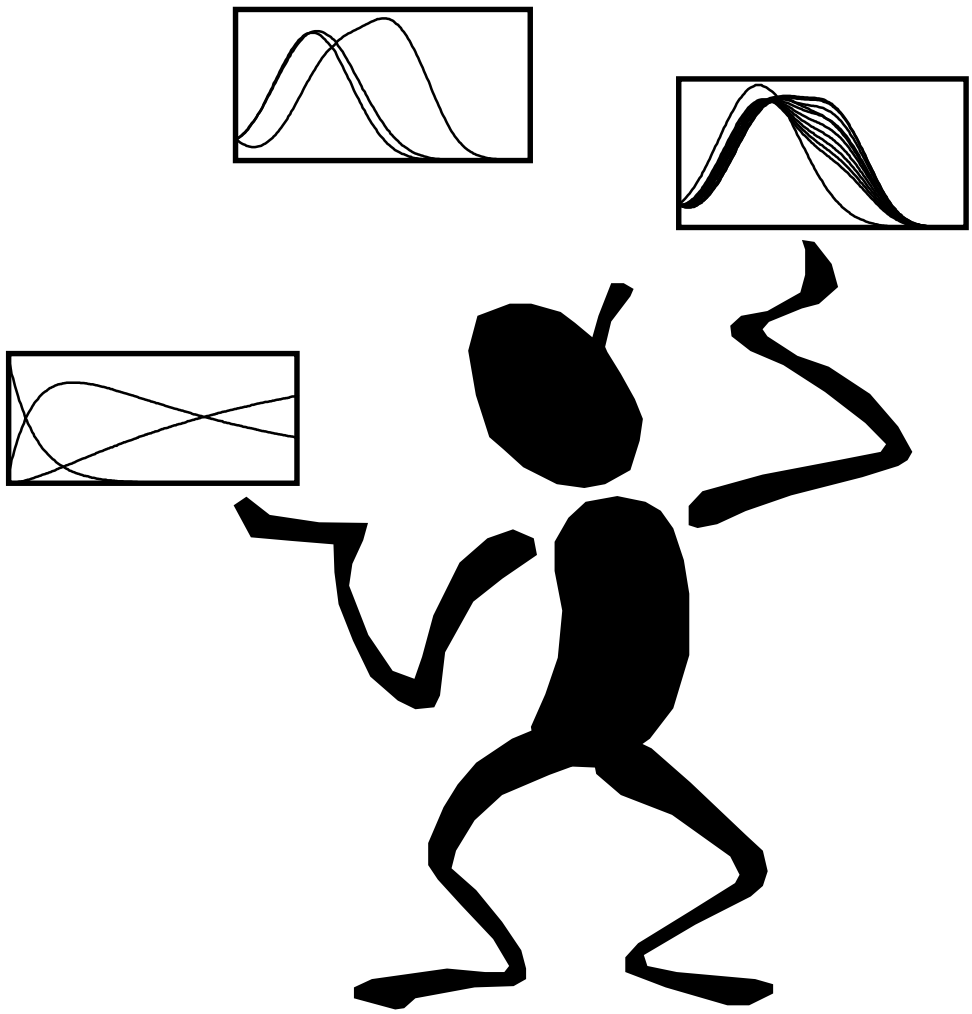

Sabina Bijlsma

2000

Estimating Rate Constants of Chemical Reactions using Spectroscopy

Printing: Ponsen & Looijen b.v. (Wageningen, The Netherlands)

Estimating Rate Constants of Chemical Reactions using Spectroscopy

ACADEMISCH PROEFSCHRIFT

ter verkrijging van de graad van doctor
aan de Universiteit van Amsterdam
op gezag van de Rector Magnificus
prof. dr. J.J.M. Franse
ten overstaan van een door het college voor promoties ingestelde
commissie in het openbaar te verdedigen in de Aula der Universiteit
op donderdag 22 juni 2000 te 10.00 uur

door

Sabina Bijlsma

geboren te Amsterdam

Promotor	: prof. dr. A.K. Smilde, University of Amsterdam
Other committee members	: prof. dr. A. Bliek, University of Amsterdam prof. dr. L.M.C. Buydens, Catholic University of Nijmegen prof. dr. H.A.L. Kiers, University of Groningen prof. dr. G.J. Koomen, University of Amsterdam prof. dr. P.J. Schoenmakers, University of Amsterdam dr. R. Tauler, University of Barcelona, Spain
Faculty:	: Faculty of Science

Aan Von en Frans

Table of Contents

Abbreviations

CCR	Classical curve resolution
CR	Curve resolution
DECRA	Direct exponential curve resolution algorithm
FSWEFA	Fixed size window evolving factor analysis
GEP	Generalized eigenvalue problem
GRAM	Generalized rank annihilation method
GRAM-LM-PAR	Generalized rank annihilation method-Levenberg-Marquardt-parallel factor analysis
HELP	Heuristic evolving latent projection
MCR	Multivariate curve resolution
PARAFAC	Parallel factor analysis
RFE	Relative fit error
SSQ	Sum of squares
SVD	Singular value decomposition
SW-NIR	Short-wavelength near-infrared
TCF	Traditional curve fitting
TFA	Target factor analysis
TLD	Trilinear decomposition
TLD-LM-PAR	Trilinear decomposition-Levenberg-Marquardt-parallel factor analysis
UV-Vis	Ultraviolet visible
WCR	Weighted curve resolution
WLS	Weighted least squares

Notation

In general, boldface capital characters denote matrices and boldface lower case characters denote vectors.

$\mathbf{A}$ ($(M\text{-}S)\times 3$)	The matrix with concentration profiles obtained from a GEP
$\mathbf{A}^{(j)}$ ($(M\text{-}S)\times 3$)	The matrix $\mathbf{A}$ after the jth iteration
$\tilde{\mathbf{A}}$ ($(M\text{-}S)\times 3$)	The new matrix $\mathbf{A}$ obtained by an initial estimate for k_1 and k_2
$\tilde{\tilde{\mathbf{A}}}$ ($(M\text{-}S)\times 2$)	The first two columns of matrix $\tilde{\mathbf{A}}$
$\mathbf{a}_i$	The ith column of matrix $\mathbf{A}$
$\mathbf{a}_i^{(j)}$	The ith column of matrix $\mathbf{A}$ after the jth iteration
$\mathbf{B}$ ($(N+1)\times 3$)	The matrix with combined spectra obtained from a GEP
$\mathbf{C}$ (2×3)	The matrix with scaling factors obtained from a GEP
$C_{U,0}$	The initial concentration of species U
$C_{U,i}$	The concentration of species U at time point i; $C_{W,i}$ and $C_{Y,i}$ for W and Y, respectively
$\mathbf{D}$ ($N\times K$)	Matrix with pure spectra
$\mathbf{E}$ ($M\times N$)	Matrix with spectral residuals
$\underline{\mathbf{E}}^*$ ($(M\text{-}S)\times(N+1)\times 2$)	Three-way array with spectral residuals
$\mathbf{F}$ ($M\times K$)	Matrix with concentration profiles
G	The step size parameter
K	Number of reacting absorbing species
k_a, k_b	Second order reaction rate constants
k_1, k_2	(Pseudo-) first order reaction rate constants
k	Equals $\frac{k_1}{(k_2 - k_1)}$
$\bar{\hat{k}}_1$, $\bar{\hat{k}}_2$	Mean estimated k_1 and k_2 calculated over the individual estimates
M	Number of time points
N	Number of wavelengths
S	The time shift parameter
t_i	The time at point i
$\mathbf{X}$ ($M\times N$)	Matrix with spectra during a certain time course
$\mathbf{X}^*$ ($M\times(N+1)$)	The augmented datamatrix
$\mathbf{X}^*_1$ ($(M\text{-}S)\times(N+1)$)	Datamatrix 1 formed by splitting $\mathbf{X}^*$

$\mathbf{X}^*_2$ ($(M\text{-}S)\times(N+1)$)	Datamatrix 2 formed by splitting $\mathbf{X}^*$
$\underline{\mathbf{X}}^*$ ($(M\text{-}S)\times(N+1)\times 2$)	Three-way array formed by stacking $\mathbf{X}^*_1$ and $\mathbf{X}^*_2$
$\tilde{\mathbf{X}}^*$ ($(M\text{-}S)\times(2N+2)$)	Matrix obtained by matricizing $\underline{\mathbf{X}}^*$
$\dot{\mathbf{X}}^*$ ($(M\text{-}S)\times 2N$)	Matrix obtained by removing the two columns of constants from $\tilde{\mathbf{X}}^*$
$\mathbf{X}^T$	Transpose of $\mathbf{X}$
$\mathbf{X}^{-1}$	Inverse of $\mathbf{X}$
$\hat{\mathbf{X}}$	Estimate of $\mathbf{X}$

Chapter 1

General Introduction

1.1 Short overview of the history of chemical kinetics

The history of chemical kinetics can be described by eight models,[1] which are summarized in Figure 1. Before the seventeenth century, the first model, *the anthropomorphic model*, was based on affinity. Affinity was defined by Greek philosophers as a concept with human properties like love and hate. However, the western alchemists believed that affinity arose from a similarity in composition. Chemical reactions were seen as the transformations in materials that were controlled by the differences in affinities.[2]

From the seventeenth century ideas about chemical kinetics became more successful. Boyle and Newton launched the idea that chemical reactions involved the constitution of invisible small particles. This was the root for *the affinity corpuscular model*. In the eighteenth century, the term attraction was introduced and was defined as the tendency of substances to combine with each other by means of forces.[3] The

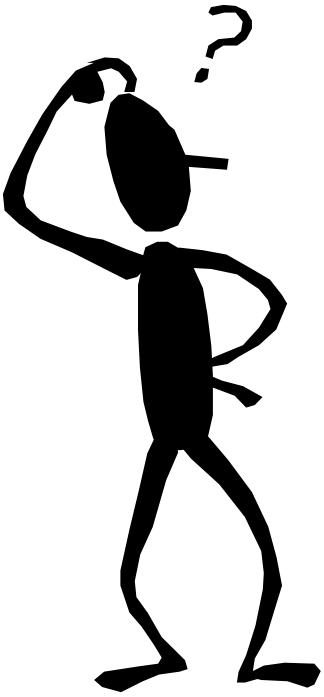

Models of Chemical Kinetics
- **The Anthropomorphic Model**
- **The Affinity Corpuscular Model**
- **The First Quantitative Model**
- **The Mechanism Model**
- **The Thermodynamics Model**
- **The Kinetic Model**
- **The Statistical Mechanics Model**
- **The Transition State Model**

Figure 1. The eight models in the history of chemical kinetics.

rate of transformation was related to different degrees of affinity/attraction between the particles. Bergman showed for the very first time in history that an increase of the reaction temperature could change the affinities of the substances.[4] Also ideas about catalysts were developed. *The affinity corpuscular model* was the first model concerned with the occurrence and the rate of chemical reactions. Predictions of the occurrence and rates were very limited. They were based on affinity tables which were empirically developed. A large drawback of the model was the absence of any mathematical treatment between the energy of a system and the reaction rate.

The use of mathematics in chemical kinetics began in Germany in 1850 with the quantitative investigation of the inversion of sucrose by Wilhelmy[5] resulting in *the first quantitative model*. He produced the first quantitative rate law for chemical reactions. He also introduced that a chemical reaction was a process in which particles interacted and affinity was not playing a role at all.

Harcourt and Esson introduced *the mechanism model* in the nineteenth century. The idea that in a chemical reaction particles interact with each other in distinct steps was born.[6] Esson developed empirical equations in which the amount of product formed and time were connected. This resulted in integrated differential equations for rates of chemical reactions. This was achieved for what we now call first order, second order and pseudo-first order reactions. By means of the introduction of mathematics in chemistry more accurate predictions of rates of chemical reactions became available. Harcourt and Esson studied also the influence of temperature on reaction rates in more detail. Within *the mechanism model*, Ostwald[7] investigated the catalysis within chemical reactions. He proposed the existence of alternative pathways in catalyzed reactions. When at the beginning of the twentieth century it became possible to detect and identify reaction intermediates using experimental techniques, catalysis was developed further.

A large step forward in the study of chemical kinetics was achieved by introduction of *the thermodynamics model*. Van ‘t Hoff[8] investigated the energy necessary for the occurrence of forward and backwards reactions in equilibrium reactions. Arrhenius[9] proposed that there is a minimum amount of energy necessary for the reaction to occur which was defined as the energy barrier. Later, the term activation energy was introduced. A key issue in *the thermodynamics model* is that a relationship was introduced between energy and energy barrier, which was not present in previous models.

In the twentieth century *the kinetic model* was introduced in which a new attribute was defined. A chemical reaction, involving the breaking and making of bonds, would be the cause of collisions between molecules.[10] This led to the introduction of a steric factor into the Arrhenius equation in order to explain why only

a proportion of the collisions occurring were effective. However, obtaining a magnitude of the steric factor was very problematic.[11] Despite these difficulties, *the kinetic model* contributed to a better understanding of the process of a chemical reaction and of the reasons why different reactions took place at different rates.

At the same time that *the kinetic model* was developed, a group of scientists applied statistical mechanics to systems of reacting molecules resulting in *the statistical mechanics model*. Mathematical equations were derived for the rate of a chemical reaction obtained from the consideration of the passage of systems through the potential energy surface.[12] Also the idea that radicals might be present in chemical reactions was born.[13]

The transition state model was a serious attempt in order to overcome the shortcomings of all previous models discussed. The new model proposed that only some of the molecules create transitional complexes. It became possible to derive the concentration at which substances pass through the critical configuration of the transition state by applying statistical methods. The model took into account the statistical properties of reactive systems as well as the microscopic details of molecular collisions.[14,15] With the development of experimental techniques to detect reaction intermediates a significant progress in the detailed understanding of the mechanisms of catalyzed reactions became possible. Some important experimental techniques are described in the next Section of this Chapter.

Nowadays, investigating rates of chemical reactions is a very popular topic.[16] If reaction rates are known it is possible to estimate when a reaction mixture approaches equilibrium, for example. Another reason for studying reaction rates is that reaction mechanisms can be unraveled into elementary steps. Rates of chemical reactions are also investigated to determine the end point of a reaction in process industry. If rapid on-line estimation methods for reaction rate constants become available then reaction rate constants of a certain chemical process can be monitored on-line in order to control the process within the desired specification limits. However, this is not applied yet and has to be developed still. This thesis can be seen as a first step in this direction, because it reports applications of novel techniques which are very suitable for rapid estimation of reaction rate constants.

1.2 Experimental techniques in kinetics

The first step in kinetic analysis is to obtain the concentrations of the reactants and products at different times after the reaction has been initiated. The temperature must be kept constant during the reaction which requires certain demands on the experimental set-up, because most chemical reactions are sensitive to the temperature.

A procedure to obtain concentrations of chemical species in time of a reacting system is the following. Samples of the reaction mixture are taken in time by means of the quenching method.[16] In the quenching method samples are cooled suddenly or added to a large amount of solvent which will stop the reaction. Subsequently, the quenched samples are analyzed using techniques like: titration, mass spectrometry, gas chromatography, polarimetry, nuclear magnetic resonance or spectroscopy, for example, in order to obtain concentrations of different species involved in the reacting system. If concentrations of different species in the reaction mixture are obtained in time, a kinetic model can be fitted to the concentration versus time data. This results in an estimation of the unknown reaction rate constants.[17-19]

The quenching procedure has some serious drawbacks. It is only applicable to reactions that are quite slow. No reaction must occur during the time it takes to quench the samples. Secondly, taking samples from the reaction mixture and analyzing these samples is expensive and very time-consuming.

A reaction in which at least one species is a gas results in a change of pressure in a system of constant volume. Hence, its progress can be followed by measuring the pressure difference in time. A disadvantage of the method is that it is far from specific, because all gas-phase species contribute to the pressure differences measured.

The use of on-line spectroscopic techniques overcomes the shortcomings of the quenching procedure discussed as shown in this thesis. On-line spectroscopic techniques are explained in the next Section of this Chapter.

1.3 Spectroscopy

Using spectroscopic techniques, for example infrared (IR) spectroscopy,[20,21] it is possible to monitor specific reacting IR absorbing species of chemical reactions without the need to take samples of the reacting system. Spectroscopic monitoring of reactions can be realized by using probes, flowcells and optical fibers. In the fingerprint area of IR, bands of functional groups are sharp. A disadvantage of IR spectroscopy is that very short light pathlengths (μm's) are required, which makes the measurements more difficult.

Nowadays, a lot of commercial software packages are available for estimating reaction rate constants from spectral data like KINSIM[22] and FITSIM.[23] However, these packages can only deal with univariate progress curves. The absorption spectra that are characteristic for spectroscopic techniques contain wide bands that might have a large spectral overlap. In such complex spectra it is difficult to find single wavelengths that are specific for only one of the reacting absorbing species. For wavelengths that are not specific for only one reacting absorbing species the molar

absorbances of the individual reacting absorbing species have to be known. Hence, in reasonably complex cases methods like KINSIM and FITSIM fail. Multivariate analysis tools can overcome the mentioned problems as is shown in this thesis.

Using near-infrared (NIR) spectroscopy, short-wavelength near-infrared (SW-NIR) spectroscopy or UV-Vis spectroscopy[20,21] it is possible to use longer light pathlengths (mm's - cm's), making the experimental set-up easier and more widely applicable. Several publications have shown applications of SW-NIR spectroscopy to monitor processes. Cavinato *et al*.[24] used SW-NIR for the determination of ethanol during the time course of a fermentation process. The measurements were performed non-invasively. Aldridge *et al*.[25] used SW-NIR to monitor the free radical polymerization of methyl-methacrylate. The conversion was obtained by a plot of one specific wavelength, representative for the monomer, of the recorded spectra versus reaction time. The reaction rate constants of the chemical reactions studied were not estimated in the publications mentioned in this paragraph.

In 1974, Sylvestre *et al.*[26] published a paper which describes the first application of spectroscopic techniques to estimate reaction rate constants from chemical reactions using multivariate analysis tools. In the literature, there are a lot of papers published on this topic.[27-34] In these publications the emphasis is not on the spectroscopic techniques used, but there is focussed on new multivariate approaches to estimate the reaction rate constants from the spectral data obtained. Important multivariate analysis tools are discussed in the next Section of this Chapter. In this thesis, new multivariate analysis tools are presented.

1.4 Multivariate analysis tools

Chemometrics is a part of chemistry that develops mathematical and statistical methods for analyzing chemical data.[35] Multivariate analysis is widely used in chemometrics. Curve resolution[36] is a group of multivariate analysis tools based on the determination of qualitative information and the recovery of response profiles, for example time profiles. Nowadays, new modifications of curve resolution techniques and applications have been published.[37-44]

The traditional curve resolution techniques can be adapted in order to estimate pure spectra of reacting absorbing species and reaction rate constants simultaneously from spectral data of the reacting system using specific kinetic model information as is shown in this thesis. In that case, equations describing the kinetics are used explicitly by the algorithm.[26-34] In the curve resolution methods, an iterative least squares optimization procedure is implemented to estimate the values of the unknown parameters. The pure spectra obtained can be used to identify chemical species using

library spectra. This is useful for checking the reaction mechanism and locating unknown side reactions.

For processes with unknown stoichiometry, curve resolution can be combined with target factor analysis (TFA).[45,46] The Kalman filter is also a very popular tool for estimating reaction rate constants from spectroscopic data.[47,48] Otto gives a short overview of the use of multivariate analysis tools in kinetic analysis.[49] The use of three-way analysis to estimate reaction rate constants from batch processes is a new approach.[50,51] In that approach different kinetic runs are analyzed simultaneously if these several runs have a certain correlation in the data structure. In a specific case it is possible to create a three-way structure from only one spectral dataset as is shown in this thesis.

1.5 Constraints in kinetics

The accuracy of reaction rate constant estimates can possibly be improved by using constraints during the optimization procedure. In the literature, constraints like unimodality of concentration profiles,[52,53] closure,[51,52] selectivity[52] and non-negativity of both concentration profiles and pure spectra[51,52] are used as constraints during optimization of the curve resolution model in order to improve the accuracy of parameter estimates. Often some of the pure spectra of the absorbing species involved in the chemical reactions of interest are known beforehand or easy to measure. This information can be implemented in adapted curve resolution methods as is shown in this thesis. In three-way analysis constraints are very often used to avoid numerical problems and to speed up the algorithms.[51,54,55] Constraints in three-way analysis are also discussed in this thesis.

1.6 Goal of the thesis

The initial aim of the work described in this thesis was to use and adapt existing curve resolution based methods to estimate reaction rate constants from spectroscopic data obtained in time of chemical reactions, to validate the obtained parameter estimates and to investigate the use of constraints within curve resolution methods. When Antalek and Windig[56] published a paper about the use of non-iterative three-way methods for estimating parameters from exponential profiles, it became a challenge to modify and apply these methods to kinetic profiles. This has been investigated in detail and new iterative three-way methods, specific for estimating reaction rate constants, have been developed. This thesis gives an overview of the theory of several two-way and three-way methods. Applications of these methods to simulated and experimental data are reported.

1.7 Structure of the thesis

This thesis is organized as follows. In **Chapter 2**, the measurement model is explained in detail and the theory of some two-way methods is presented. Also attention is paid to the use of constraints within these methods. In **Chapter 3**, the three-way methods are presented. Also in this Chapter the use of constraints is discussed. In **Chapter 4**, methods in order to achieve quality assessment of obtained reaction rate constant estimates are reported. **Chapter 5**, deals with a detailed overview of four experimental datasets used in this thesis. A short summary of the datasets can be found in the Appendix. Applications of two-way methods and three-way methods to simulated and experimental data are given in **Chapter 6** and **7**, respectively. **Chapter 8** treats the comparison between the performance of two-way and three-way methods. **Chapter 9** is concerned with the implementation of constraints within a specific curve resolution method, discussed in **Chapter 2**. General conclusions of the work presented and suggestions for further research are given in **Chapter 10**.

The methods presented in this thesis are not applied to all datasets which are described in **Chapter 5**. This is because of the large time gap between the measurements of several datasets. This thesis is organized in such a way, that **Chapter 6**, **7**, **8** and **9**, which all deal with applications, can be read independently. This also holds for **Chapter 2**, **3**, **4** and **5**, which deal with theory and the description of experimental datasets. However, all **Chapters** use the measurement model defined in **Chapter 2**, **Section 2.2**.

1.8 References

1. Justi R, Gilbert JK. 'History and philosophy of science through models: The case of chemical kinetics'. *Science and Education*, 1999; **8**: 287-307.
2. Mellor JW. *Chemical Statics and Dynamics*, Longmans Green: London, 1904.
3. Duncan A. *Law and Order in Eighteenth-Century Chemistry*, Oxford University Press: Oxford, 1996.
4. Mierzecki R. *The Historical Development of Chemical Concepts*, Kluwer: Dordrecht, 1991.
5. Farber E. 'Early studies concerning time in chemical reactions'. *Chymia*, 1961; **7**: 875-894.
6. Partington JR. *A History of Chemistry (Vol.4)*, MacMillan: London, 1964.
7. Ostwald W. *The fundamental Principles of Chemistry*, Longman Green: New York, 1909.
8. Van 't Hoff JH. *Studies in Chemical Dynamic*, Frederick Miller and Williams & Norgate: Amsterdam and London, 1896.
9. Arrhenius S. 'On the reaction velocity of the inversion of cane sugar by acids', in *Selected Readings in Chemical Kinetics*, ed. By Black MH, Laidler KJ. Pergamon Press: Oxford, 1967; 31-35.
10. Glasstone S, Laidler KJ, Eyring H. *The Theory of Rate Processes-the Kinetics of Chemical Reactions, Viscosity, Diffusion and Electrochemical phenomena*, Erlbaum: New Jersey, 1941; 3-34.

11. Rice OK, Ramsberger HC. 'Theories of unimolecular reactions at low pressures'. *J. Am. Chem. Soc.*, 1927; **49**: 1617.
12. Semenoff N. 'The oxidation of phosphorus vapour at low pressures', in *Selected Readings in Chemical Kinetics*, ed. By Black MH, Laidler KJ. Pergamon Press: Oxford, 1967; 127-153.
13. Christiansen JA. 'On the reaction between hydrogen and bromine', in *Selected Readings in Chemical Kinetics*, ed. By Black MH, Laidler KJ. Pergamon Press: Oxford, 1967; 119-126.
14. Evans MG, Polanyi M. 'Some applications of the transition state method to the calculation of reaction velocities'. *Transactions of the Faraday Society*, 1935; **31**: 875-894.
15. Evans MG. 'Thermodynamical treatment of transition state'. *Transactions of the Faraday Society*, 1938; **34**: 49-57.
16. Atkins PW. *Physical Chemistry*, Oxford University Press: Oxford, 1998, Chapter 25.
17. Kaufman D, Sterner C, Masek B, Svenningsen R, Samuelson G. 'An NMR kinetics experiment'. *J. Chem. Education*, 1982; **59**: 885-886.
18. Chrastil J. 'Determination of the first order consecutive reaction rate constants from final product'. *Comput. Chem.*, 1988; **12**: 289-292.
19. Chrastil J. 'Determination of the first-order consecutive reversible reaction kinetics'. *Comput. Chem.*, 1993; **17**: 103-106.
20. Burns DA, Ciurczak EW. *Handbook of Near-Infrared Analysis*, Dekker: New York, 1992.
21. Workman JR JJ. 'Interpretive spectroscopy for near infrared'. *Appl. Spectrosc. Reviews*, 1996; **31**: 251-320.
22. Barshop BA, Wrenn RF, Frieden C. 'Analysis of numerical methods for computer simulation of kinetic processes: Development of KINSIM-A flexible, portable system'. *Anal. Biochem.*, 1983; **130**: 134-145.
23. Zimmerle CT, Frieden C. 'Analysis of progress curves by simulations generated by numerical integration'. *Biochem. J.*, 1989; **258**: 381-387.
24. Cavinato AG, Mayes DM, Ge Z, Callis JB. 'Noninvasive method for monitoring ethanol in fermentation processes using fiber-optic near-infrared spectroscopy'. *Anal. Chem.*, 1990; **62**: 1977-1982.
25. Aldridge PK, Burns DH, Kelly JJ, Callis JB. 'Monitoring of methylmethacrylate polymerization using non-invasive SW-NIR spectroscopy'. *Process Control and Quality*, 1993; **4**: 155-160.
26. Sylvestre EA, Lawton WH, Maggio MS. 'Curve resolution using a postulated chemical reaction'. *Technometrics*, 1974; **16**: 353-368.
27. Mayes DM, Kelly JJ, Callis JB. 'Non-invasive monitoring of a two-step sequential chemical reaction with shortwave near-infrared spectroscopy', in *Near Infra-Red Spectroscopy: Bridging the Gap between Data Analysis and NIR Applications*, ed. by Hildrum KI, Isaksson T, Naes T, Tandberg A. Ellis Horwood: Chichester, 1992; 377-387.
28. Chau F-T, Mok K-W. 'Multiwavelength analysis for a first-order consecutive reaction'. *Computers Chem.*, 1992; **16**: 239-242.
29. Bugnon P, Chottard J-C, Jestin J-L, Jung B, Laurenczy G, Maeder M, Merbach AE, Zuberbühler AD. 'Second-order globalisation for the determination of activation parameters in kinetics'. *Anal. Chim. Acta*, 1994; **298**: 193-201.
30. Tam KY, Chau FT. 'Multivariate study of kinetic data for a two-step consecutive reaction using target factor analysis'. *Chemometrics Intell. Lab. Syst.*, 1994; **25**: 25-42.
31. Maeder M, Molloy KJ, Schumacher MM. 'Analysis of non-isothermal kinetic measurements'. *Anal. Chim. Acta*, 1997; **337**: 73-81.

32. Furusjö E, Danielsson L-G. 'A method for the determination of reaction mechanisms and rate constants from two-way spectroscopic data'. *Anal. Chim. Acta*, 1998; **373**: 83-94.
33. Molloy KJ, Maeder M, Schumacher MM. 'Hard modelling of spectroscopic measurements. Applications in non-ideal industrial reaction systems'. *Chemometrics Intell. Lab. Syst.*, 1999; **46**: 221-230.
34. Furusjö E, Danielsson L-G. 'Target testing procedure for determining chemical kinetics from spectroscopic data with absorption shifts and baseline drift'. *Chemometrics Intell. Lab. Syst.*, 2000; **50**: 63-73.
35. Massart DL, Vandeginste BGM, Buydens LMC, de Jong S, Lewi PJ, Smeyers-Verbeke J. *Handbook of Chemometrics and Qualimetrics*, Elsevier: Amsterdam, 1997.
36. Lawton WH, Sylvestre EA. 'Self modeling curve resolution'. *Technometrics*, 1971; **13**: 617-633.
37. Shrager RI, Hendler RW. 'Titration of individual components in a mixture with resolution of difference spectra, pK's, and redox transitions'. *Anal. Chem.*, 1982; **54**: 1147-1152.
38. Frans SD, Harris JM. 'Reiterative least-squares spectral resolution of organic acid/base mixtures'. *Anal. Chem.*, 1984; **56**: 466-470.
39. Frans SD, Harris JM. 'Least squares singular value decomposition for the resolution of pK's and spectra from organic acid/base mixtures'. *Anal. Chem.*, 1985; **57**: 1718-1721.
40. Shrager RI. 'Chemical transitions measured by spectra and resolved using singular value decomposition'. *Chemometrics Intell. Lab. Syst.*, 1986; **1**: 59-70.
41. Tauler R, Fleming S, Kowalski BR. 'Multivariate curve resolution applied to spectral data from multiple runs of an industrial process'. *Anal. Chem.*, 1993; **65**: 2040-2047.
42. Lacorte S, Barceló D, Tauler R. 'Determination of traces of herbicide mixtures in water by on-line solid-phase extraction followed by liquid chromatography with diode-array detection and multivariate self-modelling curve resolution'. *J. Chromatogr. A*, 1995; **697**: 345-355.
43. Tauler R, Izquierdo-Ridorsa A, Gargallo R, Casassas E. 'Application of a new multivariate curve resolution procedure to the simultaneous analysis of several spectroscopic titrations of the copper (II)-polyinosinic acid system'. *Chemometrics Intell. Lab. Syst.*, 1995; **27**: 163-174.
44. Casassas E, Marqués I, Tauler R. 'Study of acid-base properties of fulvic acids using fluorescence spectrometry and multivariate curve resolution methods'. *Anal. Chim. Acta*, 1995; **310**: 473-484.
45. Bonvin D, Rippin DWT. 'Target factor analysis for the identification of stochiometric models'. *Chem. Eng. Sci.*, 1990; **45**: 3417-3426.
46. Harmon JL, Duboc Ph, Bonvin D. 'Factor analytical modeling of biochemical data'. *Comp. and Chem. Eng.*, 1995; **19**: 1287-1300.
47. Jimenez-Prieto R, Velasco A, Silva M, Perez-Bendito D. 'Kalman filtering of data from first- and second-order kinetics'. *Talanta*, 1993; **40**: 1731-1739.
48. Mok K-W, Chau F-T. 'Application of the extended Kalman filter for analysis of a consecutive first-order reaction'. *Trends Anal. Chem.*, 1996; **15**: 170-174.
49. Otto M. 'Chemometrics in kinetic analysis'. *The Analyst*, 1990; **115**: 685-688.
50. Gui M, Rutan SC, Agbodjan A. 'Kinetic detection of overlapped amino acids in thin-layer chromatography with a direct trilinear decomposition method'. *Anal. Chem.*, 1995; **67**: 3293-3299.
51. Saurina J, Hernandez-Cassou S, Tauler R. 'Multivariate curve resolution and trilinear decomposition methods in the analysis of stopped-flow kinetic data for binary amino acid mixtures'. *Anal. Chem.*, 1997: **69**: 2329-2336.
52. Tauler R, Smilde A, Kowalski B. 'Selectivity, local rank, three-way data analysis and ambiguity in multivariate curve resolution'. *J. Chemometrics*, 1995; **9**: 31-58.

53. de Juan A, van der Heyden Y, Tauler R, Massart, DL. 'Assessment of new constraints applied to the alternating least squares method'. *Anal. Chim. Acta*, 1997; **346**: 307-318.
54. Saurina J, Hernandez-Cassou S., Tauler R. 'Multivariate curve resolution applied to continuous-flow spectrophotometric titrations. Reaction between amino acids and 1,2-naphthoquinone-4-sulfonic acid' *Anal. Chem.*, 1995; **67**: 3722-3726.
55. Bro R. *Multi-Way Analysis in the Food Industry: Models, Algorithms and Applications*, Doctoral Thesis, 1998.
56. Antalek B, Windig W. 'Generalized rank annihilation method applied to a single multicomponent pulsed gradient spin echo NMR data set'. *J. Am. Chem. Soc.*, 1996; **118**: 10331-10332.

Chapter 2

Theory of Two-Way Methods

2.1 Introduction

The theory of the two-way methods traditional curve fitting (TCF), classical curve resolution (CCR) and weighted curve resolution (WCR) for estimating reaction rate constants from spectroscopic data in time of chemical reactions is described in this Chapter. Constraints that can be implemented into these two-way methods are also discussed. Before algorithms and the implementation of constraints are treated in detail, the measurement model is described firstly.

2.2 The measurement model

Let matrix **X** ($M \times N$) be a collection of spectra taken in time of a certain chemical reaction with M time points at N wavelengths, K reacting absorbing species and uniform errors assumed in the data. Matrix **X** can be expressed as the following equation assuming the Beer-Lambert law:[1]

$$\mathbf{X} = \mathbf{F}\mathbf{D}^{\mathrm{T}} + \mathbf{E} \tag{1}$$

The matrices from Equation (1) have the following properties:

1) Every row in **X** denotes a spectrum measured at a certain time.
2) **F** ($M \times K$) is the matrix with concentration profiles of the reacting absorbing species. Every column in **F** denotes the concentration profile of a certain reacting absorbing species in time.
3) **D** ($N \times K$) is the matrix containing the pure spectra of the reacting absorbing species. Every column in **D** represents the pure spectrum of a certain reacting absorbing species.
4) **E** ($M \times N$) is a matrix of spectral residuals (model errors, experimental errors and instrumental noise).

Suppose the following two-step consecutive reaction is considered with second order reaction rate constant k_a ($M^{-1}min^{-1}$) and first order reaction rate constant k_2 (min^{-1}).

$$U + V \xrightarrow{k_a} W \xrightarrow{k_2} Y$$

Equation (2)-(5) describe the differential equations of species *U*, *V*, *W* and *Y*, respectively.

$$\frac{d[U]}{dt} = -k_a[U][V] \tag{2}$$

$$\frac{d[V]}{dt} = \frac{d[U]}{dt} \tag{3}$$

$$\frac{d[W]}{dt} = k_a[U][V] - k_2[W] \tag{4}$$

$$\frac{d[Y]}{dt} = k_2[W] \tag{5}$$

The first reaction step of the two-step consecutive reaction can be made pseudo-first order if reactant *V* is present in large excess. In that case, the reaction can be described as:

$$U \xrightarrow{k_1} W \xrightarrow{k_2} Y$$

with pseudo-first order reaction rate constant k_1 (min^{-1}). If the first reaction step is a pseudo-first order reaction, Equation (6)-(8) can be used to describe the concentration profiles of species *U*, *W* and *Y*, respectively.

$$C_{U,i} = C_{U,0}e^{-k_1 t_i} \tag{6}$$

$$C_{W,i} = \frac{C_{U,0}k_1}{k_2 - k_1}(e^{-k_1 t_i} - e^{-k_2 t_i}) \tag{7}$$

$$C_{Y,i} = C_{U,0} - C_{U,i} - C_{W,i} \tag{8}$$

where $C_{U,0}$ is the initial concentration of U; $C_{U,i}$, $C_{W,i}$ and $C_{Y,i}$ are the concentrations of U, W and Y at time t_i, respectively. It is assumed that only species U and species V are present at the start of the reaction. The relation given in Equation (9) links the second order reaction rate constant k_a and the pseudo-first order reaction rate constant k_1 discussed.

$$k_a = \frac{k_1}{[V]_0} \tag{9}$$

where $[V]_0$ is the initial concentration of species V.

If concentrations in time of the reacting absorbing species are available, the reaction rate constants can be obtained by fitting, for example, Equation (6)-(8) in case of pseudo-first order conditions to the time versus concentration data using mathematical techniques.[2-4] However, in practice only **X** is *known* and **F** and **D** are both *unknown*. In that case, it is impossible to estimate the reaction rate constants of the considered chemical reaction using techniques which are based on fitting the kinetic expressions to the concentration versus time data since these concentrations are not measured. Often, it is possible to obtain a part of **D** by means of measuring pure spectra of reactants and products. However, obtaining pure spectra of intermediate species can be a problem because they are difficult to isolate. Matrix **F** is *unknown*, but a model for **F** (structure) is *known* if a suitable kinetic model for the chemical reaction of interest and the initial concentrations of the different reacting absorbing species are *known*. Iterative algorithms are necessary in order to estimate the reaction rate constants of interest. Three iterative algorithms which can be used to achieve this goal are described in Sections 2.3, 2.5 and 2.6 of this Chapter. In the next Sections it is assumed that species U, W and Y are spectroscopically active whereas species V is not spectroscopically active.

2.3 Traditional curve fitting

In traditional curve fitting (TCF) reaction rate constants are estimated from the absorbance differences in time, which is a concentration profile of a certain species, obtained from one (or more) selective wavelength(s), that is (are) specific for mainly this species.[5-7] This is illustrated in Figure 2. In this figure, the pure UV-Vis spectra are shown of three reacting absorbing species involved in a certain chemical reaction. Suppose that species II is the species of interest. The wavelength $\lambda_{selective}$, indicated by the arrow, is one possible selective wavelength for species II, because the absorbances

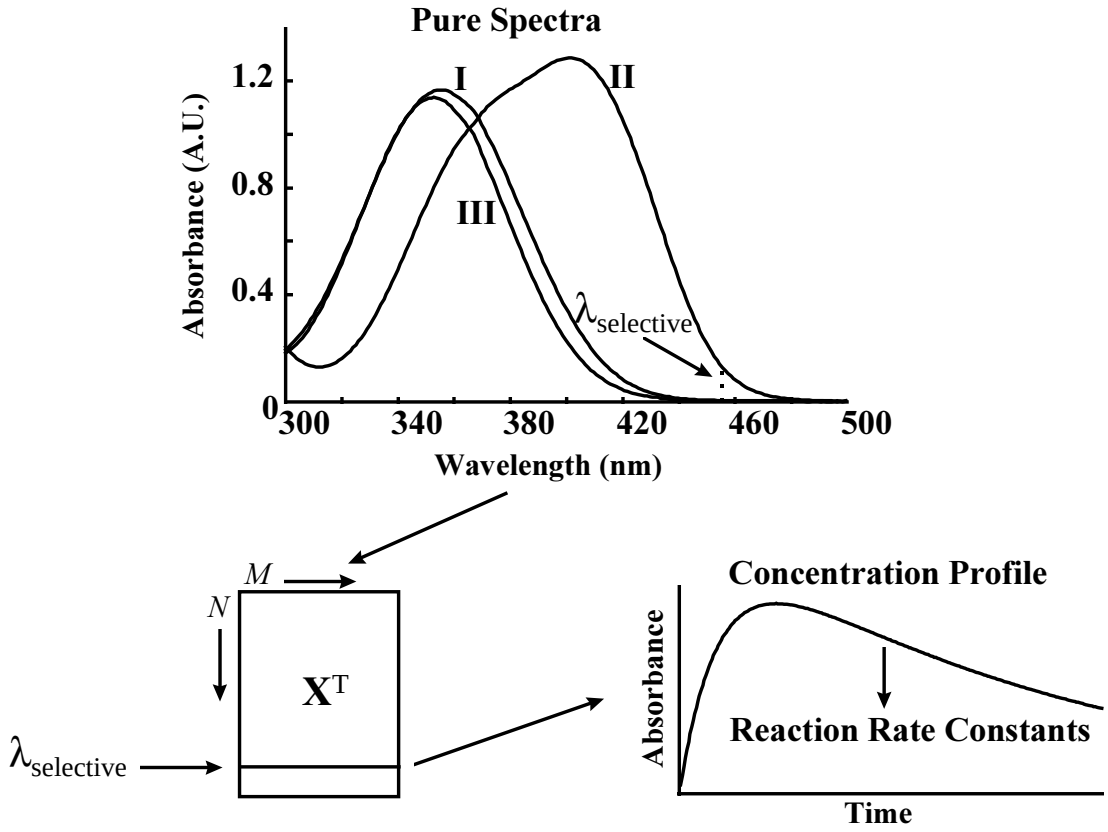

Figure 2. Traditional curve fitting.

of species I and III at this wavelength are very small. From the absorbance versus time data obtained from one or more selective wavelengths, which results in a concentration profile, unknown reaction rate constants can be estimated quite easily and fast. This is done by means of fitting the rate equation of the specific species to the obtained concentration profile. It is important to stress that TCF is an univariate method in case of one selective wavelength.

Consider the measurement model described in Section 2.2 of this Chapter. From Equation (4) in case of second order kinetics or from Equation (7) in case of pseudo-first order kinetics, it is observed that the reaction rate constants of interest, k_a and k_2 or k_1 and k_2, can be estimated from *only* the concentration profile of the intermediate species (species *W*). Hence, if one or more selective wavelengths are chosen for the intermediate species, the reaction rate constants can be estimated from the concentration profile obtained from the absorbance versus time data. Selective wavelengths for the intermediate species can be obtained using fixed-size window evolving factor analysis (FSWEFA), a local rank selection method.[8-10] Also other local rank selection methods like heuristic evolving latent projection (HELP)[11,12] could be used to obtain these selective wavelengths. In FSWEFA selective

wavelengths are obtained from a matrix containing the spectra of the reacting system in time. The FSWEFA technique is explained in more detail in the next Section.

After selective wavelengths have been obtained, the mean absorbance for the selective wavelengths chosen for every time point is calculated. This will give a concentration profile for the intermediate species. It is essential that the pure spectra of reactant and product are both known in advance. Finally, the concentration profile obtained is fitted to the equation of the theoretical concentration profile of the intermediate species using the Levenberg-Marquardt algorithm.[13] This algorithm, for finding an optimum in a response surface, smoothly varies between two methods for finding the optimum, the steepest decent method, that is used *far* from the optimum, and the inverse Hessian method, that is used *close* to the optimum.

2.4 Fixed-size window evolving factor analysis

Fixed size window evolving factor analysis (FSWEFA)[8-10] is applicable if the rows or columns of a matrix have a certain structure, for example the appearance and disappearance of chemical species in time. In FSWEFA a window of rows or columns is selected which is moved over the dataset. Typically a window size equal to the number of expected reacting absorbing chemical species, for example, is chosen. At each position of the window a singular value decomposition (SVD)[14] is calculated and the associated singular values are plotted as a function of the position of the window. In this way, local rank can be estimated. This procedure is illustrated in Figure 3.

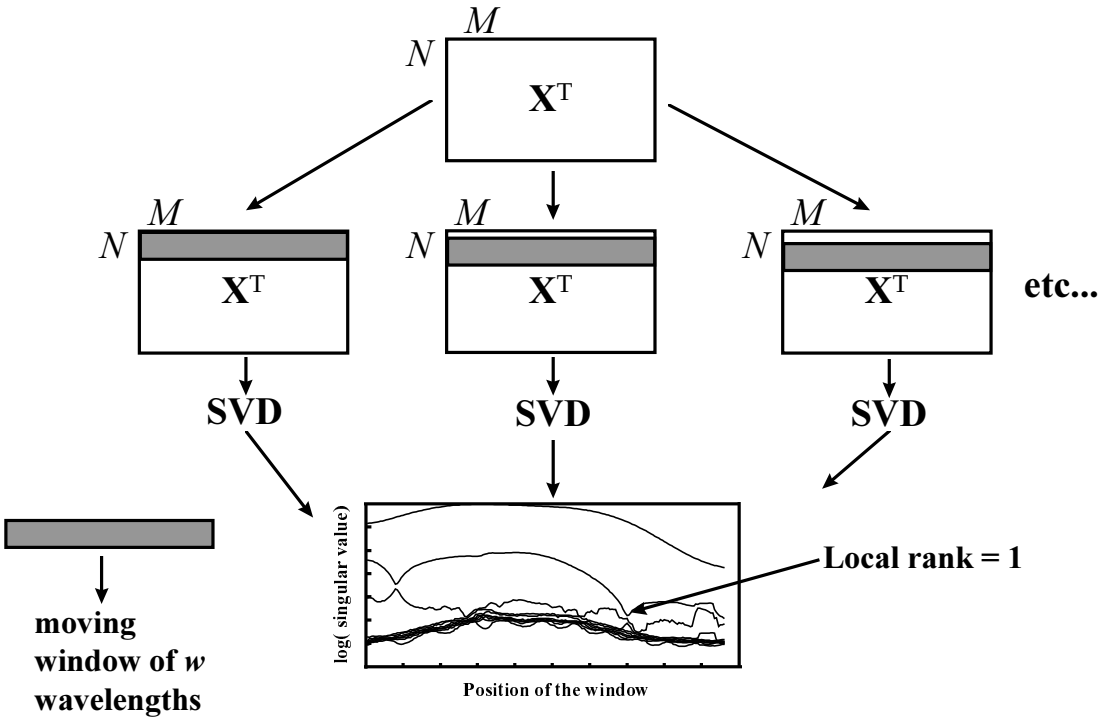

Figure 3. Fixed size window evolving factor analysis (FSWEFA).

In this thesis, FSWEFA has been applied in the spectral domain, because selective wavelengths have to be located. Therefore, a fixed size window of three wavelengths has been moved over the rows of datamatrix $\mathbf{X}^T$, because it is known that three reacting absorbing species are involved in the reacting system in case of the reaction described in Section 2.2 of this Chapter. However, in Figure 3, a fixed size window of ten wavelengths has been moved over the rows of $\mathbf{X}^T$. From the plots of the log (singular value) versus position of the window, local rank of one, representing the presence of mainly the intermediate, is detected. From these plots it is obvious that three reacting absorbing species are involved and hence it is sufficient to use a fixed window size of three wavelengths instead of ten wavelengths. The approach presented can only be applied, if the pure spectra of reactant and product are both known in advance. The pure spectrum of reactant and product are both shown in Figure 2 of the previous Section indicated by species I and species III, respectively. Because the position of the window corresponds to a certain sequence of three wavelengths, selective wavelengths for the intermediate are obtained quite easily.

2.5 Classical curve resolution

Curve resolution[15,16] is a set of techniques based on the determination of qualitative information and the recovery of response profiles, for example time profiles. If parameters of interest, for example reaction rate constants, are incorporated as unknowns in curve resolution this results in modifications of curve resolution techniques, because specific kinetic information is used explicitly. One of these modifications is the classical curve resolution (CCR) algorithm.[17] In CCR, an estimate for k_a and k_2 in case of second order kinetics or an estimate of k_1 and k_2 in case of pseudo-first order kinetics and an estimate of **D** can be obtained simultaneously by minimization of the sum of squares (SSQ) of residuals defined in Equation (10).

$$SSQ = \sum_{m=1}^{M} \sum_{n=1}^{N} e_{mn}^2 \qquad (10)$$

where the residual e_{mn} is the m,n^{th} element of matrix **E** from Equation (1).

The differential equations in case of second order kinetics are solved numerically using the Runge-Kutta (4,5) formula.[13] In that case, numerical integration is part of the algorithm. Stepwise the algorithm works as follows according to an alternating least squares scheme.

Initialization

Construct the estimate of $\mathbf{F}$, $\hat{\mathbf{F}}$, using Equation (2)-(5) in case of second order kinetics or Equation (6)-(8) in case of pseudo-first order kinetics and the starting values for the reaction rate constants.

Minimization of SSQ

Repeat step 1 up to step 5 of the following minimization loop until the SSQ has been minimized.

1) Minimize Equation (11) with respect to $\hat{\mathbf{D}}$, where $\hat{\mathbf{D}}$ is obtained using Equation (12) which represents an ordinary least squares step.

$$\min_{\hat{\mathbf{D}}} \left\| \mathbf{X} - \hat{\mathbf{F}}\hat{\mathbf{D}}^{\mathrm{T}} \right\|^2 \tag{11}$$

$$\hat{\mathbf{D}} = \mathbf{X}^{\mathrm{T}}\hat{\mathbf{F}}(\hat{\mathbf{F}}^{\mathrm{T}}\hat{\mathbf{F}})^{-1} \tag{12}$$

2) Update the reaction rate constants using the Levenberg-Marquardt[13] algorithm according to Equation (13).

$$\min_{\hat{k}_1,\hat{k}_2} \left\| \mathbf{X} - \hat{\mathbf{F}}\hat{\mathbf{D}}^{\mathrm{T}} \right\|^2 \tag{13}$$

3) Calculate $\hat{\mathbf{X}}$, according to Equation (14).

$$\hat{\mathbf{X}} = \hat{\mathbf{F}}\hat{\mathbf{D}}^{\mathrm{T}} \tag{14}$$

4) Calculate matrix $\mathbf{E}$ by applying Equation (15).

$$\mathbf{E} = \mathbf{X} - \hat{\mathbf{X}} \tag{15}$$

5) Calculate SSQ.

It is important to stress that step 1 and step 2 reduce the sum of squares of residuals and convergence is guaranteed. This is the principle of alternating least squares. The columns of matrix $\hat{\mathbf{F}}$ are *all* updated simultaneously in *every* iteration. Hence, *all* concentration profiles are updated simultaneously in *every* iteration. Moreover, only starting values for the reaction rate constants are required and no

initial estimates of the pure spectra are needed. In the Appendix a proof is given that assuming the kinetic model proposed in this thesis is sufficient for uniqueness of the solution of the curve resolution model and no rotational freedom of the solution is present.

CCR can account for non-uniform errors present in the data by using weighted least squares (WLS) if the structure of the measurement error is known.[18] However, the use of WLS is beyond the scope of this thesis, since the structure of this measurement error is unknown.

2.6 Weighted curve resolution

Equation (16) shows the SVD of $\mathbf{X}^T$ ($N \times M$) assuming $M \leq N$. For the cases where $N<M$ is valid $\mathbf{X}$ can be used instead of $\mathbf{X}^T$.

$$\mathbf{X}^T = \mathbf{U}\mathbf{S}\mathbf{V}^T \tag{16}$$

with $\mathbf{U}^T\mathbf{U} = \mathbf{I}$, $\mathbf{V}^T\mathbf{V} = \mathbf{V}\mathbf{V}^T = \mathbf{I}$, $\mathbf{U}$ ($N \times M$), $\mathbf{V}$ ($M \times M$) and $\mathbf{S}$ ($M \times M$) is a diagonal matrix with the non-negative singular values arranged in decreasing order on the diagonal. Equation (17) shows the truncated version of Equation (16) to the first L significant singular values.

$$\overline{\mathbf{X}}^T = \overline{\mathbf{U}}_L \overline{\mathbf{S}}_L \overline{\mathbf{V}}_L^T \quad \text{or} \quad \overline{\mathbf{X}} = \overline{\mathbf{V}}_L \overline{\mathbf{S}}_L \overline{\mathbf{U}}_L^T \tag{17}$$

$\overline{\mathbf{U}}_L$ ($N \times L$) contains the first L columns of $\overline{\mathbf{U}}$, $\overline{\mathbf{S}}_L$ ($L \times L$) is the upper left part of $\overline{\mathbf{S}}$, $\overline{\mathbf{V}}_L$ ($M \times L$) represents the first L columns of $\overline{\mathbf{V}}$, $\overline{\mathbf{U}}_L^T\overline{\mathbf{U}}_L = \mathbf{I}$ and $\overline{\mathbf{V}}_L^T\overline{\mathbf{V}}_L = \mathbf{I}$. The estimate of $\mathbf{F}$, $\hat{\mathbf{F}}$, is reconstructed using the valid kinetic equations and the starting values for the reaction rate constants. If Equation (1) from Section 2.2 holds then $\hat{\mathbf{F}}$ and $\overline{\mathbf{V}}_L$ span the same space and are connected with each other by means of a transformation matrix $\mathbf{H}$ according to Equation (18).

$$\overline{\mathbf{V}}_L = \hat{\mathbf{F}}\hat{\mathbf{H}} \tag{18}$$

with

$$\hat{\mathbf{H}} = (\hat{\mathbf{F}}^T\hat{\mathbf{F}})^{-1}\hat{\mathbf{F}}^T\overline{\mathbf{V}}_L \tag{19}$$

Following the target factor analysis (TFA) approach used by Maeder *et al.*[19-21] the objective function given in Equation (20) is minimized over k_1 and k_2 ensuring that for the proper k_1 and k_2 the minimum of zero will be attained.

$$\min_{\hat{k}_1,\hat{k}_2} \left\| (\overline{\mathbf{V}}_L - \hat{\mathbf{F}}\hat{\mathbf{H}})\overline{\mathbf{S}}_L \right\|^2 \tag{20}$$

where $\overline{\mathbf{V}}_L$ and $\overline{\mathbf{S}}_L$ are both fixed during optimization. Because the columns of $\overline{\mathbf{V}}_L$ are weighted by $\overline{\mathbf{S}}_L$ in order to account for the differences in the order of magnitude of importance of the different columns of $\overline{\mathbf{V}}_L$ as suggested by Shrager,[22] the algorithm is called weighted curve resolution (WCR). This approach can be very valuable in case of data with a poor signal to noise ratio. If Equation (20) is used without weighting the columns of $\overline{\mathbf{V}}_L$, the algorithm is called curve resolution (CR) in this thesis.

From Equation (20) it is obvious that WCR reflects a separable problem, because the concentration space and spectral space are separated. This is an important difference between CCR and WCR. In WCR only reaction rate constant estimates are obtained whereas in CCR reaction rate constant estimates and pure spectra estimates are obtained simultaneously. In WCR, the matrix with concentration profiles, $\hat{\mathbf{F}}$, can be reconstructed using the optimal values of the reaction rate constants found. An estimate of the pure spectra of the reacting absorbing species, $\hat{\mathbf{D}}$, can be obtained by applying Equation (12) from the previous Section.

If the reaction rate constants are estimated, the relative fit error can be calculated according to Equation (21) and (22) for CR and WCR, respectively.

$$\text{Relative fit error} = \frac{\left\| \overline{\mathbf{V}}_L - \hat{\mathbf{F}}\hat{\mathbf{H}} \right\|}{\left\| \overline{\mathbf{V}}_L \right\|} * 100\% \tag{21}$$

$$\text{Relative fit error} = \frac{\left\| (\overline{\mathbf{V}}_L - \hat{\mathbf{F}}\hat{\mathbf{H}})\overline{\mathbf{S}}_L \right\|}{\left\| \overline{\mathbf{V}}_L \overline{\mathbf{S}}_L \right\|} * 100\% \tag{22}$$

where a number of 0% indicates that there are no residuals left.

2.7 Implementation of constraints

In Chapter 1, it has been explained already that the use of constraints implemented into optimization algorithms can be very useful with respect to the accuracy of reaction rate constant estimates. Three different types of constraints are considered in this thesis. In *constraint R* only the pure spectrum of the reactant is used in the optimization procedure. In *constraint RP* the pure spectra of reactant and product are both used in the optimization procedure. In *constraint NNLS* the pure spectra are updated in each iteration of the optimization procedure using a non-negative least squares step.[23] Implementation of the three constraints mentioned in the optimization procedure is only possible in case of CCR. In TCF and WCR, the pure spectra of reacting absorbing species are not used during optimization of the reaction rate constants and hence implementation of the constraints discussed is not possible. In the next Chapter, the use of constraints within three-way methods is reported.

Using constraint R, the first column of matrix $\hat{\mathbf{D}}$ will be fixed during the whole optimization procedure. Only the reaction rate constants and the pure spectra of the intermediate and the product (second and third column of $\hat{\mathbf{D}}$, respectively) are updated simultaneously during the optimization procedure. Using constraint RP, the first and third column of matrix $\hat{\mathbf{D}}$ will be fixed during the whole procedure. Only the reaction rate constants and the pure spectrum of the intermediate (second column of $\hat{\mathbf{D}}$) are updated simultaneously during the optimization procedure. In the CCR algorithm described in Section 2.5 the pure spectra are estimated using an ordinary least squares step. In *constraint NNLS* the pure spectra are updated in each iteration using a non-negative least squares step.

2.8 References

1. Burns DA, Ciurczak EW. *Handbook of Near-Infrared Analysis*, Dekker: New York, 1992.
2. Kaufman D, Sterner C, Masek B, Svenningsen R, Samuelson G. 'An NMR kinetics experiment'. *J. Chem. Education*, 1982; **59**: 885-886.
3. Chrastil J. 'Determination of the first order consecutive reaction rate constants from final product'. *Comput. Chem.*, 1988; **12**: 289-292.
4. Chrastil J. 'Determination of the first-order consecutive reversible reaction kinetics'. *Comput. Chem.*, 1993; **17**: 103-106.
5. Drobnica L, Sturdik E. 'The reaction of carbonyl cyanide phenylhydrazones with thiols'. *Biochim. Biophys. Acta*, 1979; **585**: 462-476.
6. Bisby RH, Thomas EW. 'Kinetic analysis by the method of nonlinear least squares'. *J. Chemical Education*, 1986; **63**: 990-992.
7. Chau F-T, Mok K-W. 'Multiwavelength analysis for a first-order consecutive reaction'. *Computers Chem.*, 1992; **16**: 239-242.
8. Maeder M, Zuberbuehler AD. 'The resolution of overlapping chromatographic peaks by evolving factor analysis'. *Anal. Chim. Acta*, 1986; **181**: 287-291.

9. Maeder M. 'Evolving factor analysis for the resolution of overlapping chromatographic peaks'. *Anal. Chem.*, 1987; **59**: 527-530.
10. Keller HR, Massart DL. 'Peak purity control in liquid chromatography with photodiode-array detection by a fixed size moving window evolving factor analysis'. *Anal. Chim. Acta*, 1991; **246**: 379-390.
11. Kvalheim OM, Liang Y-Z. 'Heuristic evolving latent projections: Resolving two-way multicomponent data. 1. Selectivity, latent-projective graph, datascope, local rank, and unique resolution'. *Anal. Chem.*, 1992; **64**: 936-946.
12. Liang Y-Z, Kvalheim OM, Keller HR, Massart DL, Kiechle P, Erni F. 'Heuristic evolving latent projections: Resolving two-way multicomponent data. 2. Detection and resolution of minor constituents'. *Anal. Chem.*, 1992; **64**: 946-953.
13. Press WH, Teukolsky SA, Vetterling WT, Flannery BP. *Numerical Recipes*, Cambridge University Press: New York, 1992.
14. Martens H., Naes T. *Multivariate Calibration*, Wiley: Chichester, 1989.
15. Lawton WH, Sylvestre EA. 'Self modeling curve resolution'. *Technometrics*, 1971; **13**: 617-633.
16. Sylvestre EA, Lawton WH, Maggio MS. 'Curve resolution using a postulated chemical reaction'. *Technometrics*, 1974; **16**: 353-368.
17. Frans SD, Harris JM. 'Reiterative least-squares spectral resolution of organic acid/base mixtures'. *Anal. Chem.*, 1984; **56**: 466-470.
18. Kiers HAL. 'Weighted least squares fitting using ordinary least squares algorithms', *Psychometrika*, 1997; **62**: 251-266.
19. Bugnon P, Chottard J-C, Jestin J-L, Jung B, Laurenczy G, Maeder M, Merbach AE, Zuberbühler AD. 'Second-order globalisation for the determination of activation parameters in kinetics'. *Anal. Chim. Acta*, 1994; **298**: 193-201.
20. Maeder M, Molloy KJ, Schumacher MM. 'Analysis of non-isothermal kinetic measurements'. *Anal. Chim. Acta*, 1997; **337**: 73-81.
21. Molloy KJ, Maeder M, Schumacher MM. 'Hard modelling of spectroscopic measurements. Applications in non-ideal industrial reaction systems'. *Chemometrics Intell. Lab. Syst.*, 1999; **46**: 221-230.
22. Shrager RI. 'Chemical transitions measured by spectra and resolved using singular value decomposition'. *Chemometrics Intell. Lab. Syst.*, 1986; **1**: 59-70.
23. Bro R, de Jong S. 'A fast non-negativity-constrained least squares algorithm'. *J. Chemometrics*, 1997; **11**: 393-402.

Chapter 3

Theory of Three-Way Methods

3.1 Introduction

In this Chapter, non-iterative and iterative three-way methods for estimating reaction rate constants from spectroscopic data are described. It is possible to use constraints within three-way methods. This is discussed in Section 3.7. Before the algorithms are explained in detail the principle on which the three-way methods are based is explained in the next Section.

3.2 Shifting an exponential function

Let an array of exponentially decaying numbers, called array one, be equal to 162, 54, 18, 6. Next, suppose array one is shifted one position which results into array two according to Figure 4. In this figure, the ratio, *R*, between two numbers listed in one row is the same from row to row. In this case the ratio equals three.

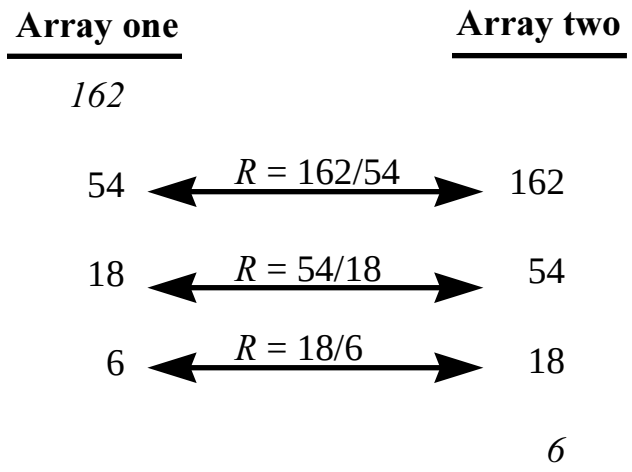

Figure 4. Array one and array two.

Equation (23) represents an exponential function describing the reaction kinetics of a first order process.

$$C = e^{-k_1 t} \tag{23}$$

where k_1 is a reaction rate constant and C is the concentration of a certain species at time t. If the exponent is shifted in time, by means of introducing shift parameter S, Equation (23) can be written as Equation (24).

$$C_s = e^{-k_1(t+S)} \tag{24}$$

where C_s is the "shifted concentration". The ratio of Equation (23) and (24), called λ is an indirect measure for k_1 as is shown in Equation (25).

$$\lambda = \frac{C}{C_s} = \frac{e^{-k_1 t}}{e^{-k_1(t+S)}} = e^{-k_1 t + k_1(t+S)} = e^{k_1 S} \Rightarrow k_1 = \frac{\ln(\lambda)}{S} \tag{25}$$

Hence, the reaction rate constant k_1 is calculated easily from the ratio of the non-shifted and the shifted exponential function.

3.3 The trilinear structure

Consider the first reaction step, described in Section 2.2 of Chapter 2, under pseudo-first order conditions. Equation (6) from Section 2.2 of Chapter 2, describes the concentration profile of the reactant (species U). In this Section, it is supposed, for convenience, that the initial concentration of species U, $C_{U,0}$, is equal to 1 moll^{-1}. Assume that matrix $\mathbf{X}$ (M×N), as defined in Section 2.2 of Chapter 2, contains spectroscopic measurements of only species U in time. This matrix contains two-way data and no trilinear structure is present at first sight. However, it is possible to build a trilinear structure according to the following procedure developed by Windig and Antalek.[1,2]

Two matrices, $\mathbf{X}_1$ and $\mathbf{X}_2$, are created from $\mathbf{X}$ by means of a time shift S, which can be any positive integer value between 1 and (M-1). This results in: $\mathbf{X}_1 = (\mathbf{X}([1 \ldots (M\text{-}S)])\times N)$ and $\mathbf{X}_2 = (\mathbf{X}([(1+S) \ldots M])\times N)$. These two matrices created by means of splitting $\mathbf{X}$ are visualized in Figure 5, where $\mathbf{d}_U$ (N×1) is the pure spectrum of species U, $\mathbf{f}_U$ (M×1) is the concentration profile of species U, $\mathbf{f}_1$ ((M-S)×1) and $\mathbf{f}_2$ ((M-S)×1) are the concentration profiles of species U with time shift S in matrices $\mathbf{X}_1$ and $\mathbf{X}_2$, respectively.

The matrices $\mathbf{X}_1$ and $\mathbf{X}_2$ formed by splitting $\mathbf{X}$ can be put into a trilinear or PARAFAC[3,4] model by means of stacking as shown in Figure 6 to construct a three-way array $\underline{\mathbf{X}}$ ((M-S)×N×2). Vector $\mathbf{c}$ (2×1) contains the scaling factors of

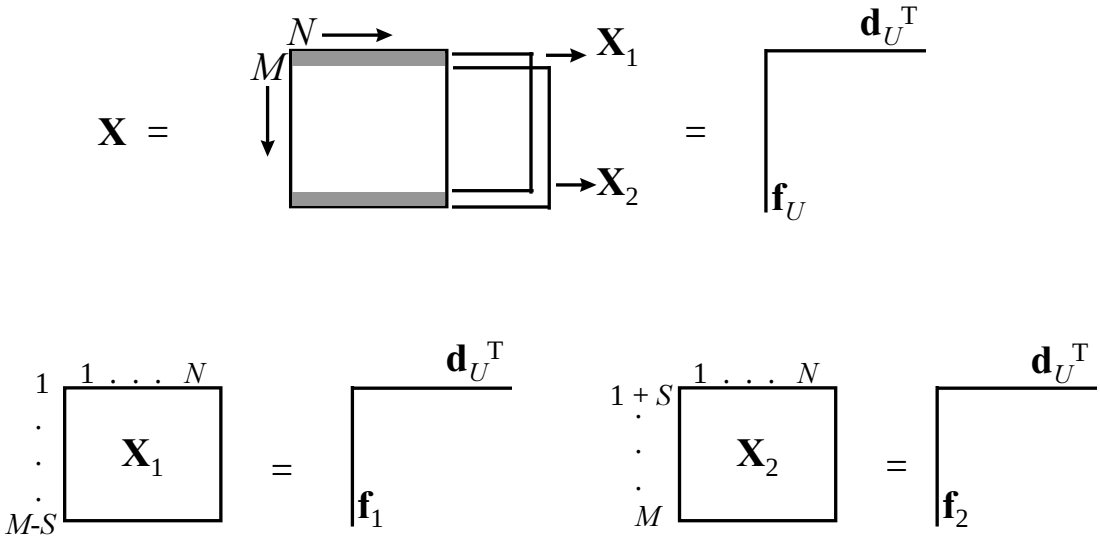

Figure 5. Illustration of X_1 and X_2 created from X by means of a time shift.

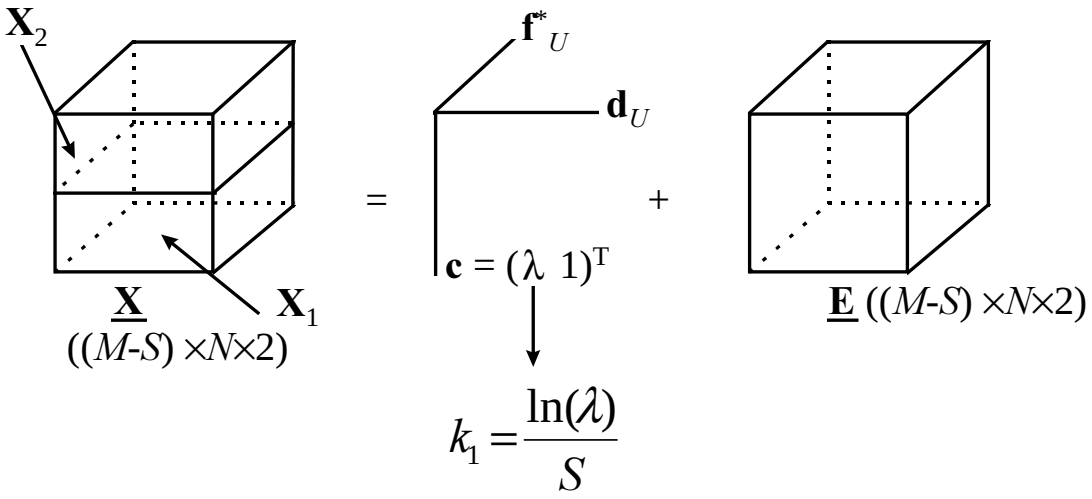

Figure 6. The trilinear structure created by means of stacking X_1 and X_2.

$\mathbf{X}_1$ and $\mathbf{X}_2$ and $\mathbf{f}^*_U$ ((*M*-*S*)×1) is the concentration profile.

From **c** the reaction rate constant k_1 can be estimated if the time shift is known as shown in Figure 6. The parameter λ contains de ratio between the non-shifted and the shifted equation of the concentration profile of species *U*. An element x_{mnp} from $\underline{\mathbf{X}}$ with dimension (*M*×*N*×*P*) is modeled by means of a one-factor PARAFAC model according to Equation (26).

$$x_{mnp} = a_{m1} b_{n1} c_{p1} + e_{mnp} \qquad (26)$$

If two exponentially decaying functions are considered this will result in a two component PARAFAC model. If more complex reaction schemes and therefore more

exponential functions are considered Equation (26) can be generalized into a PARAFAC model with multiple components according to Equation (27).

$$x_{mnp} = \sum_{q=1}^{Q} a_{mq} b_{nq} c_{pq} + e_{mnp} \qquad (27)$$

Define the vectors $\mathbf{a}_q$ (M×1), $\mathbf{b}_q$ (N×1) and $\mathbf{c}_q$ (2×1) as vectors with the elements a_{mq}, b_{nq} and c_{pq}, respectively. The multiplication of a_{mq}, b_{nq} and c_{pq} for each m, n, p gives the qth triad. Hence, every independent exponentially decaying function expresses itself in a triad. Note, that there is a permutation freedom between triads. The **C**-matrix contains the scaling factors from which the different reaction rate constants can be estimated as has been shown in Figure 6 in case of one reaction rate constant. Later in this Section, it is discussed how more reaction rate constants are calculated from matrix **C** if more than one exponential function is involved in the model. Hence, every combination of exponential functions can be modeled, but every combination has to be written as a sum of separate exponential components. This condition has to be fulfilled in order to apply the method presented. This will be explained in more detail further on in this Section.

Next, both reaction steps of the reaction, described in Section 2.2 of Chapter 2, are considered under pseudo-first order conditions. Assume again that matrix **X** (M×N) contains spectroscopic measurements of the reacting system. Species U, species W and species Y are spectroscopically active. Hence, in case of noiseless data, the rank of **X** is equal to three. Equation (6) and Equation (7) from Section 2.2 of Chapter 2 are already a sum of exponential functions, but Equation (8) is not a sum of exponential functions. Equation (8) can be written into Equation (28) using Equation (6) and Equation (7).

$$C_{Y,i} = 1 - e^{-k_1 t_i} - k(e^{-k_1 t_i} - e^{-k_2 t_i}) = e^0 - e^{-k_1 t_i} - ke^{-k_1 t_i} + ke^{-k_2 t_i} \qquad (28)$$

where $k = k_1/(k_2 - k_1)$. Equation (28) is now a sum of separate exponentially decaying functions. To make sure that the term e^0 is present in the dataset a column with constants (M×1), for example $(1\ldots1)^T$ (a column with ones) is added to datamatrix **X** (M×N) resulting in an augmented datamatrix $\mathbf{X}^*$ (M×(N+1)).[1,2] The reason to add the column of ones is explained in more detail further on in this Chapter. It is important to realize that the rank of $\mathbf{X}^*$ is equal to the rank of **X** and hence equal to three. The augmented datamatrix $\mathbf{X}^*$ is visualized in Figure 7, where $\mathbf{d}_U$, $\mathbf{d}_W$ and $\mathbf{d}_Y$ with dimensions ((N+1)×1) are the pure spectra of species U, W and Y,

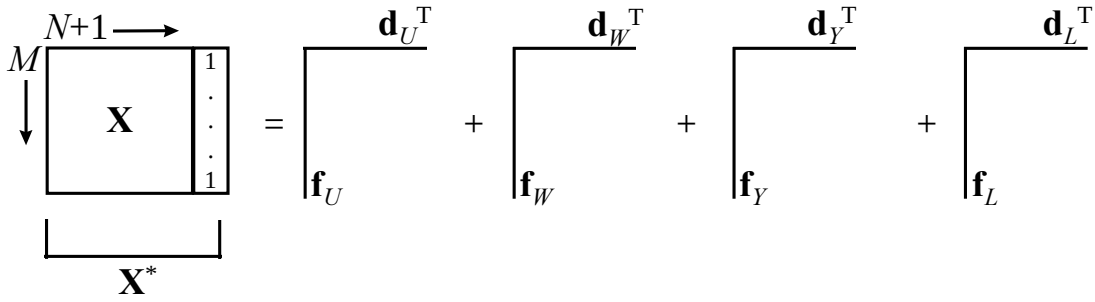

Figure 7. Visualization of the augmented datamatrix $\mathbf{X}^*$.

respectively; $\mathbf{f}_U$, $\mathbf{f}_W$ and $\mathbf{f}_Y$ with dimensions (M×1) are the concentration profiles of species U, W and Y, respectively. The vector $\mathbf{d}_L$ ((N+1)×1) is the "spectrum" of the added column with constants equal to: $(0\ 0\ 0\ 0\ \ldots\ 0\ 1)^{\mathrm{T}}$. The vector $\mathbf{f}_L$ (M×1) is the "concentration profile" of the added column with constants with "concentration" C_L equal to e^0.

A mathematical representation of $\mathbf{X}^*$ is given in Equation (29).

$$\mathbf{X}^* = \mathbf{f}_U\mathbf{d}_U^{\mathrm{T}} + \mathbf{f}_W\mathbf{d}_W^{\mathrm{T}} + \mathbf{f}_Y\mathbf{d}_Y^{\mathrm{T}} + \mathbf{f}_L\mathbf{d}_L^{\mathrm{T}} \tag{29}$$

Equation (29) can be rewritten into Equation (30) after rewriting the vectors with the concentration profiles from Equation (28) using Equation (6), (7) and the relation $k = k_1/(k_2 - k_1)$.

$$\begin{aligned}&\mathbf{X}^* = (e^{-k_1\mathbf{t}})\mathbf{d}_U^{\mathrm{T}} + k(e^{-k_1\mathbf{t}})\mathbf{d}_W^{\mathrm{T}} - k(e^{-k_2\mathbf{t}})\mathbf{d}_W^{\mathrm{T}} + e^{0\mathbf{t}}\mathbf{d}_Y^{\mathrm{T}} - (e^{-k_1\mathbf{t}})\mathbf{d}_Y^{\mathrm{T}} - k(e^{-k_1\mathbf{t}})\mathbf{d}_Y^{\mathrm{T}} \\ &+ k(e^{-k_2\mathbf{t}})\mathbf{d}_Y^{\mathrm{T}} + e^{0\mathbf{t}}\mathbf{d}_L^{\mathrm{T}} = \\ &e^{-k_1\mathbf{t}}(\mathbf{d}_U + k\mathbf{d}_W - \mathbf{d}_Y - k\mathbf{d}_Y)^{\mathrm{T}} + e^{-k_2\mathbf{t}}(-k\mathbf{d}_W + k\mathbf{d}_Y)^{\mathrm{T}} + e^{0\mathbf{t}}(\mathbf{d}_Y + \mathbf{d}_L)^{\mathrm{T}} = \\ &\mathbf{a}_1\mathbf{b}_1^{\mathrm{T}} + \mathbf{a}_2\mathbf{b}_2^{\mathrm{T}} + \mathbf{a}_3\mathbf{b}_3^{\mathrm{T}}\end{aligned} \tag{30}$$

where $e^{-k_1\mathbf{t}}$ is a shorthand notation for $[e^{-k_1t_1}...e^{-k_1t_n}]$, $e^{-k_2\mathbf{t}}$ is a shorthand notation for $[e^{-k_2t_1}...e^{-k_2t_n}]$, $\mathbf{a}_1 = e^{-k_1\mathbf{t}}$, $\mathbf{a}_2 = e^{-k_2\mathbf{t}}$, $\mathbf{a}_3 = e^{0\mathbf{t}}$, $\mathbf{b}_1^{\mathrm{T}} = (\mathbf{d}_U + k\mathbf{d}_W - \mathbf{d}_Y - k\mathbf{d}_Y)^{\mathrm{T}}$, $\mathbf{b}_2^{\mathrm{T}} = (-k\mathbf{d}_W + k\mathbf{d}_Y)^{\mathrm{T}}$ and $\mathbf{b}_3^{\mathrm{T}} = (\mathbf{d}_Y + \mathbf{d}_L)^{\mathrm{T}}$. Equation (29) and the mathematical manipulation in Equation (30) are visualized in Figure 8. The concentration profiles, $\mathbf{f}_U$, $\mathbf{f}_W$ and $\mathbf{f}_Y$, are rearranged into the exponential functions $\mathbf{a}_1$, $\mathbf{a}_2$ and $\mathbf{a}_3$. The response matrix $\mathbf{X}^*$ consists of a sum of exponential functions.

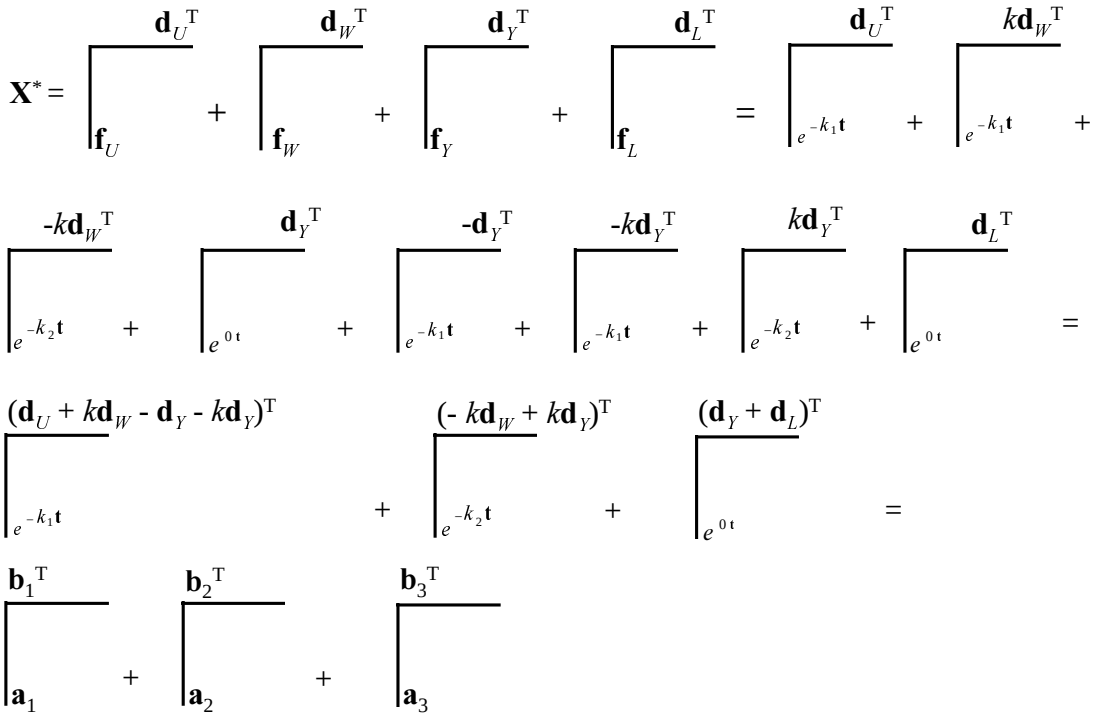

Figure 8. Visualization of Equation (29) and Equation (30).

$\mathbf{X}^*$ is used to create two datamatrices, $\mathbf{X}^*_1$ and $\mathbf{X}^*_2$ using a time shift S. The matrices $\mathbf{X}^*_1$ ((M-S)×(N+1)) and $\mathbf{X}^*_2$ ((M-S)×(N+1)) formed by splitting $\mathbf{X}^*$ are used to construct the three-way array $\underline{\mathbf{X}}^*$ ((M-S)×(N+1)×2) by means of stacking and is modeled with PARAFAC as shown in Figure 9. From the three-way array $\underline{\mathbf{X}}^*$, the following three loading matrices can be constructed.

$\mathbf{A} = [\mathbf{a}_1 \ \mathbf{a}_2 \ \mathbf{a}_3]$ ((M-S)×3) with k-rank[5] equal to 3

$\mathbf{B} = [\mathbf{b}_1 \ \mathbf{b}_2 \ \mathbf{b}_3]$ ((N+1)×3) with k-rank equal to 3

$\mathbf{C} = [\mathbf{c}_1 \ \mathbf{c}_2 \ \mathbf{c}_3]$ (2×3) with k-rank equal to 2, assuming $k_1 \neq k_2$.

The k-rank is defined as follows. Suppose a matrix has H columns. If any combination of L columns of the matrix are independent and this is not valid for L+1, then the k-rank of the matrix is equal to L. The decomposition of the three-way array in the matrices **A**, **B** and **C** is unique if the Kruskal criterion[6] is fulfilled. According to the Kruskal criterion, the decomposition is unique if Equation (31) is valid.

$$k\text{-rank}(\mathbf{A}) + k\text{-rank}(\mathbf{B}) + k\text{-rank}(\mathbf{C}) \geq 2K + 2. \qquad (31)$$

where K is equal to the rank of **X** and $\mathbf{X}^*$, which is equal to the number of reacting

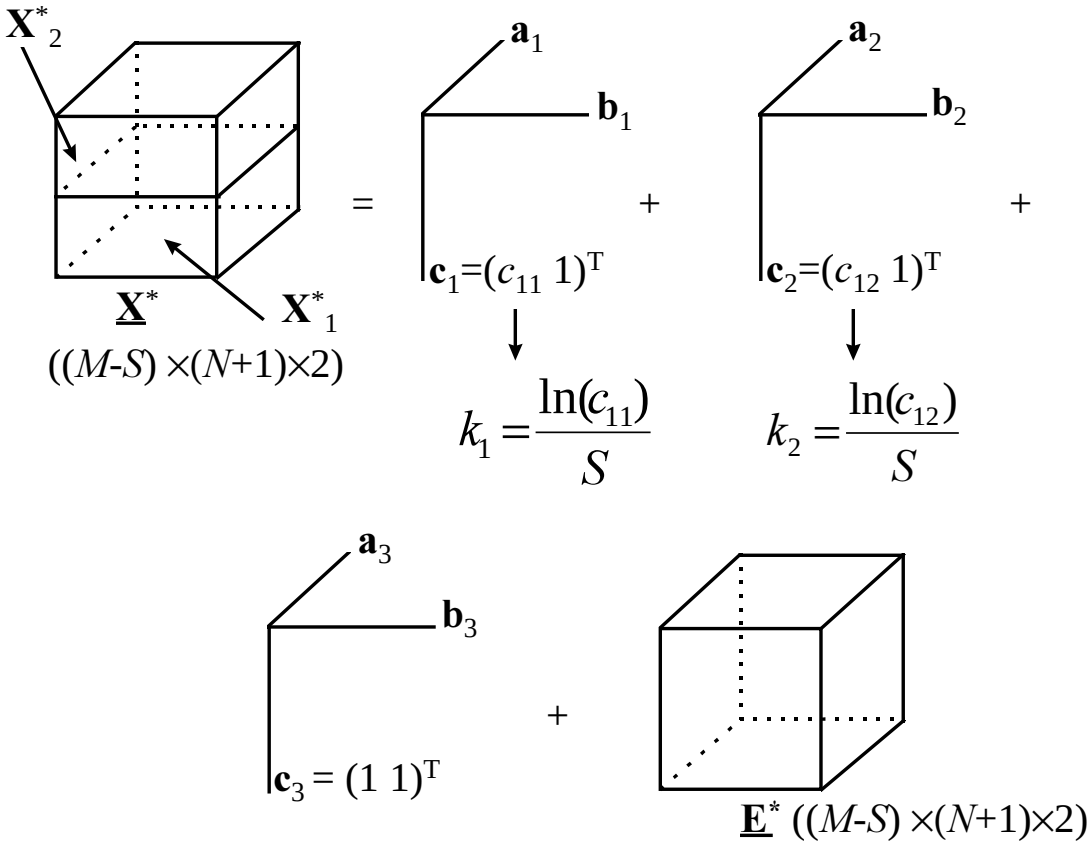

Figure 9. The trilinear structure created by means of stacking $\mathbf{X}^*_1$ and $\mathbf{X}^*_2$.

absorbing species. In this example, the number of reacting absorbing species is equal to three, as already mentioned earlier. In this case $(3 + 3 + 2) \geq (2\times3 + 2) \Rightarrow 8 \geq 8$ and hence the decomposition of the three-way array is unique. This means that no rotational freedom of the resolved temporal profiles and spectra is present.

From the third loading matrix, **C**, the reaction rate constants k_1 and k_2 can be extracted very easily if the time shift parameter S is known as shown in Figure 9. The structure of **C** is shown in Equation (32).

$$\mathbf{C} = \begin{pmatrix} c_{11} & c_{12} & 1 \\ 1 & 1 & 1 \end{pmatrix} \tag{32}$$

where k_1 and k_2 are equal to $\ln(c_{11})/S$ and $\ln(c_{12})/S$, respectively. This is analogous to the example given in Section 3.2 of this Chapter and the example shown in Figure 6. However, in that figure only one exponential function has been considered whereas in the present example three exponential functions are involved. In practice, it is not always the case that the first column of **C** represents k_1, because of the presence of permutation freedom. It is necessary to know the order of magnitude of the reaction

rate constants in advance to judge which column represents k_1, for example. So far, the whole procedure is valid if $\mathbf{X}^*$ is splitted into two datasets.

It is possible to split $\mathbf{X}^*$ in more than two datasets using a certain step size. Creating more than two datasets from $\mathbf{X}^*$ can be advantageous with respect to noise reduction. Assume for simplicity that $\mathbf{X}^*$ is splitted into three datamatrices or slabs, $\mathbf{X}^*_1$, $\mathbf{X}^*_2$ and $\mathbf{X}^*_3$ using a step size G. This is visualized in Figure 10. From this figure it is observed that the step size between $\mathbf{X}^*_1$ and $\mathbf{X}^*_2$ is in this case equal to the step size between $\mathbf{X}^*_2$ and $\mathbf{X}^*_3$. Other step sizes are also possible. The three matrices which are created by separating $\mathbf{X}^*$ are used to construct the three-way array $\underline{\mathbf{X}}^*$ ($(M-(G\times2))\times(N+1)\times3$) by means of stacking and can be modeled with PARAFAC similar to the procedure shown in Figure 9. The loading matrices can be constructed and from the third loading matrix according to Equation (33) estimates for k_1 and k_2 can be extracted which can be averaged.

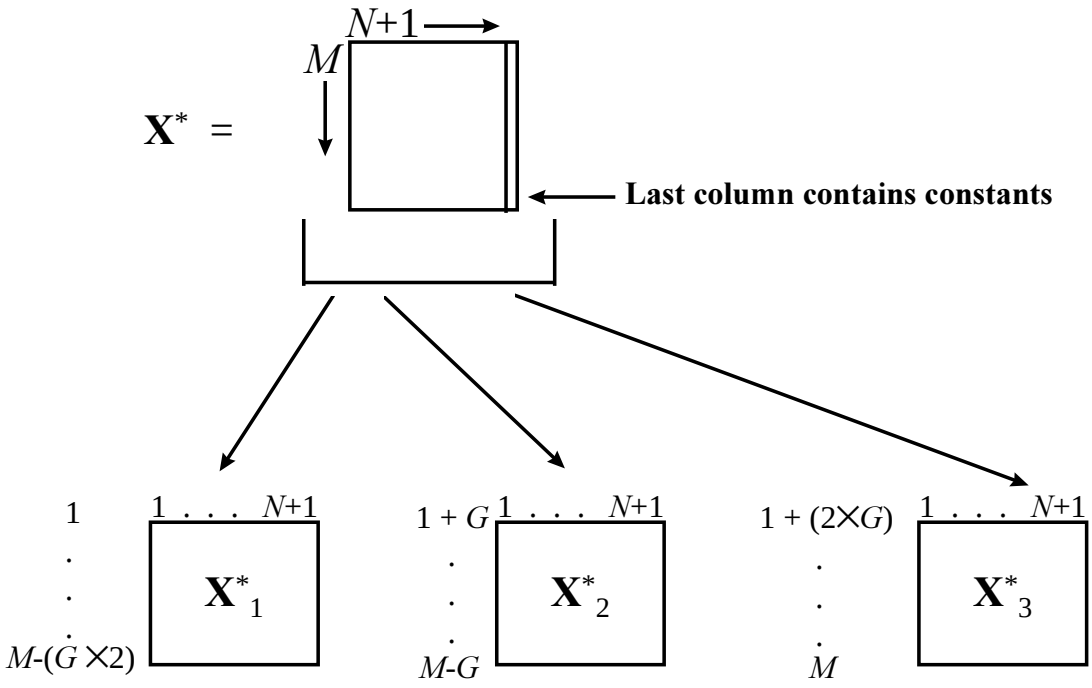

Figure 10. Splitting $\mathbf{X}^*$ into three datamatrices, $\mathbf{X}^*_1$, $\mathbf{X}^*_2$ and $\mathbf{X}^*_3$.

$$\mathbf{C} = \begin{pmatrix} c_{11} & c_{12} & 1 \\ c_{21} & c_{22} & 1 \\ 1 & 1 & 1 \end{pmatrix} \qquad (33)$$

where $\ln(c_{11}/c_{21}) = \ln(c_{21}) = k_1$ and $\ln(c_{12}/c_{22}) = \ln(c_{22}) = k_2$ for the noiseless case. Hence, two estimates for both k_1 and k_2 are obtained if three slabs are created from $\mathbf{X}^*$.

These estimates can be averaged. Likewise, three estimates of reaction rate constants are obtained from four slabs, etc…

The trilinear structure discussed in this Section is the root of the non-iterative and the iterative algorithms which are discussed in the next Sections. However, using these algorithms it is necessary that the exponential functions involved have to be written as a sum of exponential functions. This is a drawback, because that makes three-way modelling as presented in this Chapter only suitable for (pseudo-) first order kinetic problems. In case of, for example, second order kinetics two-way methods described in the previous Chapter have to be used to obtain reaction rate constant estimates.

3.4 Non-iterative three-way methods

Consider again the two reaction steps from the reaction, described in Section 2.2 of Chapter 2, under pseudo-first order conditions and matrix **X** with spectroscopic measurements of the reaction. Two slabs are created from $\mathbf{X}^*$ resulting in the three-way array $\underline{\mathbf{X}}^*$ ($(M\text{-}S)\times(N+1)\times 2$). From this structure the reaction rate constants can be estimated according to the following steps.

1) Start with a generalized eigenvalue problem (GEP)[7] which gives the two loading matrices **A** and **B**. The third loading matrix, **C**, is obtained by a least squares step. In order to solve the GEP, the matrices $\mathbf{X}^*_1$ and $\mathbf{X}^*_2$ need to be transferred into square matrices. This can be done by using a common space[8] onto which both matrices are projected. In this paper, the common space was based on $\mathbf{X}^*_1 + \mathbf{X}^*_2$.

2) Recognize the triad which is constant and permute the model such that the third triad models the added constant. For the noiseless case or in case of adding a column with constants (soft constraint), where the order of magnitude of the constants is large compared to the order of magnitude of the signal in **X**, the third column of **A**, $\mathbf{a}_3$, is constant and vector $\mathbf{c}_3$, the third column of **C**, is equal to $(1\ 1)^T$. In case of adding a column with constants, where the order of magnitude of the constants is comparable to the order of magnitude of the signal, the third column of **C** is not equal to $(1\ 1)^T$. If the order of magnitude of the reaction rate constants is known in advance, the reaction rate constants k_1 and k_2 can be estimated directly from the scaling factors listed in the first two columns of the **C** matrix if the time shift is known.

Note, that the GEP not always gives satisfactory results, because it can produce complex results. The third column of **A** and **C** are known beforehand.

However, this knowledge cannot be implemented at first sight. However, if a column with constants is added to **X** as mentioned earlier, the third column of **A** and **C** are forced to be constant. In case of data with a moderate signal to noise ratio, the third column of the two matrices is often not constant. That problem is solved by adding a column with constants to **X**, where the order of magnitude of the constant is large compared to the signal present in **X**. Using this approach, the columns are forced to be constant. Comparing the results of GEP with the third column of **A** and **C** gives a check on the quality of the results obtained.

The procedure described is a modification of the generalized rank annihilation method (GRAM). In this thesis, the modified GRAM procedure is just called GRAM. Windig and Antalek used this new GRAM procedure for obtaining parameters from NMR signals.[9,10] They called the new procedure the direct exponential curve resolution algorithm (DECRA). GRAM is a non-iterative algorithm and hence no starting values are needed for the reaction rate constants. The time necessary to obtain the reaction rate constants is known in advance. These properties make GRAM suitable for cases where fast estimates of parameters are desired.

Consider that three slabs are created from $\mathbf{X}^*$ resulting in the three-way array $\underline{\mathbf{X}}^*$ ((M-(G×2))×(N+1)×3). It is not possible to estimate reaction rate constants using GRAM. In this case, the trilinear decomposition (TLD) algorithm which is well described in the literature by Booksh *et al.*,[11] has to be used. Here, a short description is given.

1) The three-way array $\underline{\mathbf{X}}^*$ ((M-(G×3))×(N+1)×3) is decomposed into three loading matrices **A**, **B** and **C**. The matrices **A** and **B** are both obtained by solving a GEP and **C** is obtained by means of a three-way least squares fit (PARAFAC fit) from $\underline{\mathbf{X}}^*$, **A** and **B**. A common space of $\mathbf{X}^*_1 + \mathbf{X}^*_3$ is used for solving the GEP.

2) Estimate the reaction rate constants from the scaling factors listed in **C**.

3) Average the estimates for k_1 and k_2. This yields a mean estimated k_1 and k_2.

Also in case of TLD the time needed to obtain the reaction rate constants is known in advance and because of the non-iterative nature of the algorithm no starting values are required for the kinetic parameters.

3.5 Iterative three-way methods

Loading matrices **A** and **C** contain information about the reaction rate constants of interest. Loading matrix **B** contains linear combinations of pure spectra of the reacting absorbing species. In case of spectroscopic data with a poor signal to noise ratio rough estimates of reaction rate constants can be obtained using GRAM or TLD. However, the results from GRAM or TLD, which are both no least squares methods, can be used as an excellent set of starting values of the kinetic parameters for the iterative three-way algorithms generalized rank annihilation method-Levenberg-Marquardt-parallel factor analysis (GRAM-LM-PAR) and trilinear decomposition-Levenberg-Marquardt-parallel factor analysis (TLD-LM-PAR), respectively. In these three-way algorithms the concentration profiles stored in loading matrix **A** and the reaction rate constants listed in loading matrix **C** are both updated using the Levenberg-Marquardt algorithm. The linear combinations of spectra from loading matrix **B** are updated using an alternating least squares step of the PARAFAC model. The different steps of GRAM-LM-PAR and TLD-LM-PAR are described in detail in this Section. The steps of GRAM-LM-PAR are described first.

The first two steps of GRAM-LM-PAR are equal to GRAM. Let the three matrices **A**, **B** and **C** obtained from the first step of GRAM described in Section 3.4 be equal to $\mathbf{A}^{(0)}$, $\mathbf{B}^{(0)}$ and $\mathbf{C}^{(0)}$, respectively. The superscript zero indicates, that no iterations have occurred yet. Let the estimated k_1 and k_2 obtained by the second step of GRAM be start-k_1 and start-k_2, respectively. The LM-PAR part of GRAM-LM-PAR is an alternating least squares algorithm. In every iteration the sum of squares is reduced. This process is repeated until convergence is obtained. The LM-PAR part of GRAM-LM-PAR works as follows.

1) The $\mathbf{C}^{(0)}$ matrix from the first step of GRAM has the following form:

$\mathbf{C}^{(0)} = \begin{pmatrix} u & v & 1 \\ x & y & 1 \end{pmatrix}$. Define $\tilde{\mathbf{C}}^{(0)}$ according to Equation (34).

$$\tilde{\mathbf{C}}^{(0)} = \begin{pmatrix} 1 & 1 & 1 \\ d_1 & d_2 & 1 \end{pmatrix} \qquad (34)$$

where $d_1 = x/u$ and $d_2 = y/v$. Because the $\mathbf{C}^{(0)}$ matrix has been transformed into $\tilde{\mathbf{C}}^{(0)}$, a transformed matrix $\tilde{\mathbf{B}}^{(0)}$ has to be constructed too. This is done by a three-way least squares fit (PARAFAC fit) from the three-way array $\underline{\mathbf{X}}^{*}$, $\tilde{\mathbf{C}}^{(0)}$ and $\tilde{\mathbf{A}}^{(0)}$, where $\tilde{\mathbf{A}}^{(0)}$

is a matrix with the reconstructed exponentially decaying functions using start-k_1 and start-k_2 for k_1 and k_2, respectively, according to Equation (35).

$$\tilde{\mathbf{A}}^{(0)} = [\tilde{\tilde{\mathbf{A}}}^{(0)}, \mathbf{a}_3^{(0)}] = [\tilde{\tilde{\mathbf{a}}}_1^{(0)}, \tilde{\tilde{\mathbf{a}}}_2^{(0)}, \mathbf{a}_3^{(0)}] \tag{35}$$

where the matrix with a double tilde consist of the first two columns of the considered matrix, $\tilde{\tilde{\mathbf{a}}}_1^{(0)} = e^{-k_1\mathbf{t}}$ and $\tilde{\tilde{\mathbf{a}}}_2^{(0)} = e^{-k_2\mathbf{t}}$. The vector $(e^{-k_1 t_1} ... e^{-k_1 t_{(M-S)}})^{\mathrm{T}}$ is reduced to the shorthand notation $e^{-k_1\mathbf{t}}$ and $\mathbf{t} = (t_1 ... t_{(M-S)})^{\mathrm{T}}$. The first two columns of $\tilde{\mathbf{A}}^{(0)}$, $\tilde{\tilde{\mathbf{A}}}^{(0)}$, are a function of d_1 and d_2, respectively and, hence, these are a function of k_1, k_2 and S. The third column of $\tilde{\mathbf{A}}^{(0)}$, $\mathbf{a}_3^{(0)}$, is constant. This column is fixed during the GRAM-LM-PAR algorithm.

2) Matricize $\underline{\mathbf{X}}^*$ into $\tilde{\mathbf{X}}^*$ ($(M\text{-}S)\times(2N+2)$). In chemometrics matricizing is often denoted as "unfolding". However, in psychometrics this has another meaning.[12] Subtract the contribution of the columns of constants from $\tilde{\mathbf{X}}^*$ resulting in $\dot{\mathbf{X}}^*$ ($(M\text{-}S)\times(2N+2)$).

$$\dot{\mathbf{X}}^{*(0)} = \tilde{\mathbf{X}}^* - \mathbf{a}_3^{(0)}(\mathbf{c}_3^{(0)} \otimes \tilde{\mathbf{b}}_3^{(0)})^{\mathrm{T}} \tag{36}$$

where $\otimes$ denotes the Kronecker product[12] and $\mathbf{c}_3$ is the third column of $\tilde{\mathbf{C}}^{(0)}$ equal to $(1\ 1)^{\mathrm{T}}$.

3) Next, matrices are partitioned:

$$\tilde{\mathbf{B}}^{(0)} = [\tilde{\tilde{\mathbf{B}}}^{(0)}, \tilde{\mathbf{b}}_3^{(0)}] \tag{37}$$

$$\tilde{\mathbf{C}}^{(0)} = [\tilde{\tilde{\mathbf{C}}}^{(0)}, \begin{pmatrix} 1 \\ 1 \end{pmatrix}] \tag{38}$$

where the matrices with a double tilde consist of the first two columns of the considered matrix.

4) Equation (39) is minimized for fixed $\tilde{\tilde{\mathbf{B}}}^{(0)}$ over k_1 and k_2 ensuring that for the proper k_1 and k_2 this minimum will be attained.

$$\min_{\hat{k}_1,\hat{k}_2} \left\| \dot{\mathbf{X}}^{*(0)} - \tilde{\tilde{\mathbf{A}}}^{(0)} (\tilde{\tilde{\mathbf{C}}}^{(0)} \odot \tilde{\tilde{\mathbf{B}}}^{(0)})^{\mathrm{T}} \right\|^2 \tag{39}$$

where $\odot$ denotes the column-wise Kronecker product also known as the Khatri-Rao product.[12]

Update $\tilde{\tilde{\mathbf{A}}}^{(0)}$ and $\tilde{\tilde{\mathbf{C}}}^{(0)}$ simultaneously using the optimal values for k_1 and k_2 according to the Levenberg-Marquardt algorithm.

5) Update $\tilde{\mathbf{B}}^{(0)}$ (all three columns!) using a least-squares PARAFAC step.

6) Calculate the loss function according to Equation (40).

$$f^{(i)} = SSQ(\dot{\mathbf{X}}^{*(i)} - \tilde{\tilde{\mathbf{A}}}^{(i)} (\tilde{\tilde{\mathbf{C}}}^{(i)} \odot \tilde{\tilde{\mathbf{B}}}^{(i)})^{\mathrm{T}}) \tag{40}$$

where SSQ is the sum of squares. If Equation (41) holds the iterations are stopped.

$$\frac{f^{(i-1)} - f^{(i)}}{f^{(i)}} < 10^{-6} \tag{41}$$

The TLD-LM-PAR algorithm is exactly the same algorithm as GRAM-LM-PAR except that in TLD-LM-PAR the TLD results are used as an initial set of starting values for k_1 and k_2 instead of the GRAM results for the reaction rate constants. Only the first two steps of the TLD-LM-PAR algorithm differ from those of the GRAM-LM-PAR algorithm. For TLD-LM-PAR the first two steps are given below.

1) Applying TLD gives loading matrices $\mathbf{A}^{(0)}$, $\mathbf{B}^{(0)}$, $\mathbf{C}^{(0)}$ and multiple reaction rate constant estimates. The reaction rate constant estimates are averaged resulting in $\bar{\hat{k}}_1$ and $\bar{\hat{k}}_2$.

2) Define $\tilde{\mathbf{A}}^{(0)}$, $\tilde{\mathbf{B}}^{(0)}$ and $\tilde{\mathbf{C}}^{(0)}$. The first column of $\mathbf{A}^{(0)}$ represents $e^{-k_1 \mathbf{t}}$ and the second column of $\mathbf{A}^{(0)}$ represents $e^{-k_2 \mathbf{t}}$. Hence, k_1 and k_2 can be replaced by $\bar{\hat{k}}_1$ and $\bar{\hat{k}}_2$, respectively, resulting in $\tilde{\mathbf{A}}^{(0)}$ which is a reconstruction of the concentration profiles using the averaged reaction rate constant estimates. $\tilde{\mathbf{C}}^{(0)}$ is a reconstruction of $\mathbf{C}^{(0)}$

where the last row and last column are set to a row vector and a column vector of ones, respectively, and $\bar{\hat{k}}_1$ and $\bar{\hat{k}}_2$ are used for the reconstruction of $\mathbf{C}^{(0)}$. Matrix $\tilde{\mathbf{B}}^{(0)}$ is constructed by means of a three-way least squares fit (PARAFAC fit) from $\underline{\mathbf{X}}^*$, $\tilde{\mathbf{C}}^{(0)}$ and $\tilde{\mathbf{A}}^{(0)}$.

The next steps are equal to the GRAM-LM-PAR algorithm.

3.6 The relative fit error

If reaction rate constants are estimated with GRAM, TLD, GRAM-LM-PAR or TLD-LM-PAR, the relative fit error can be estimated. This is done as follows. Matricize the three-way matrix $\underline{\mathbf{X}}^*$ resulting in $\tilde{\mathbf{X}}^*$. Estimate $\tilde{\tilde{\mathbf{X}}}^*$, $\hat{\tilde{\mathbf{X}}}^*$, according to Equation (42).

$$\hat{\tilde{\mathbf{X}}}^* = \tilde{\mathbf{A}}(\tilde{\mathbf{C}} \odot \tilde{\mathbf{B}})^{\mathrm{T}} \tag{42}$$

Delete the two columns with constants from $\tilde{\tilde{\mathbf{X}}}^*$ and $\hat{\tilde{\mathbf{X}}}^*$ to construct $\dot{\mathbf{X}}^*$ ((*M*-*S*)×2*N*) and $\dot{\hat{\mathbf{X}}}^*$ ((*M*-*S*)×2*N*), respectively. The relative fit error (RFE) can be estimated according to Equation (43).

$$\mathrm{RFE} = \sqrt{\frac{\sum_{i=1}^{I}\sum_{j=1}^{J}(\dot{\mathbf{X}}^* - \dot{\hat{\mathbf{X}}}^*)_{ij}^2}{\sum_{i=1}^{I}\sum_{j=1}^{J}(\dot{\mathbf{X}}^*)_{ij}^2}} \tag{43}$$

where $I = (M\text{-}S)$, $J = 2N$, $i = 1, 2, \ldots, I$ and $j = 1, 2, \ldots, J$. From Equation (43) it can be seen that it is necessary to delete the columns with constants from the two-way arrays, because otherwise the denominator will dominate.

3.7 Implementation of constraints

The use of constraint R, constraint RP and constraint NNLS, as discussed in Section 2.7 of Chapter 2, is only possible for the iterative three-way methods (GRAM-LM-PAR and TLD-LM-PAR). Using *a priori* known pure spectra of reacting absorbing species within three-way methods is more complicated compared to

two-way methods, because loading matrix **B** contains linear combinations of pure spectra. The use of pure spectra of reacting absorbing species as constraints in iterative three-way methods is beyond the scope of this thesis.

In case of non-iterative three-way methods (GRAM and TLD), the following soft constraint is implemented. The third column of loading matrix **C** is forced to be constant by means of adding a column with constants to matrix **X**, where the order of magnitude of the constants is large compared to the order of magnitude of the signal in **X**.

The following constraints have been used in this thesis in case of GRAM-LM-PAR and TLD-LM-PAR. The third column of loading matrix **A** and loading matrix **C** are fixed during the whole least squares part of the three-way algorithms. In case of GRAM-LM-PAR and TLD-LM-PAR the structure of **C** given in Equation (32) and Equation (33), respectively, is implemented.

3.8 References

1. Antalek B, Windig W. 'Generalized rank annihilation method applied to a single multicomponent pulsed gradient spin echo NMR data set'. *J. Am. Chem. Soc.*, 1996; **118**: 10331-10332.
2. Windig W, Antalek B. 'Direct exponential curve resolution algorithm (DECRA): A novel application of the generalized rank annihilation method for a single spectral mixture data set with exponentially decaying contribution profiles'. *Chemometrics Intell. Lab. Syst.*, 1997; **37**: 241-254.
3. Harshman RA, Lundy ME. 'PARAFAC: Parallel factor analysis'. *Computational Statistics & Data Analysis*, 1994, **18**: 39-72.
4. Smilde AK. 'Three-way analyses problems and prospects'. *Chemometrics Intell. Lab. Syst.*, 1992; **15**: 143-157.
5. Kruskal JB. in *Multiway Data Analysis*, ed. by Coppi R, Bolasco S. Elsevier: Amsterdam, 1989; 7-18.
6. Kruskal JB, Harshman RA, Lundy ME. in *Multiway Data Analysis*, ed. by Coppi R, Bolasco S. Elsevier: Amsterdam, 1989; 115-122.
7. Sanchez E, Kowalski BR. 'Generalized rank annihilation factor analysis'. *Anal. Chem.*, 1986; **58**: 496-499.
8. Wilson B, Sanchez E, Kowalski BR. 'An improved algorithm for the generalized rank annihilation method'. *J. Chemometrics*, 1989; **3**: 493-498.
9. Windig W, Hornak JP, Antalek B. 'Multivariate image analysis of magnetic resonance images with the direct exponential curve resolution algorithm (DECRA). Part 1: Algorithm and model study'. *J. Magn. Reson.*, 1998; **132**: 298-306.
10. Antalek B, Hornak JP, Windig W. 'Multivariate image analysis of magnetic resonance images with the direct exponential curve resolution algorithm (DECRA). Part 2: Application to human brain images'. *J. Magn. Reson.*, 1998; **132**: 307-315.
11. Booksh KS, Lin Z, Wang Z, Kowalski BR. 'Extension of trilinear decomposition method with an application to the flow probe sensor'. *Anal. Chem.*, 1994; **66**: 2561-2569.
12. Kiers HAL. 'Towards a standardized notation and terminology in multiway analysis'. *J. Chemometrics*, 2000; in press.

Chapter 4

Quality Assessment of Reaction Rate Constant Estimates

4.1 Introduction

If reaction rate constants are estimated from spectroscopic data of repeated batch runs, these estimates have a certain accuracy. The accuracy of reaction rate constant estimates is influenced by model errors, experimental errors and instrumental noise which are always present. Examples of experimental errors are: initial concentration errors of reactants at the start of the reaction and temperature fluctuations during the reaction. Instrumental noise is caused by variations of the instrument. If, for example, a suitable kinetic model for the data is used and the Beer-Lambert law is valid, model errors can be kept very small compared to experimental errors and instrumental noise.

Assume a batch process with reaction rate constant k_1. Suppose that model errors are negligible compared to the experimental errors and instrumental noise present. For each individual batch process run the reaction rate constant, k_1, can be estimated. A standard deviation can be obtained, from the k_1 estimates of n repeated individual batch process runs, which represents the upper error bound.

A lower level of standard deviation, the lower error bound, represents the influence of mainly instrumental noise on the k_1 estimates. It can be estimated using a jackknife based resampling method described in Section 4.3.[1,2]

4.2 Accuracy of reaction rate constant estimates

The accuracy of a parameter can be divided into the precision and the bias of the parameter according to equation (44).

$$E(\hat{k} - k_{true})^2 = E(\hat{k} - E(\hat{k}))^2 + (E(\hat{k}) - k_{true})^2 \qquad (44)$$

Accuracy **Precision** **Bias**

where E indicates the expectation operator. The accuracy, bias and precision of a parameter can be estimated by applying Equation (45), (46) and (47), respectively.

$$\text{Accuracy} = \frac{1}{N}\sum_{n=1}^{N}(\hat{k}_n - k_{true})^2 \quad (45)$$

$$\text{Bias} = (\bar{\hat{k}} - k_{true})^2 \quad (46)$$

$$\text{Precision} = \frac{1}{N-1}\sum_{n=1}^{N}(\hat{k}_n - \bar{\hat{k}})^2 \quad (47)$$

where

$$\bar{\hat{k}} = \frac{1}{N}\sum_{n=1}^{N}\hat{k}_n \text{ , } n = 1, 2, 3, \ldots, N. \quad (48)$$

A good accuracy and precision is associated with a small value of Equation (45) and Equation (47), respectively, whereas a poor accuracy and precision is associated with a large value of Equation (45) and Equation (47), respectively. In this thesis, relative errors are reported according to Equation (49).

$$\text{Relative error} = \frac{\sqrt{\text{accuracy}}}{\text{true value}} * 100\% \quad (49)$$

In practice, the accuracy of estimates cannot be obtained, because the true values for the reaction rate constants are unknown.

4.3 A jackknife based method

Assume 21 spectra are measured in time of a certain chemical process which results in two-way data and a jackknife interval of four spectra. First, spectra number 1, 5, 9, 13 and 17 are left out and the remaining spectra are used to estimate the rate constants. Secondly, spectra number 1, 5, 9, 13 and 17 are left in and spectra number 2, 6, 10, 14 and 18 are left out and the remaining spectra are used again to estimate the rate constants. This will lead to a certain number of rate constant estimates. The standard deviation obtained represents the lower error bound of mainly instrumental noise. In case of three-way data spectra are left out from $\underline{\mathbf{X}}$ according to the same procedure as described. In this thesis, the jackknife based procedure described has been applied to the mean batch process run obtained by averaging the individual batch process runs.

4.4 References

1. Shao J, Tu D. *The Jackknife and Bootstrap*, Springer: New York, 1995.
2. Efron B, Tibshirani R.J. *An Introduction to the Bootstrap*, Chapman & Hall: New York, 1993.

Chapter 5

Description of Datasets and Experimental Set-Up

5.1 Introduction

In this Chapter, four different experimental datasets used in this thesis are described. A short summary of the datasets can be found in the Appendix. Dataset 1 contains short-wavelength near-infrared (SW-NIR)[1,2] measurements of a two-step epoxidation performed under pseudo-first order conditions. Dataset 2 contains ultraviolet-visible (UV-Vis)[1,2] measurements of a two-step biochemical reaction also performed under pseudo-first order conditions at a certain pH. At a different pH the same reaction has been monitored using UV-Vis spectroscopy performed under pseudo-first order conditions and second order conditions, resulting in dataset 3 and dataset 4, respectively.

For dataset 2, 3 and 4, pure spectra of some of the reacting absorbing species involved in the reaction have been measured. This is described in this Chapter together with the experimental set-up, dataprocessing and the repeatability of experiments.

5.2 A two-step epoxidation reaction

5.2.1 Description of the reaction

The two-step consecutive epoxidation of 2,5-di-*tert*-butyl-1,4-benzoquinone using *tert*-butyl hydroperoxide and Triton B catalyst[3,4] was monitored in time using SW-NIR spectroscopy. The reaction consists of the following two steps:[i]

$$U + V \xrightarrow{k_a} W + Z$$
$$W + V \xrightarrow{k_b} Y + Z$$

[i] In this thesis, reaction rate constants with Arabic subscript are second order reaction rate constants and reaction rate constants with numerical subscript are (pseudo-) first order reaction rate constants.

with second order reaction rate constants k_a and k_b both in $M^{-1}min^{-1}$. Species *U*, *V*, *W*, *Y* and *Z* are specified in Table 1.

Table 1. The species involved in the SW-NIR dataset.

Species	
U	2,5-di-*tert*-butyl-1,4-benzoquinone
V	*tert*-butyl hydroperoxide
W	2,5-di-*tert*-butyl mono-epoxide-1,4-benzoquinone
Y	cis and trans 2,5-di-*tert*-butyl di-epoxide-1,4-benzoquinone
Z	*tert*-butyl alcohol

No distinction was made between the cis and trans product (species *Y*) of the second step of the reaction, because the spectral differences are negligible in SW-NIR.[4]

The first and second reaction step are both second order reactions. However, if species *V* is present in large excess, the first and second reaction step become both pseudo-first order reactions with pseudo-first order reaction rate constants k_1 (min^{-1}) and k_2 (min^{-1}), respectively. Hence, Equation (6)-(8), defined in Section 2.2 of Chapter 2, can be used in order to describe the concentration profiles of the reactant (species *U*), intermediate (species *W*) and main-product (species *Y*) of the reaction, respectively.

5.2.2 Sample preparation

A cuvette was filled with 0.264 g (1.2 mmol) of 2,5-di-*tert*-butyl-1,4-benzoquinone, as synthesized by the procedure described by Hairfield *et al*.[3] A melting point of 152-153°C was obtained for 2,5-di-*tert*-butyl-1,4-benzoquinone. The reported melting point is 152.5°C.[5] Next, 2,5-di-*tert*-butyl-1,4-benzoquinone was dissolved in 15 ml dioxane (Acros 99$^+$%) and 1.55 ml (12 mmol) of a *tert*-butylhydroperoxide 70% (Acros) solution in water and 13.21 ml ethanol (BDH Laboratory Supplies, pro analysis) were both added. After the target reaction temperature had been reached, data collection was started immediately after addition of 0.24 ml ice-cold Triton B catalyst (Acros, 40 wt. % in methanol) in 0.50 ml ethanol and 0.60 ml dioxane. The excess of *tert*-butylhydroperoxide in moles was ten times 2,5-di-*tert*-butyl-1,4-benzoquinone. At this excess, pseudo-first order kinetics may be assumed.

5.2.3 Experimental set-up

The experimental set-up is shown in Figure 11. To measure SW-NIR spectra, a Hewlett Packard 8453 UV-Vis spectrophotometer with diode array detection was used. A quartz cuvette with 10.00 cm pathlength (Hellma Benelux) was used to obtain spectra of the reaction mixture. On both sides of the cuvette, a small unit of glass was glued to be able to thermostate the cuvette. The cuvette contained two stirring modules. Water was pumped from a constant temperature bath (Neslab) through the cooling units of the cuvette. A Pt-100, which is a thermocouple, connected to the constant temperature bath was used inside the cuvette to control the temperature. To obtain a temperature below room temperature an immersion cooler (Haake) was used to cool the water of the constant temperature bath.

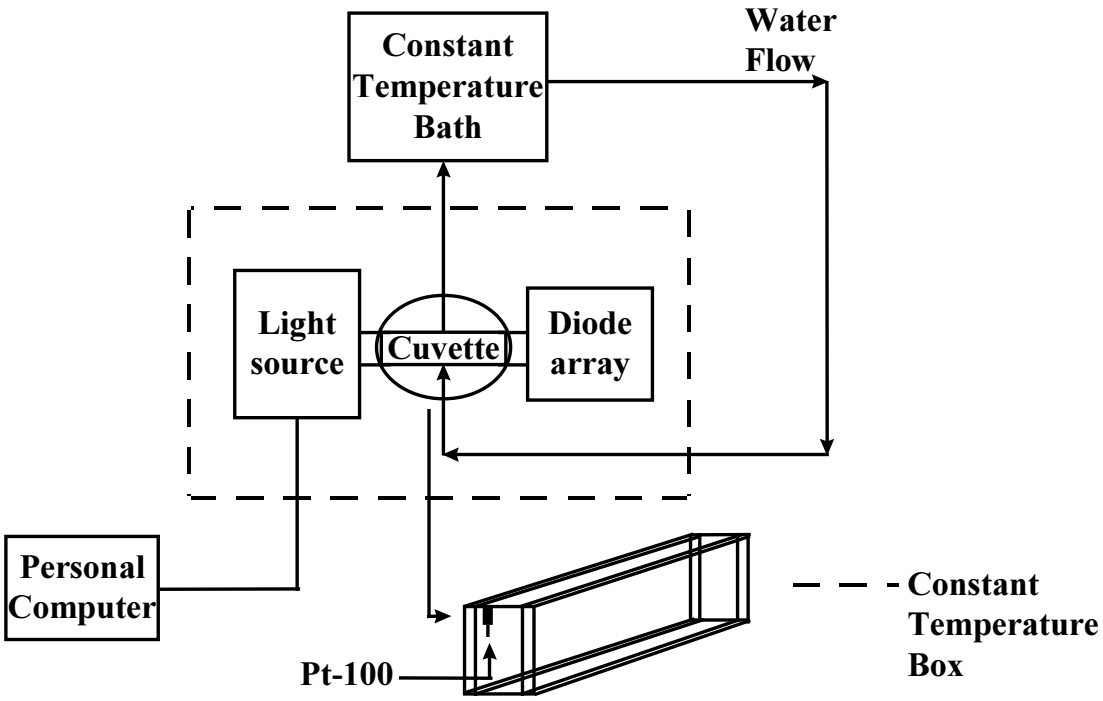

Figure 11. The experimental set-up.

The cuvette was placed in a special constructed cell holder. The spectrophotometer and the cuvette were placed in a home-made air thermostated box, to avoid the influence of temperature fluctuations of the surroundings. The box temperature was controlled by a constant temperature bath (Haake). A Hewlett Packard Vectra XM2 Chemstation (IntelDX4-100 MHz with 16 MB RAM and a 800 MB harddisk) using the Hewlett Packard software was used to collect and store the data. The experimental conditions are listed in Table 2. Eight individual batch process runs were performed at identical conditions which are labeled dataset 1 in this thesis.

Table 2. Experimental conditions.

Reaction Temperature	17 °C
Integration Time	1 s
Sampling Time	5 s
Total Run Time	1200 s
Wavelength Range	800-1100 nm
Wavelength interval	1.0 nm
Number of Measured Spectra	241

5.2.4 Dataprocessing

In order to remove offset and drift, second-derivative spectra were estimated using a Savitzky-Golay filter[6] using a window size of 15 wavelengths. To stress the spectral features of the appearing and disappearing species, second derivative difference spectra were calculated after subtracting the fourth measured spectrum from all the other spectra remaining. The first three measured spectra were not used for dataprocessing because of the moderate reproducibility of these spectra. The small wavelength range 860-880 nm was used for dataprocessing. If this wavelength range is used the spectral features are only caused by the three species which were monitored (species *U*, *W* and *Y*).[4] The second-derivative difference spectra of one individual batch process run are shown in Figure 12. The first and last measured spectra are indicated. From Figure 12 it is obvious that a moderate signal to noise ratio is present.

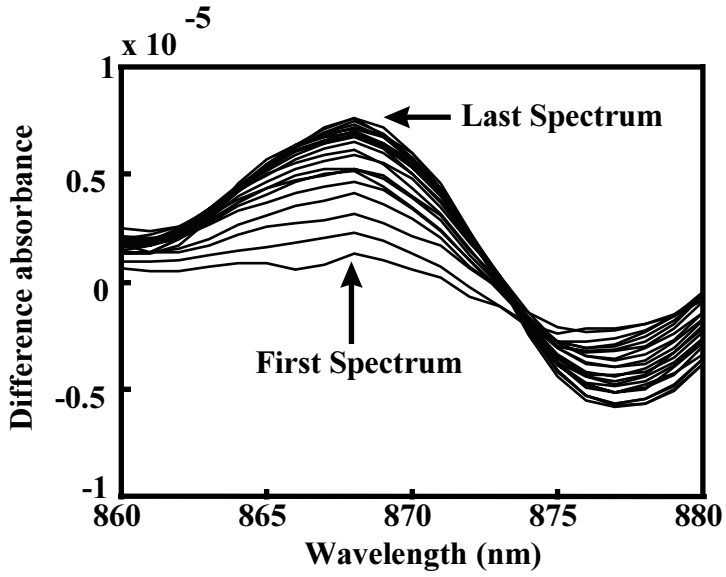

Figure 12. The second derivative difference spectra of one individual batch process run.

In case of using the WCR algorithm, described in Section 2.6 of Chapter 2, the datamatrix with measured spectra of the reacting system was truncated into three singular values. For the two-way methods starting values of 0.30 min^{-1} and 0.05 min^{-1} were used for k_1 and k_2, respectively, based on the estimates of these reaction rate constants obtained by others.[3,4]

Data processing was performed in the Matlab environment (Version 5.2, The Mathworks Inc.) on a Pentium 133 MHz Computer with 64 MB RAM and a 1.2 GB harddisk.

5.2.5 The repeatability of experiments

The repeatability, R_{batch}, for I batch process runs was calculated using Equation (50).[7]

$$R_{batch} = \frac{\sqrt{\frac{1}{I}\sum_{i=1}^{I}\left\|\mathbf{X}_i - \overline{\mathbf{X}}\right\|^2}}{\left\|\overline{\mathbf{X}}\right\|} * 100\% \qquad (50)$$

where $\mathbf{X}_i$ is the spectral matrix for experiment i and $\overline{\mathbf{X}}$ is the averaged spectral matrix obtained from the I individual experiments.

The repeatability was equal to 23.28% for dataset 1. This poor repeatability is mainly a consequence of the small differences in absorbances of the species and the error propagation due to taking the second derivative.

5.3 A two-step biochemical reaction

5.3.1 Description of the reaction

The two-step consecutive reaction of 3-chlorophenylhydrazonopropane dinitrile with 2-mercaptoethanol[8,9] was monitored using UV-Vis spectroscopy. The reaction consists of the following two steps:

$$U + V \xrightarrow{k_a} W$$
$$W \xrightarrow{k_2} Y + Z$$

with second order reaction rate constant k_a ($M^{-1}min^{-1}$) and first order reaction rate constant k_2 (min^{-1}). Species U, V, W, Y and Z are specified in Table 3.

If species V is present in large excess the first step of the reaction becomes pseudo-first order with pseudo-first order reaction rate constant k_1 (min^{-1}). Hence, Equation (6)-(8), from Section 2.2 of Chapter 2, can be used in order to describe the

concentration profiles of *U*, *W* and *Y*, respectively. A detailed reaction mechanism of the reaction described is given in Figure 13.

Table 3. The species involved in the UV-Vis dataset.

Species	
U	3-chlorophenylhydrazono-propane dinitrile
V	2-mercaptoethanol
W	intermediate adduct
Y	3-chlorophenylhydrazono-cyanoacetamide
Z	ethylenesulphide

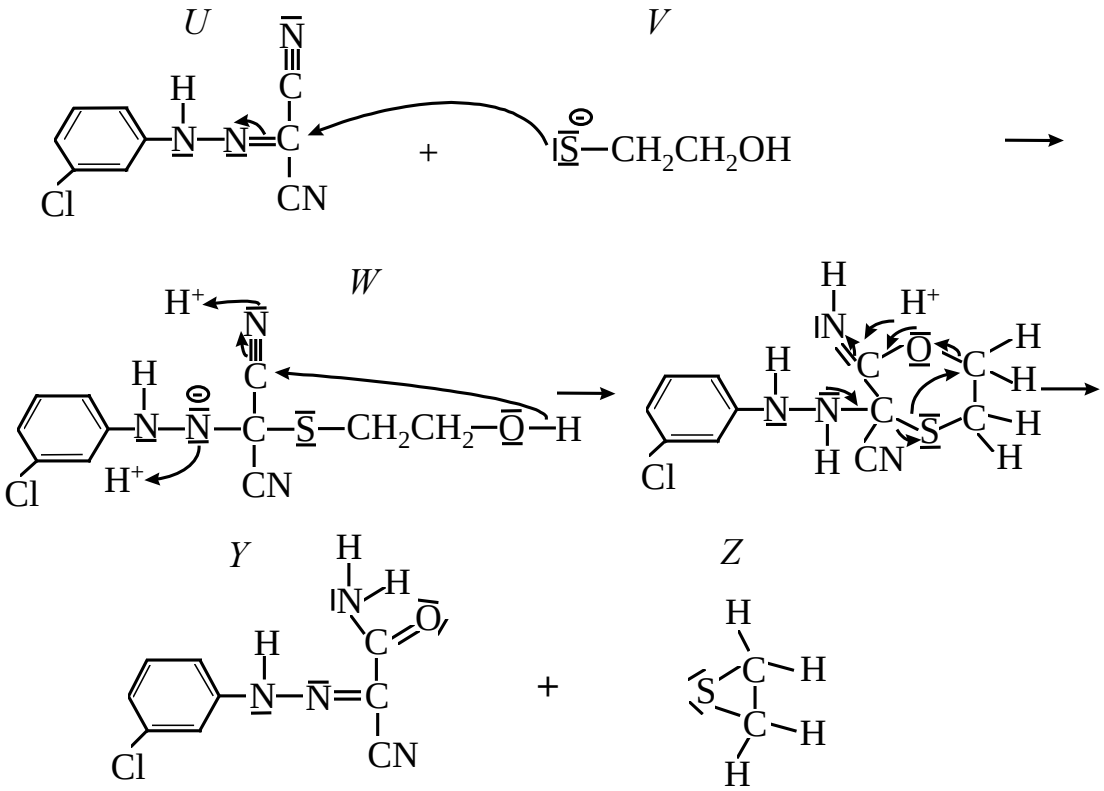

Figure 13. The reaction mechanism.

5.3.2 Sample preparation

All chemicals were used as received without further purification. An amount of 0.0529 g (0.2585 mmol) of species *U* (Acros, 99^{+}%) was dissolved in water using a minimum volume of 0.1 moll^{-1} NaOH (Baker Chemicals, 98.8%) to give a stock solution of 1.034 mmoll^{-1}. This stock solution was diluted into a working solution containing 51.71 µmoll^{-1} of species *U*, buffered with KH_2PO_4 (Acros, pro analysis 0.2 moll^{-1}, pH 4.4). The pH of the working solution was equal to 5.4. This working solution had to be prepared freshly every day. At this pH, species *U* was

supersaturated and slowly crystallized from the solution after a couple of days. This was not observed by Bisby and Chau.[8,9] The cuvette was filled with 2.5 ml of the working solution. When the temperature inside the cuvette had reached the target temperature, data collection was started upon addition of 10 µl of a *V*-solution, which contained 35.65 µmol of species *V*, by means of a pipette. This *V*-solution consisted of 250 µl pure *V* (Acros, 99%) and 750 µl KH_2PO_4 buffer solution. However, if pure species *V* is added it will take some time to mix with the reaction mixture. This mixing time can be reduced if species *V* is already in the same buffer solution as the buffer solution used to create the reaction mixture. The excess of species *V* in moles was 276 times species *U*.

The reaction described was also performed using an other pH of the working solution. At a pH of 5.2 of this solution, experiments were performed where the excess of species *V* in moles was 265 times species *U*. The reaction was also investigated under second order conditions for three specific ratio's of initial concentration of both reactants (species *U* and species *V*). The ratio's $C_{U,0}$:$C_{V,0}$ were chosen equal to 1:4, 1:5 and 1:6. The pH of the working solution in case of second order kinetic experiments was also equal to 5.2.

5.3.3 Experimental set-up

The experimental set-up used, was equal to the experimental set-up described in Section 5.2.3 of this Chapter. However, in this case a quartz cuvette with 1.00 cm pathlength was used to obtain spectra of the reaction mixture. The experimental conditions are given in Table 4 for pseudo-first order experiments.

For second-order experiments, the experimental conditions were equal to those listed in Table 4 apart from the sampling time and total run time, which were equal to 20s and 5400s, respectively.

In case of a pH of the working solution equal to 5.4, ten experiments were performed at identical pseudo-first order conditions which are labeled dataset 2 in this thesis. For a pH of 5.2 the pseudo-first order experiment was repeated 32 times which is labeled dataset 3 in this thesis. At the same pH, the second order experiment was repeated six times for three specific ratio's of initial concentrations of both reactants. Hence, in total 18 second order experiments were performed which are labeled dataset 4 in this thesis. The spectra of one individual batch process run are shown in Figure 14 for pseudo-first order conditions and second order conditions using a pH of the working solution of 5.2 in both cases. The spectra obtained under pseudo-first order conditions are similar for a pH of 5.4 and a pH of 5.2. From Figure 14 it is

Table 4. The experimental conditions.

Reaction Temperature	25 °C
Integration Time	1 s
Sampling Time	10 s
Total Run Time	2700 s
Wavelength Range	200-600 nm
Wavelength interval	1.0 nm
Number of Measured Spectra	271

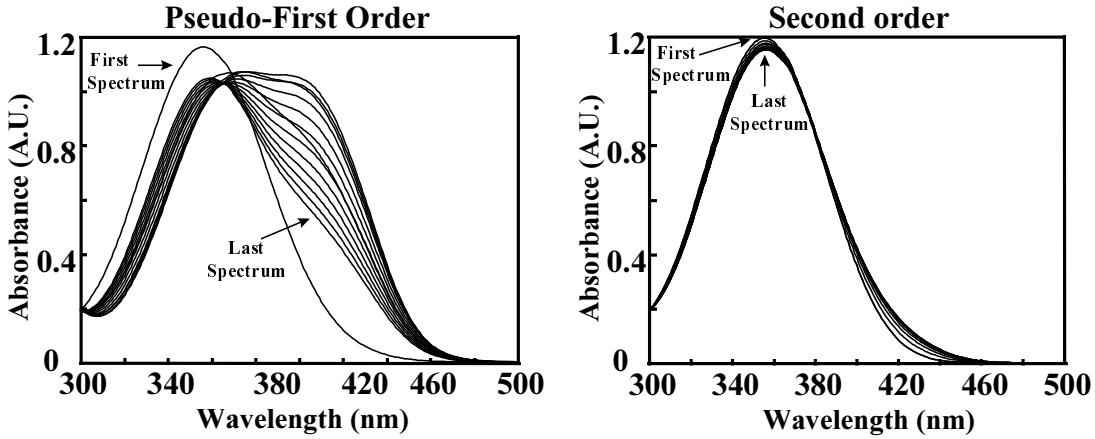

Figure 14. The spectra of one individual batch process run performed under pseudo-first order and second order conditions.

obvious that in case of second order conditions, very small absorbances differences are obtained in time compared to the absorbance differences for pseudo-first order conditions. A reason for this, is that if second order conditions are chosen the first reaction step is very slow, which results in these small absorbance differences in time. Because of the slow first reaction step, the intermediate formed reacts fast into the product.

5.3.4 Pure spectra

In order to obtain the pure spectrum of the reactant, species *V* was not added and 21 spectra were taken of the reactant for the wavelength range 300-500 nm. The averaged spectrum is an estimate of the pure individual spectrum of species *U*. In case of dataset 3 and dataset 4, 21 spectra of the reactant were measured and averaged for every individual batch process run. Hence, every individual batch process run is connected with an averaged pure spectrum of the reactant.

The pure spectrum of the product was obtained by taking 21 spectra of the reaction mixture after a reaction time of eight hours. This procedure was repeated two

times and every set of 21 spectra was averaged. Hence, two averaged pure spectra of the product are available. After eight hours, it is assumed that no species *U* and species *W* are left in the reaction mixture and hence there is approximately 100% conversion. Only species *V*, species *Y* and species *Z* are present. However, species *V* and species *Z* both have no absorbances in the wavelength range considered. Therefore, it can be assumed that the averaged measured spectrum of the reaction mixture represents the pure spectrum of product species *Y*. From the reaction rate constant estimates reported in Chapter 6, 7, 8 and 9 of this thesis, it is reasonable to assume that no reactant and intermediate are left after eight hours. The averaged measured pure spectrum of reactant and product are both shown in Figure 15. From this figure it is observed that the spectral overlap between both pure spectra shown is very large.

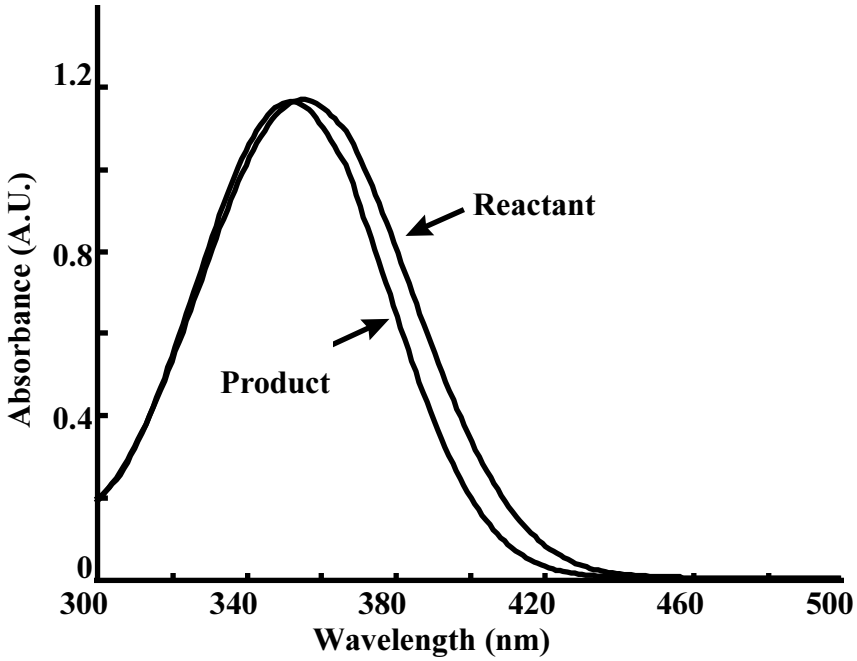

Figure 15. The measured pure spectrum of reactant and product.

5.3.5 Dataprocessing

A spectrum of KH_2PO_4 buffer solution was used as blank. The wavelength range 300-500 nm was used for dataprocessing. Using this spectral range there are only spectral features caused by species *U*, *W* and *Y*. At $\lambda < 300$ nm species *V* absorbs and by-product *E* shows an increasing absorbance. At $\lambda > 500$ nm there is no significant contribution of the reacting species to the absorbance. The first measured spectrum was not used for dataprocessing because of the moderate reproducibility of this spectrum. In case of using two-way methods for estimating reaction rate constants,

starting values of 0.30 min^{-1} and 0.05 min^{-1} were used for k_1 and k_2, respectively, based on the estimates obtained by others.[8,9]

Data processing was performed in the Matlab environment (Version 5.2, The Mathworks Inc.) on a Pentium 133 MHz Computer with 64 MB RAM and a 1.2 GB harddisk.

5.3.6 The repeatability of experiments

The repeatability was calculated for the UV-Vis datasets using Equation (50) from Section 5.2.5 of this Chapter. The repeatability was equal to 0.54% and 1.60% for dataset 2 and dataset 3, respectively. For dataset 4, three repeatability numbers were calculated, because there were three different ratio's of initial concentrations of the reactants involved. For a ratio of 1:4, 1:5 en 1:6 the repeatability was equal to 1.28%, 2.15% and 1.15%, respectively. Hence, it can be concluded that dataset 3 and dataset 4 have a similar repeatability. The repeatability of dataset 2 is excellent for spectroscopic measurements.

5.4 References

1. Workman JJ Jr. 'Interpretive spectroscopy for near infrared'. *Appl. Spectrosc. Rev.*, 1996; **31**: 251-320.
2. Burns DA, Ciurczak EW. *Handbook of Near-Infrared Analysis*, Dekker: New York, 1992.
3. Hairfield EM, Moomaw EW, Tamburri RA, Vigil RA. 'The epoxidation of 2,5-di-tert-butyl-1,4-benzoquinone'. *J. Chemical Education*, 1985; **62**: 175-177.
4. Mayes DM, Kelly JJ, Callis JB. 'Non-invasive monitoring of a two-step sequential chemical reaction with shortwave near-infrared spectroscopy', in *Near Infra-Red Spectroscopy: Bridging the Gap between Data Analysis and NIR Applications*, ed. by Hildrum KI, Isaksson T, Naes T, Tandberg A. Ellis Horwood: Chichester, 1992; 377-387.
5. Weast RC. *Handbook of Chemistry and Physics*, 1st Student Edition, Press CRC: Florida, 1988.
6. Savitzky A, Golay MJE. 'Smoothing and differentiation of data by simplified least squares procedures'. *Anal. Chem.*, 1964; **36**: 1627-1639.
7. Smilde AK, Tauler R, Henshaw JM, Burgess LW, Kowalski BR. 'Multicomponent Determination of Chlorinated Hydrocarbons Using a Reaction-Based Chemical Sensor. 3. Medium-Rank Second-Order Calibration with Restricted Tucker Models'. *Anal. Chem.*, 1994; **66**: 3345-3351.
8. Bisby RH, Thomas EW. 'Kinetic analysis by the method of nonlinear least squares'. *J. Chemical Education*, 1986; **63**: 990-992.
9. Chau F-T, Mok K-W. 'Multiwavelength analysis for a first-order consecutive reaction'. *Computers Chem.*, 1992; **16**: 239-242.

Chapter 6

Applications of Two-Way Methods

6.1 Introduction

In this Chapter,[i] the results of the two-way methods traditional curve fitting (TCF) combined with fixed size window evolving factor analysis (FSWEFA), classical curve resolution (CCR), weighted curve resolution (WCR) and curve resolution (CR), applied to the four datasets described in Chapter 5, are presented. A short summary of the four datasets is given in the Appendix. The theory of the two-way methods used has already been described in Chapter 2 of this thesis. Note, that CR is the same algorithm as WCR without weighting certain matrices during the optimization procedure (see Section 2.6, Chapter 2). The starting values of the reaction rate constants used for the two-way methods have been reported in Section 5.2.4 and Section 5.3.5 of Chapter 5. If other sets of starting values were used, similar results were obtained.

6.2 SW-NIR data

6.2.1 Introduction

CR and WCR, which are described in Section 2.6 of Chapter 2, are applied to estimate reaction rate constants from dataset 1. Dataset 1 contains SW-NIR measurements in time of a two-step consecutive epoxidation reaction as described in Section 5.2 of Chapter 5. Some simulations with synthetic spectra from a simple two-step process

[i] This Chapter is based on the following papers:

- Bijlsma S, Louwerse DJ, Smilde AK. 'Rapid estimation of rate constants of batch processes using on-line SW-NIR'. *AIChE J.*, 1998; **44**: 2713-2723.
- Bijlsma S, Smilde AK. 'Application of curve resolution based methods to kinetic data'. *Anal. Chim. Acta*, 1999; **396**: 231-240.
- Bijlsma S, Boelens HFM, Smilde AK. 'Rapid determination of rate constants in second order kinetics'. submitted.
- Bijlsma S, Boelens HFM, Hoefsloot HCJ, Smilde AK. 'Estimating reaction rate constants: comparison between traditional curve fitting and curve resolution'. submitted.

are used to show that the methods can be applied to estimate unknown reaction rate constants in cases where the pure spectra of the reacting absorbing species involved are extremely overlapped. For the reaction rate constant estimates obtained from dataset 1, upper and lower error bounds are estimated in order to perform quality assessment as described in Section 4.3 of Chapter 4. For the simulated data and dataset 1, the performance of CR and WCR are compared.

6.2.2 Simulation set-up

For the simulations, the two-step consecutive reaction valid for dataset 1 was considered. Concentration profiles (matrix **F**) were simulated for 21 time points for species *U*, *W* and *Y* corresponding to a k_1 value of 0.30 min^{-1}, a k_2 value of 0.05 min^{-1} and an initial concentration of species *U* of 1 $moll^{-1}$. The time range was chosen from 0 min to 20 min with increments of 1 min. Pure SW-NIR spectra (matrix **D**) were simulated for the three individual reacting absorbing species for the wavelength range 850-1050 nm with increments of 1 nm using Gaussian peaks with a peak sigma of 15 nm. The maximum of the pure spectra of species *U*, *W* and *Y* corresponded to different wavelengths to control the amount of spectral overlap of the individual spectra of these three species. The simulated spectra for datamatrix **X** were calculated according to Equation (1) of Section 2.2, Chapter 2. Normally distributed white noise was added to datamatrix **X**. The sigma of the white noise added was defined as a certain percentage of the maximum absorbance of the simulated SW-NIR spectrum at time 0.

The amount of spectral overlap presented in the pure SW-NIR spectra of the different reacting absorbing species involved was varied by moving the individual spectrum of species *U* and *Y* along the wavelength axis. The pure spectra of the individual reacting absorbing species with a small and a strong spectral overlap are shown in Figure 16. A small spectral overlap corresponded to an absorbance maximum of the pure spectra at 900 nm, 950 nm and 1000 nm for species *U*, *W* and *Y*, respectively (solid line). A strong overlap corresponded to a maximum of the pure spectra at 930 nm, 950 nm and 970 nm for the species *U*, *W* and *Y*, respectively (dotted line). One hundred sets of SW-NIR spectra were simulated according to two different noise levels (1% and 4%). For data reduction using the SVD, three singular values were chosen, because three species were involved in the simulated SW-NIR spectra. For every noise level 100 k_1 and k_2 values were estimated. The starting values for k_1 and k_2 were always equal to 0.20 min^{-1} and 0.04 min^{-1}, respectively.

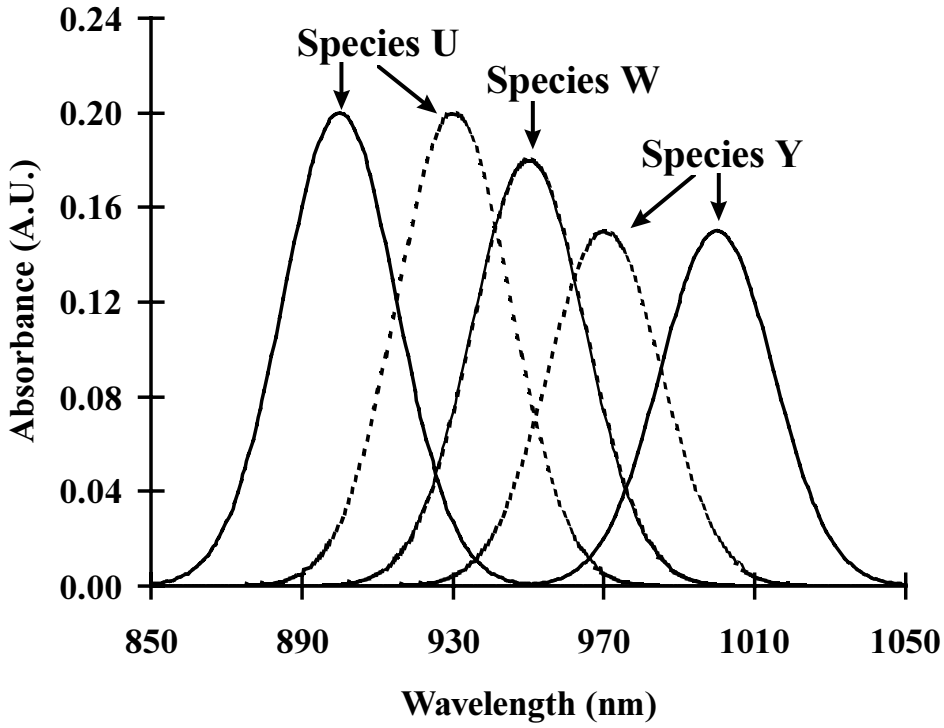

Figure 16. The pure spectra of species *U*, *W* and *Y* in the SW-NIR simulations.

6.2.3 Results and discussion

SIMULATIONS

The mean values of one hundred reaction rate constant estimates and the corresponding individual standard deviations are listed in Table 5 for CR and WCR. From the precision of the reaction rate constant estimates for both algorithms used it is obvious that a higher noise level will result in a poorer precision of reaction rate constant estimates (higher estimation error). If the noise level is constant and the spectral overlap is varied, the precision of reaction rate constant estimates becomes poorer for a larger spectral overlap. However, the methods can both still be applied successfully if there is a large amount of overlap in the pure spectra of the different reacting absorbing species present.

If the reaction rate constant estimates for CR are compared to the estimates for WCR, it is obvious that there is an improvement in precision of reaction rate constant estimates if WCR is used instead of CR. Hence, using WCR can be extraordinarily valuable if spectral data are noisy. In all cases, no biased reaction rate constant estimates are obtained.

Table 5. Mean reaction rate constant estimates and corresponding individual standard deviations (STD) using CR and WCR (values between parenthesis) for 100 simulated sets of SW-NIR spectra using two different noise levels and four different amounts of spectral overlap. $P_{max,i}$ indicates the spectral position of the maximum of the pure spectrum of species *i*.

$P_{max,U}$ (nm)	$P_{max,W}$ (nm)	$P_{max,Y}$ (nm)	Noise level (%)	Mean k_1 (min^{-1})	STD k_1 (min^{-1})	Mean k_2 (min^{-1})	STD k_2 (min^{-1})
900	950	1000	1	0.2999 (0.3000)	0.0034 (0.0021)	0.0500 (0.0497)	0.0026 (0.0018)
			4	0.2993 (0.2998)	0.0123 (0.0073)	0.0510 (0.0504)	0.0085 (0.0075)
910	950	990	1	0.2997 (0.2997)	0.0035 (0.0023)	0.0500 (0.0502)	0.0027 (0.0019)
			4	0.2994 (0.3013)	0.0139 (0.0080)	0.0511 (0.0497)	0.0115 (0.0082)
920	950	980	1	0.2999 (0.3001)	0.0038 (0.0025)	0.0501 (0.0498)	0.0031 (0.0023)
			4	0.2997 (0.2981)	0.0157 (0.0091)	0.0506 (0.0516)	0.0127 (0.0089)
930	950	970	1	0.2994 (0.3000)	0.0059 (0.0032)	0.0501 (0.0498)	0.0043 (0.0028)
			4	0.2971 (0.3001)	0.0305 (0.0138)	0.0507 (0.0501)	0.0181 (0.0115)

EXPERIMENTS

Reaction rate constant estimates

The mean datamatrix of dataset 1 has been obtained by averaging the datamatrices of the eight repeated individual batch process runs. A k_1 and a k_2 value have been estimated with CR and WCR. The relative fit errors have been estimated also according to Equation (21) and Equation (22) of Section 2.6, Chapter 2. The results are listed in Table 6. Because of their small values it can be concluded that the kinetic model used is satisfactory.

Table 6. Reaction rate constant estimates for the mean data matrix obtained over eight averaged individual batch process runs using CR and WCR (values between parenthesis).

Estimated k_1 (min^{-1})	Estimated k_2 (min^{-1})	Relative fit error in %
0.30 (0.26)	0.04 (0.07)	2.59 (2.63)

Table 6 gives no information about the fluctuation of the reaction rate constant estimates from batch to batch. Therefore, upper and lower error bounds have been estimated.

Estimation of the upper error bound

The reaction rate constants of dataset 1 have been estimated for eight individual batch process runs using CR and WCR. The mean values for both reaction rate constant estimates and their corresponding individual standard deviations are listed in the first part of Table 7. These standard deviations represent the upper error bound (worst case), because both experimental errors and instrumental noise are involved. Hence, there is no averaging effect. From Table 7 it is also obvious, that WCR performs better for k_1 compared to CR. There is a factor three improvement in the precision of the k_1 estimates. This is because of the fact that certain matrices are weighted in WCR during the optimization procedure as described in Section 2.6, Chapter 2. For both algorithms the precision of k_2 is poor. This is due to the dominance of the reactant (k_1) at the start of the reaction and the moderate signal to noise ratio present in the data.

Table 7. The mean reaction rate constant estimates and individual standard deviations (STD) according to the upper and lower error bound using CR and WCR (values between parenthesis).

Type of error bound	Mean k_1 (min^{-1})	STD k_1 (min^{-1})	Mean k_2 (min^{-1})	STD k_2 (min^{-1})
Upper	0.31 (0.26)	0.09 (0.03)	0.05 (0.07)	0.03 (0.03)
Lower	0.30 (0.26)	$6.80 \cdot 10^{-3}$ ($1.00 \cdot 10^{-3}$)	0.04 (0.07)	$3.10 \cdot 10^{-3}$ ($1.80 \cdot 10^{-3}$)

From Table 7, it is obvious that the reaction rate constant estimates obtained by others[1,2] are close to the estimates obtained in this Section. Hairfield *et al.*[1] obtained a mean estimate for k_1 and k_2 of 0.24 min^{-1} and 0.05 min^{-1}, respectively. Mayes *et al.*[2] obtained a mean estimate for k_1 and k_2 of 0.30 min^{-1} and 0.05 min^{-1}, respectively.

The correlation coefficient, r, has been estimated between the eight k_1 and the eight k_2 estimates for both algorithms. The value of r can be positive or negative. If r is negative this means that k_1 and k_2 are negatively correlated. In that case, a larger value of k_1 is associated with a smaller value of k_2 and the other way round. The absolute value for r gives an indication about the quality of the algorithm used. A small absolute value of r indicates that the algorithm can distinguish between k_1 and k_2

during the optimization procedure very easily. The correlation coefficient is -0.77 if CR has been used and -0.61 if WCR has been used, which means that it is easier for WCR to distinguish between k_1 and k_2 compared to CR because a weaker correlation is obtained for WCR. The reconstructed concentration profiles for the three benzoquinone species are shown in Figure 17 if the mean reaction rate constant estimates for WCR from Table 7 are used.

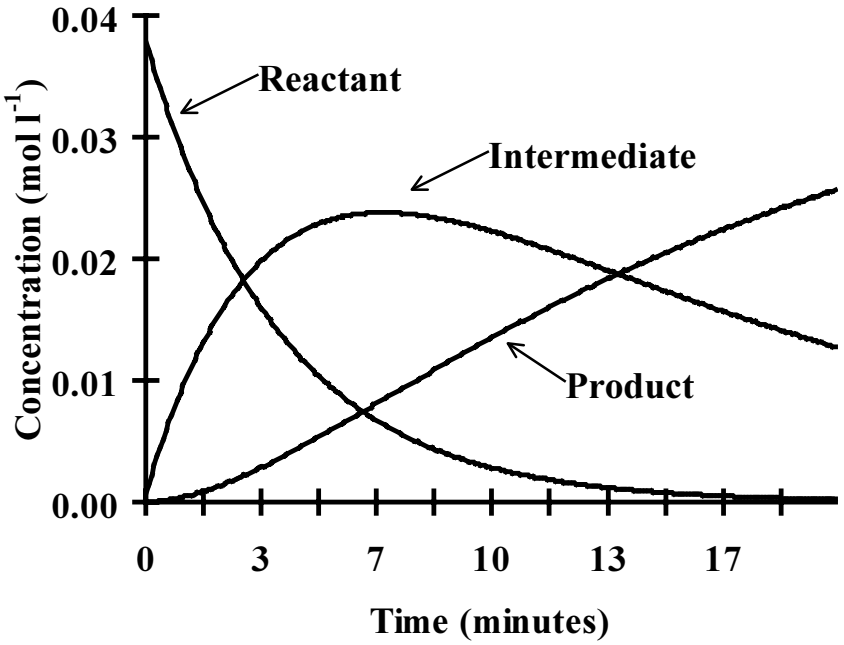

Figure 17. The reconstructed concentration profiles.

Estimation of the lower error bound

The lower error bound has been estimated according to the jackknife based procedure described in Section 4.3, Chapter 4, of this thesis. Spectra have been left out from the mean batch run using a jackknife interval of 31 spectra. This resulted in ten jackknife estimates for k_1 and k_2 for the mean batch process run. The jackknife procedure has been applied for both algorithms. The mean values obtained for the reaction rate constant estimates and the corresponding individual standard deviation for CR and WCR are listed in the last part of Table 7. The individual standard deviation estimates (lower error bound) represent the influence of mainly instrumental noise on the reaction rate constant estimates. There is an improvement in the precision of the k_1 and k_2 estimates (factor seven and two, respectively) if WCR is used instead of CR.

SUMMARY RESULTS

Using WCR, the mean estimated k_1 value is 0.26 min^{-1} with an error between $1.00 \cdot 10^{-3}$ min^{-1} (lower error bound) and 0.03 min^{-1} (upper error bound). With this algorithm the mean estimated k_2 value is 0.07 min^{-1} with an error between $1.80 \cdot 10^{-3}$ min^{-1} (lower error bound) and 0.03 min^{-1} (upper error bound). These values show that it is possible to estimate the reaction rate constants with good precision even in case of high spectral overlap and a high noise level. For all k_1 and k_2 estimates, too high k_1 estimates tend to occur with too low k_2 estimates and vice versa due to the moderate correlation (-0.61) between both reaction rate constants.

6.2.4 Conclusions

Reaction rate constants have been estimated from dataset 1 using CR and WCR. This dataset has been used as an example batch process to illustrate that the algorithms can be applied successfully if there is a strong spectral overlap of the pure spectra of the different reacting absorbing species and a high noise level are present in the data. An advantage of the procedure described is the rapid estimation of the reaction constants. Also upper and lower error bounds of the reaction rate constants can be estimated which is very important for quality assessment. Simulations have shown that the presented algorithms can be still applied successfully in case of an extreme overlap of the spectra of the individual species involved in the considered process. From the reaction rate constant estimates obtained from experimental and simulated data it can be concluded that WCR performed the best with respect to the precision of reaction rate constant estimates.

Because of the rapid estimation of the reaction rate constants from on-line SW-NIR measurements, the use of the procedures presented can have many applications in the field of obtaining information about batch processes and statistical control of batch processes using fast on-line SW-NIR sensors. The expansion to more complicated processes, e.g. batch polymerization processes is also possible.

6.3 UV-Vis data (1)

6.3.1 Introduction

In Section 2.7 of Chapter 2 the use of constraints in CCR has been discussed in detail. If pure spectra of some reacting absorbing species are known *a priori* these can be incorporated in CCR as a constraint resulting in constraint R or constraint RP. It is expected that this will result in a better accuracy of kinetic parameter estimates compared to methods which do not use this specific *a priori* spectral information. In this Section, constraint RP is implemented in CCR. Hence, the pure spectra of reactant and product are both implemented in the CCR algorithm.

Dataset 2 is used to estimate reaction rate constants and pure spectra of the reacting absorbing species involved. This dataset has been described in Section 5.3 of Chapter 5. The true values for the reaction rate constants are unknown. It is therefore not possible to check if the reaction rate constant estimates obtained are biased. WCR is compared to CCR, where constraint RP is implemented in the optimization procedure of CCR. Quality assessment of the estimated reaction rate constants is applied using the jackknife based method as described Section 4.3 of Chapter 4.

6.3.2 Results and discussion

REACTION RATE CONSTANT ESTIMATES AND PURE SPECTRA ESTIMATES

WCR results

For the mean batch process run, obtained by averaging the ten individual batches performed at identical conditions, the reaction rate constants, k_1 and k_2, have been estimated using WCR. The reaction rate constants have been estimated also for the individual batches. The mean reaction rate constant estimates and corresponding individual standard deviations are listed in Table 8. The standard deviations obtained represent the upper error bounds.

Table 8. The reaction rate constant estimates and corresponding standard deviations using WCR.

Batch process number	Estimated k_1 (min^{-1})	Estimated k_2 (min^{-1})
1	0.3103	0.0264
2	0.3117	0.0261
3	0.3112	0.0265
4	0.3189	0.0262
5	0.3089	0.0264
6	0.3069	0.0262
7	0.3248	0.0245
8	0.3245	0.0260
9	0.3317	0.0232
10	0.2995	0.0266
	$\bar{k}_1$ = 0.3148 STD = $0.9835 \cdot 10^{-2}$	$\bar{k}_2$ = 0.0258 STD = $0.1093 \cdot 10^{-2}$
Mean batch process	0.3146	0.0258

From Table 8 it is observed that a good precision of reaction rate constant estimates is obtained in all cases. For the reaction rate constant estimates for the individual batch processes the correlation coefficient has been calculated. Hence, the

correlation coefficient has been calculated between ten k_1 estimates and ten k_2 estimates. The correlation coefficient is equal to -0.82, which indicates a strong correlation.

For the estimated k_1 and k_2 for the mean batch process the concentration profiles have been reconstructed. These are shown in Figure 18. From this figure it is obvious that the assumption that no reactant and product will be left after eight hours, made earlier in Section 5.3.4 of Chapter 5, is reasonable.

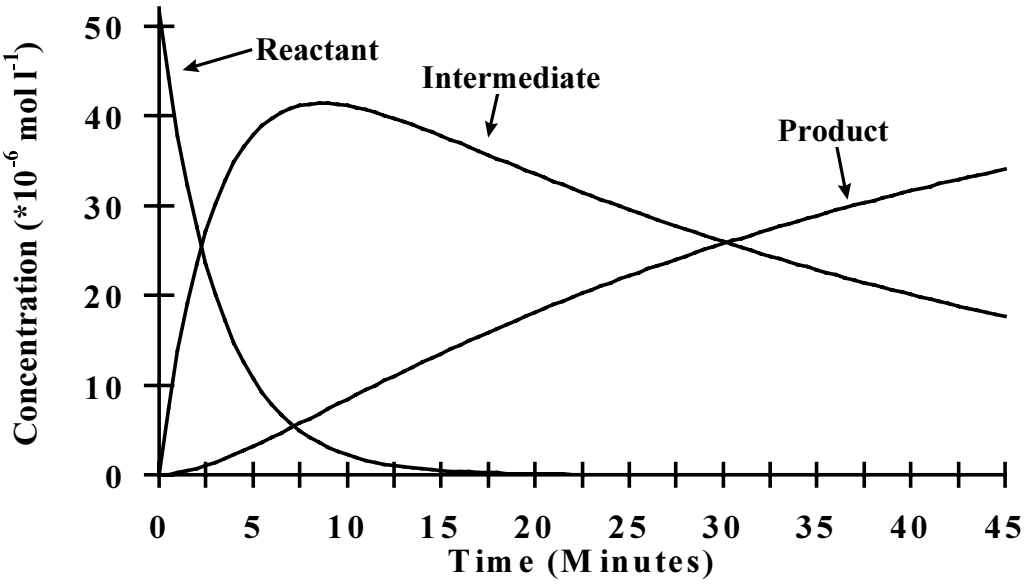

Figure 18. The reconstructed concentration profiles.

Pure spectra estimates

The pure spectrum of reactant, intermediate and product have been estimated using the reconstructed concentration profiles, the spectra of the mean batch process and non-negative least squares. Hence, the constraint that pure spectra of reacting absorbing species are non-negative has been used as a constraint. This constraint is labeled constraint NNLS in Section 2.7 of Chapter 2. Difference spectra have been calculated by subtracting the estimated pure spectrum from the measured pure spectrum, which is only possible for the reactant and product. The difference spectra for the reactant and product are shown in Figure 19 and Figure 20, respectively. The maximum absorbance of the measured mean pure spectrum of reactant and product is approximately equal to 1.2 A.U. as can be seen from Figure 15, Section 5.3.4, Chapter 5. In that figure the measured pure spectra of reactant and product are both shown.

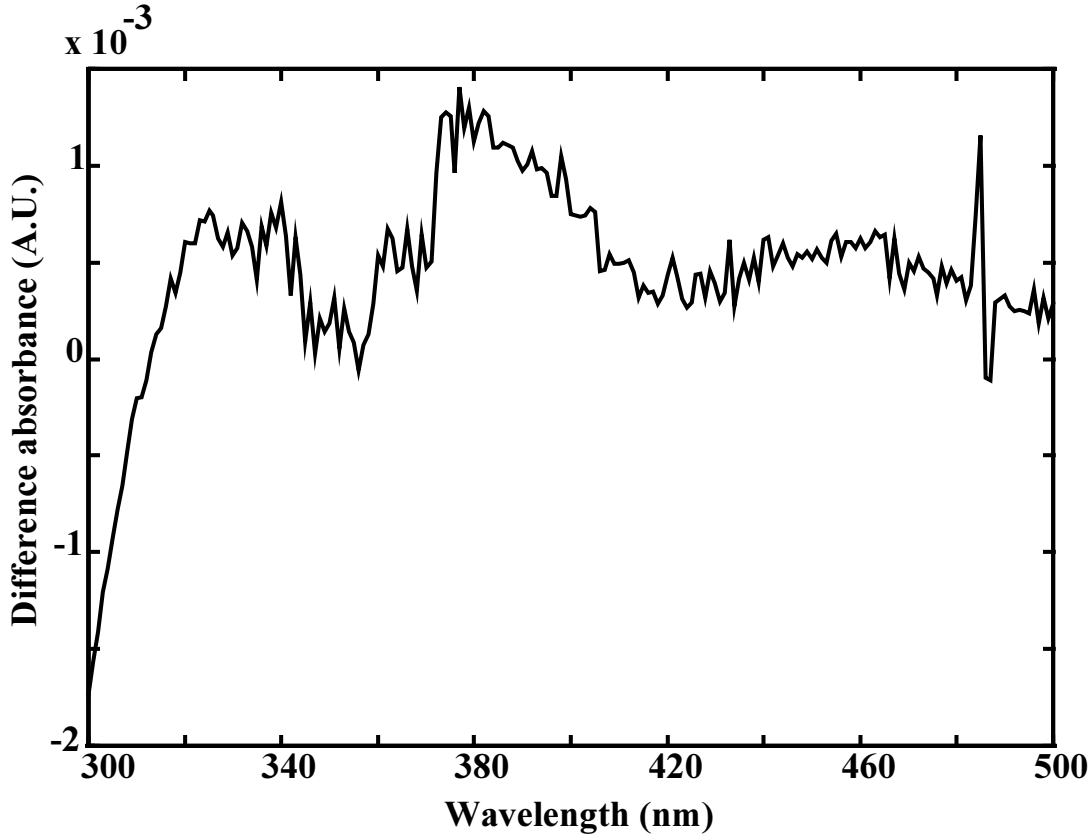

Figure 19. Difference spectrum of the reactant for WCR.

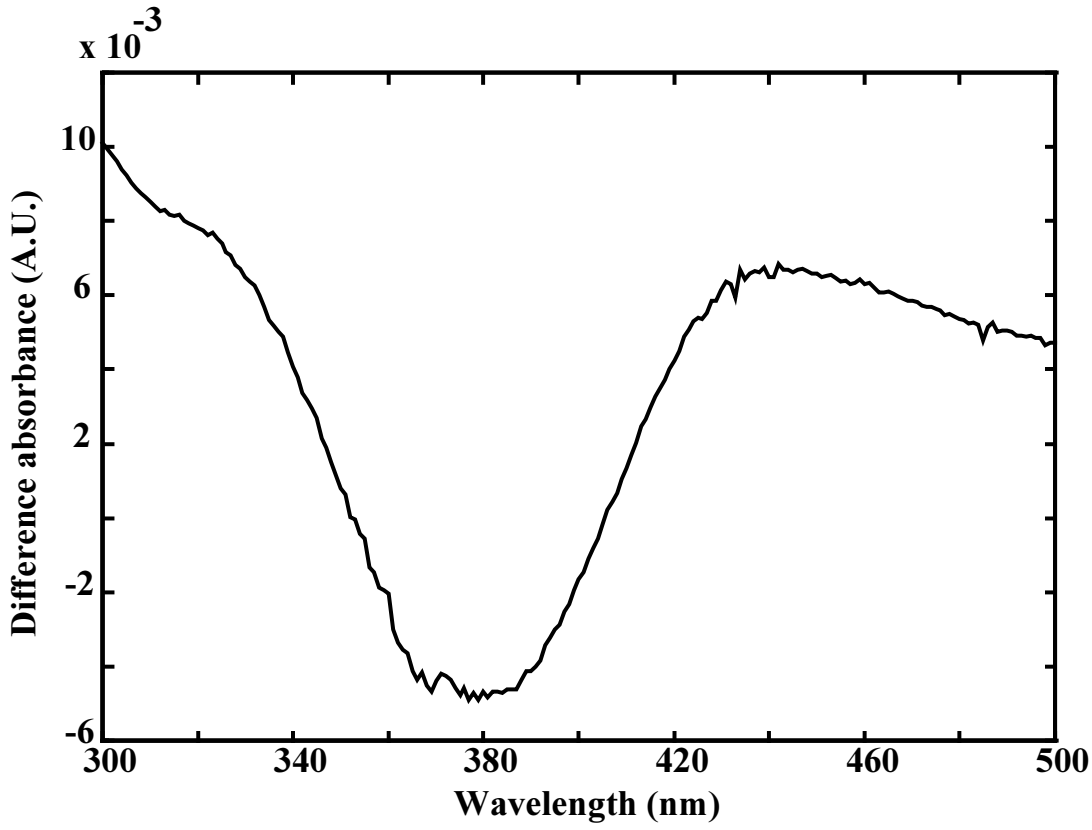

Figure 20. Difference spectrum of the product for WCR.

From Figure 19 and 20 it can be observed that the residuals are the smallest for the reactant. However, it seems that there is some structure present in the residuals. This can be caused by non-linear drift of the spectrophotometer, for example. Because of the small residuals the kinetic model fitted very well. For the reaction rate constants obtained from the individual batches the pure spectra for reactant and product have been estimated also. Next, the cosine of the angle between the estimated and measured pure spectrum has been calculated. For both the reactant and product the cosine is equal to 0.99 or higher for all cases, indicating an almost perfect match.

CCR results

For the mean batch process of dataset 2 and ten individual batch processes the reaction rate constants, k_1 and k_2, have been estimated using CCR with constraint RP implemented in the algorithm. The reaction rate constant estimates and corresponding individual standard deviations are listed in Table 9. The standard deviations obtained represent the upper error bound. The correlation coefficient between the k_1 and k_2 values obtained for the individual bath processes has been calculated also. The correlation coefficient is equal to -0.54.

Table 9. The reaction rate constant estimates and corresponding individual standard deviations using CCR.

Batch process number	Estimated k_1 (min^{-1})	Estimated k_2 (min^{-1})
1	0.3127	0.0258
2	0.3147	0.0257
3	0.3138	0.0258
4	0.3215	0.0258
5	0.3087	0.0259
6	0.3107	0.0258
7	0.3293	0.0255
8	0.3255	0.0260
9	0.3288	0.0254
10	0.2986	0.0258
	$\bar{k}_1$ = 0.3164 STD = $0.9774 \cdot 10^{-2}$	$\bar{k}_2$ = 0.0257 STD = $0.1713 \cdot 10^{-3}$
Mean batch process	0.3162	0.0257

If Table 8 is compared to Table 9 it can be observed that there is an improvement in precision of the reaction rate constant estimates if CCR is used

instead of WCR. Especially for k_2 there is a large improvement in precision. Because the pure spectrum of reactant and product are both implemented in CCR, k_1 and k_2 can be estimated much easier. If the absolute value of the correlation coefficient between the k_1 and k_2 estimates of both algorithms are compared it appears that the correlation between the two kinetic parameters is the lowest for CCR. This means that it is easier to distinguish between k_1 and k_2 using CCR instead of WCR due to the implementation of *a priori* spectral information in the CCR algorithm.

Pure spectra estimates for the intermediate

The pure spectrum of the intermediate has been estimated using the WCR results of the reaction rate constant estimates, as has been already mentioned earlier, and CCR. The estimated pure spectra of the intermediate obtained with WCR and CCR are both shown in Figure 21. The difference between the estimated pure spectrum for both algorithms for the intermediate is shown in Figure 22. From these figures it is obvious that the difference is not that large, but a certain structure is present.

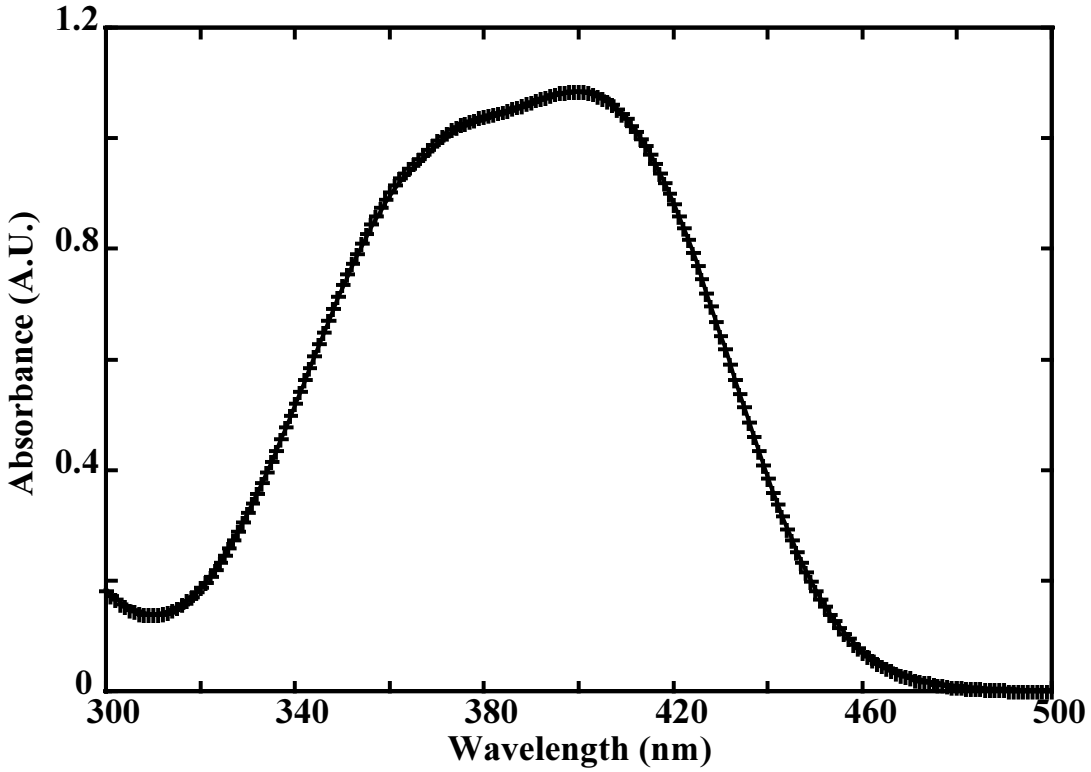

Figure 21. The pure spectra estimates of the intermediate using WCR (solid line) and CCR (+).

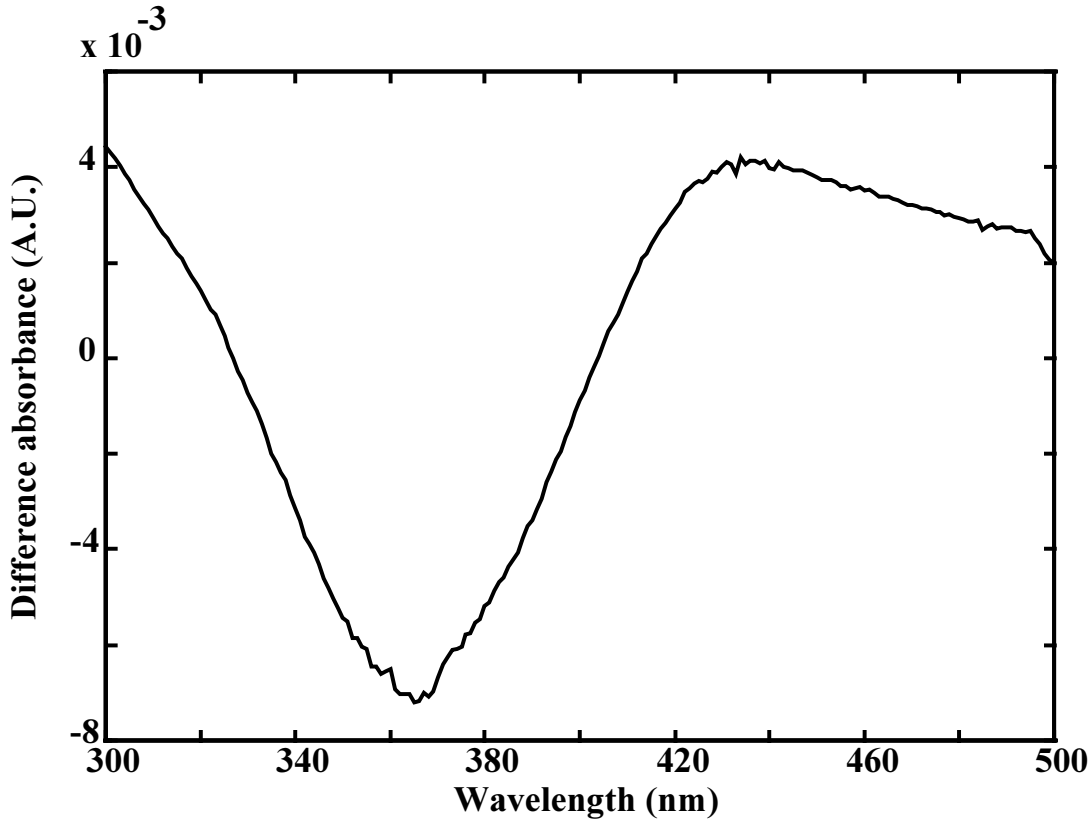

Figure 22. The difference spectrum of the intermediate from Figure 21.

JACKKNIFE RESULTS FOR WCR AND CCR

For both algorithms the jackknife based procedure has been applied using a jackknife interval of 27 spectra. This resulted in ten jackknife estimates for both algorithms. A mean k_1 and k_2 and their corresponding standard deviations are calculated over ten jackknife estimates. The results are listed in Table 10. The standard deviations from this table represent the lower error bounds. From Table 10 it can be observed that the precision of the reaction rate constant estimates is better for CCR compared to WCR, especially for k_2.

Table 10. The jackknife results for the mean batch process obtained with WCR and CCR.

Algorithm	Mean k_1 (min^{-1})	STD k_1 (min^{-1})	Mean k_2 (min^{-1})	STD k_2 (min^{-1})
WCR	0.3147	$0.1229 \cdot 10^{-3}$	0.0258	$0.1341 \cdot 10^{-4}$
CCR	0.3162	$0.2592 \cdot 10^{-4}$	0.0257	$0.7613 \cdot 10^{-6}$

6.3.3 Conclusions

WCR and CCR performed both very well. Constraint RP has been implemented in CCR which cannot be realized for WCR. Reaction rate constants and the pure spectra of the reacting absorbing species have been estimated simultaneously from dataset 2

using both algorithms. From the standard deviations obtained it can be concluded that there is a gain in precision of the reaction rate constant estimates if CCR is used instead of WCR. If the pure spectra estimates obtained with both algorithms are compared it can be concluded that the difference is quite small. Hence, using information about pure spectra that is known in advance is very useful since it will result in more precise results. The absolute value of the correlation coefficient between the estimates of both reaction rate constants appeared to be the lowest for CCR. This indicates that it is easier to distinguish between both reaction rate constants if a constraint is implemented. Quality assessment of the estimated reaction rate constants for both algorithms has been performed by applying a jackknife based procedure. From the results it can be concluded again that the precision of the reaction rate constant estimates is better for CCR compared to WCR.

In general, using CCR with *a priori* spectral information implemented gives the best results and hence this algorithm is very powerful in cases where information about the pure spectra of different species, involved in the chemical process, is available.

6.4 UV-Vis data (2)

6.4.1 Introduction

Dataset 3, performed under pseudo-first order conditions, and dataset 4, performed under second order conditions, have been both described in detail in Section 5.3 of Chapter 5. The spectra of dataset 3 have large absorbance differences in time whereas the spectra of dataset 4 have small absorbance differences in time as is obvious from Figure 14, Section 5.3.3, Chapter 5. The reaction rate constants and pure spectra of reacting absorbing species have been estimated both from dataset 3 and dataset 4 using TCF and CCR without constraints implemented. The goal of this Section is to compare both approaches with respect to the precision of the reaction rate constant estimates, the recovery of pure spectra and to investigate the advantages and disadvantages of the two methods. The true values for the reaction rate constants are unknown. Therefore it is not possible to check if the reaction rate constant estimates obtained are biased. For the measurements obtained under second order conditions, curve resolution and numerical integration have been combined, which makes the procedure more general applicable.

6.4.2 Results and discussion

DETERMINATION OF SELECTIVE WAVELENGTHS

Selective wavelengths for the intermediate have been chosen by means of FSWEFA with a fixed size moving window of three wavelengths as described in Section 2.4

from Chapter 2. In Figure 23 the FSWEFA plots (log (singular value) as a function of the position of the window) are shown for one individual batch process run under pseudo-first order conditions and one individual batch process run obtained under second order conditions. FSWEFA plots obtained for other individual batches are comparable.

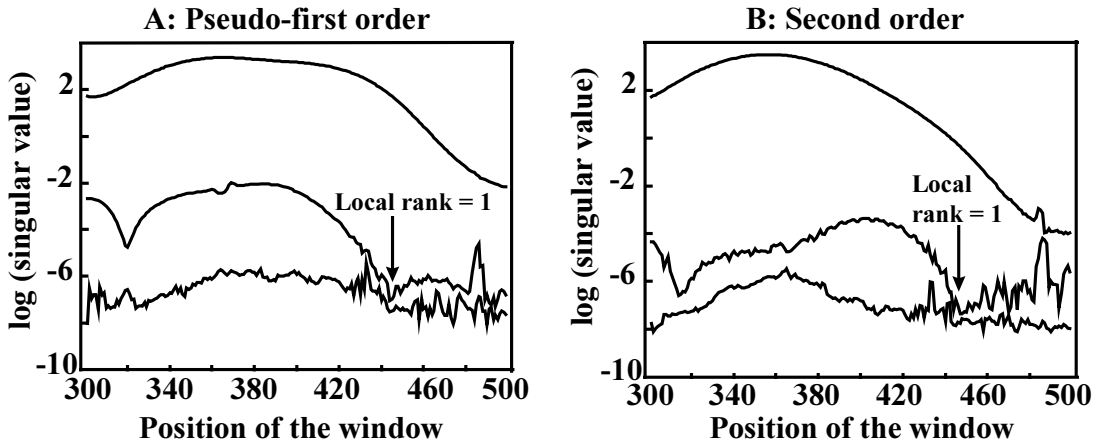

Figure 23. Plots of log (singular value) versus position of the FSWEFA window.

In Figure 23, the position of the window equal to 301 means wavelength range 300-302 nm, the position of the window equal to 340 corresponds to 339-341 nm, etc… If Figure 23 is examined critically it can be observed that the local rank case of interest (local rank equals 1), is at position number 444. This corresponds to the wavelength range 443-445 nm. Hence, at this window absorbance differences are mainly caused by one species. It is known that the pure spectra of reactant and product have no absorbances in the wavelength range 443-445 nm (see Figure 15, Section 5.3.4, Chapter 5). Therefore it is reasonable to assume that the absorbances at this wavelength range are mainly caused by the intermediate.

REACTION RATE CONSTANT ESTIMATES

In this Section, the focus will be mainly on the precision of the reaction rate constant estimates. TCF and CCR have both been applied to the pseudo-first order dataset (dataset 3) and the second order dataset (dataset 4). The reaction rate constant estimates for every individual batch for the two methods are shown in Figure 24.

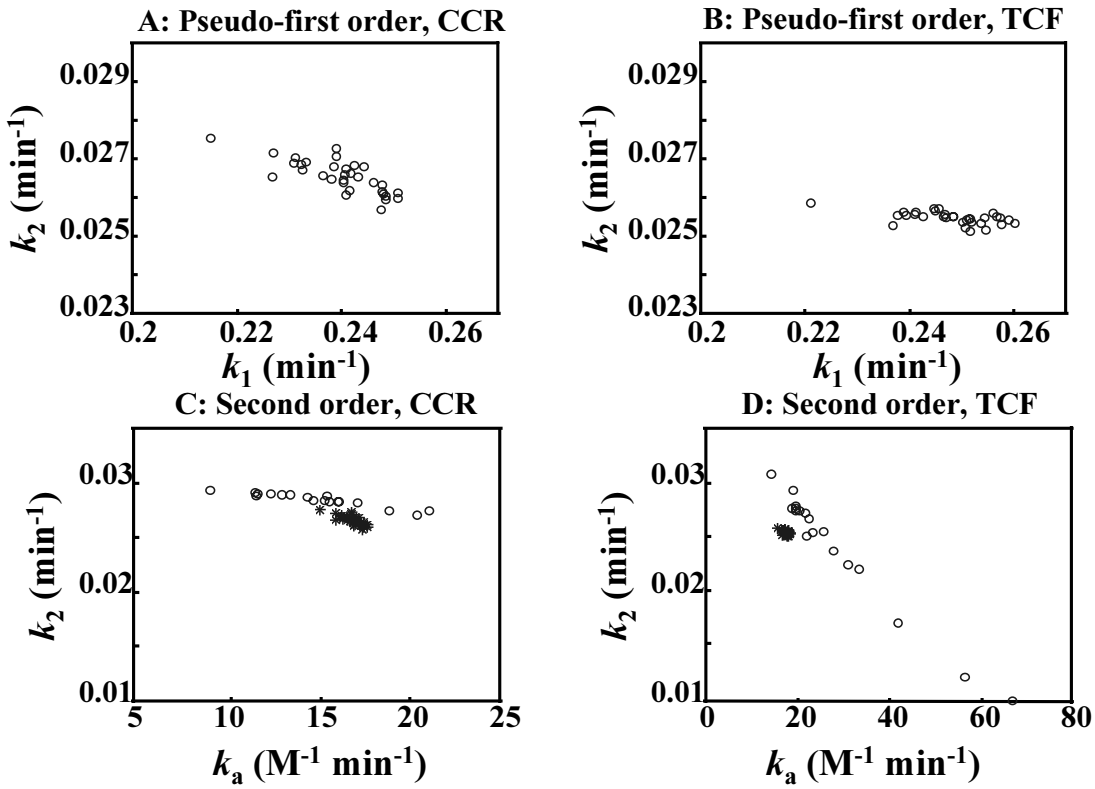

Figure 24. The individual reaction rate constant estimates indicated by "o". The second order reaction rate constant estimates indicated by '*' are obtained by transforming the pseudo-first order reaction rate constant estimates.

From Figure 24, the following can be observed:

1) For the pseudo-first order dataset the precision of the k_2 estimates is better (approximately a factor 1.4) using TCF whereas the precision of the k_1 estimates is the same for CCR and TCF (compare Figure 24A and 24B).
2) For the second order dataset the precision of the k_a and k_2 estimates is better using CCR than for TCF (compare Figure 24C and 24D). Note the scale difference for the k_a axis in the plots.
3) There is a small systematic difference between the k_2 estimates for the pseudo-first order dataset and the k_2 estimates for the second order dataset using CCR (compare Figure 24A and 24C).

An explanation of the results obtained is that in case of second order conditions less information about the kinetics is present in matrix **X** compared to pseudo-first order conditions because of the small absorbance differences in time for second order conditions. Especially TCF suffers from this lack of absorbance difference in second order conditions.

The pseudo-first order rate constant estimates from Figure 24A and 24B have been transformed into second order rate constant estimates using Equation (9) from Section 2.2 of Chapter 2 and are plotted in Figure 24C and 24D, respectively, indicated with a '*'. If the second order rate constant estimates from Figure 24C and 24D for the pseudo-first order dataset (*) are compared to the second order rate constant estimates for the second order dataset (o) also shown in Figure 24C and 24D, it can be observed that for CCR and TCF the precision of the second order rate constant estimates, obtained by transformation of the pseudo-first order rate constant estimates (*), is better compared to the precision of the second order rate constant estimates obtained for the second order batches (o) (compare Figure 24C and 24D). This is again due to the larger absorbance differences for pseudo-first order conditions.

For the pseudo-first order dataset TCF performs the best with respect to the precision of the reaction rate constant estimates. However, since CCR accounts for spectral overlap it is reasonable to assume that the CCR results are closer to the real values compared to the TCF results. Using TCF there will always be some spectral overlap in this case which is not accounted for even if the best selective wavelengths for the intermediate species using FSWEFA are selected. As already mentioned in this Chapter, it is not possible to check if the reaction rate constant estimates are biased, because the true values are unknown. Chapter 9 of this thesis, describes simulations in order to check if biased reaction rate constant estimates can be obtained in case of CCR with and without different constraints implemented in the algorithm. For the second order dataset the best precision is obtained using CCR. A very poor precision of the reaction rate constant estimates is obtained for TCF.

PURE SPECTRA ESTIMATES

For the individual batches of the pseudo-first order and second order dataset the pure spectra of reactant, intermediate and product have been estimated. The pure spectra estimates obtained for the reactant and product for CCR and TCF for both datasets have been compared to their measured spectra by means of calculating the difference spectra. The difference spectra have been calculated by subtracting the measured pure spectrum from the estimated pure spectrum. In Figure 25 the difference spectra are shown for one individual pseudo-first order batch and one individual second order batch obtained with both CCR and TCF. The difference spectra obtained for other individual pseudo first order and second order batches are comparable to those shown in Figure 25. From this figure the following can be observed:

1) For the pseudo-first order batch, CCR and TCF yield comparable pure spectra estimates (compare Figure 25A and 25B). The difference spectra show some structure, but the order of magnitude of these difference absorbances is small compared to the order of magnitude of the absorbances of the original pure spectra (see Figure 15, Section 5.3.4, Chapter 5).
2) For the second order batch the difference spectra obtained with CCR and TCF are comparable (compare Figure 25C and 25D).
3) For the CCR algorithm the difference spectra obtained for the pseudo-first order batch and the second order batch are comparable for the reactant (compare Figure 25A and 25C). For the product the order of magnitude of the difference spectra differ (compare Figure 25A and 25C). This is also observed for TCF (compare Figure 25B and 25D).

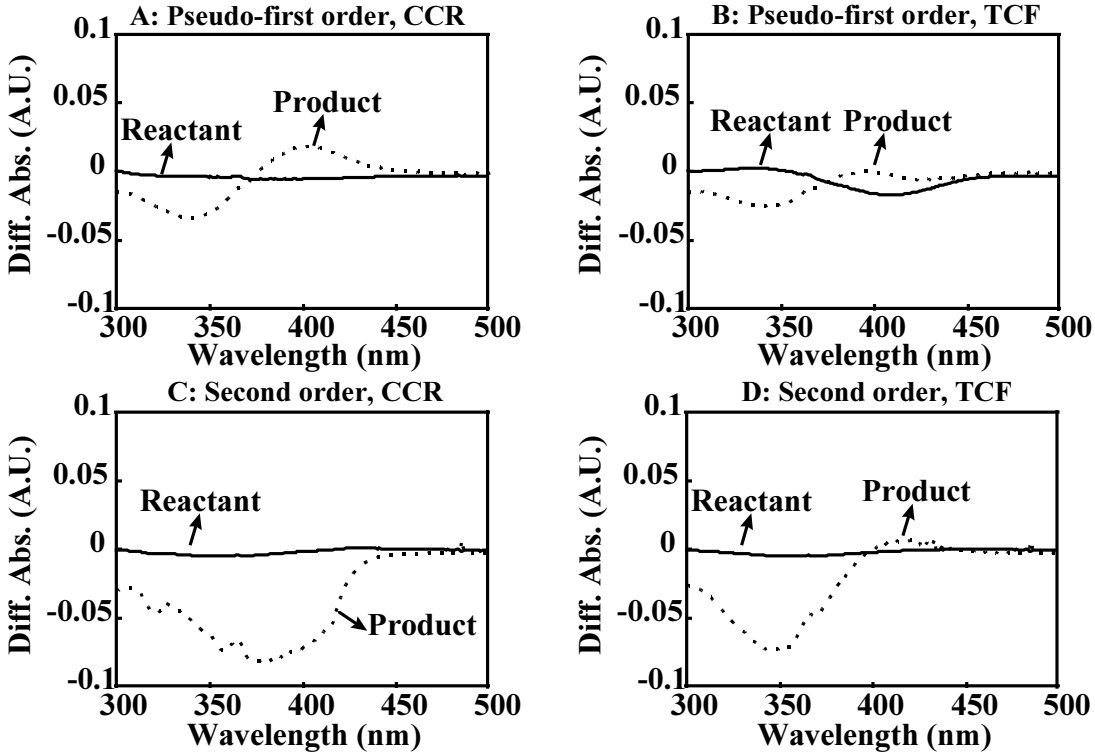

Figure 25. The difference spectra for the reactant and product.

The fact that the difference spectra for the product are always larger than the difference spectra of the reactant (compare Figure 25A, 25B, 25C and 25D) might be caused by the fact that species *U* and species *W* were still present in low concentrations when the pure spectrum of the product was measured. Therefore, it is possible that the pure spectrum of the product is slightly misestimated.

For all individual batches, the correlation coefficient between estimated and measured pure spectrum for the reactant and product has been calculated. If the

correlation coefficient is equal to 1 this indicates a perfect match of estimated and measured pure spectrum. For the pseudo-first order and second order dataset using CCR and TCF the values for the correlation coefficient of the pure spectra estimates and the measured pure spectra are equal to 0.99 or higher for all individual batches.

As already mentioned earlier, it is not possible to compare estimates of the pure spectrum of the intermediate with its measured pure spectrum. In Figure 26 the pure spectra estimates for the intermediate are shown for three individual pseudo-first order batches (Figure 26A and 26B) and three individual second order batches (Figure 26C and 26D) obtained with CCR and TCF. Two of the three individual batches chosen for both datasets correspond to the two most extreme cases with respect to reaction rate constant estimates from Figure 24. The third individual batch chosen corresponds to a compromise with respect to reaction rate constant estimates shown in Figure 24. From Figure 26, the following can be observed:

1) For the individual pseudo-first order batches chosen, the fluctuation of the pure spectrum estimates and the shape of the pure spectra are similar for both CCR and TCF (compare Figure 26A and 26B).
2) For the three individual second order batches chosen, the fluctuation of the pure spectrum estimates is large for both TCF and CCR (compare Figure 26C and 26D).
3) The pure spectra estimates for the pseudo-first order and second order batches differ for both algorithms (compare Figure 26A and 26C and compare Figure 26B and 26D).

The observation that the pure spectrum estimates of the intermediate for the second order batches using TCF differ from the results obtained with CCR and the results obtained for the pseudo-first order batches using TCF and CCR can be explained as follows. The absorbance differences in time are very small using second order conditions. For TCF, this means that the kinetic information in the absorbances in time of selective wavelengths is less excited compared to cases with large absorbance differences in time (pseudo-first order kinetics). Also in case of CCR less spectral information is present in the signal in case of second order conditions in order to estimate reaction rate constants compared to pseudo-first order conditions. However, because CCR uses more wavelengths than TCF, more spectral information is available.

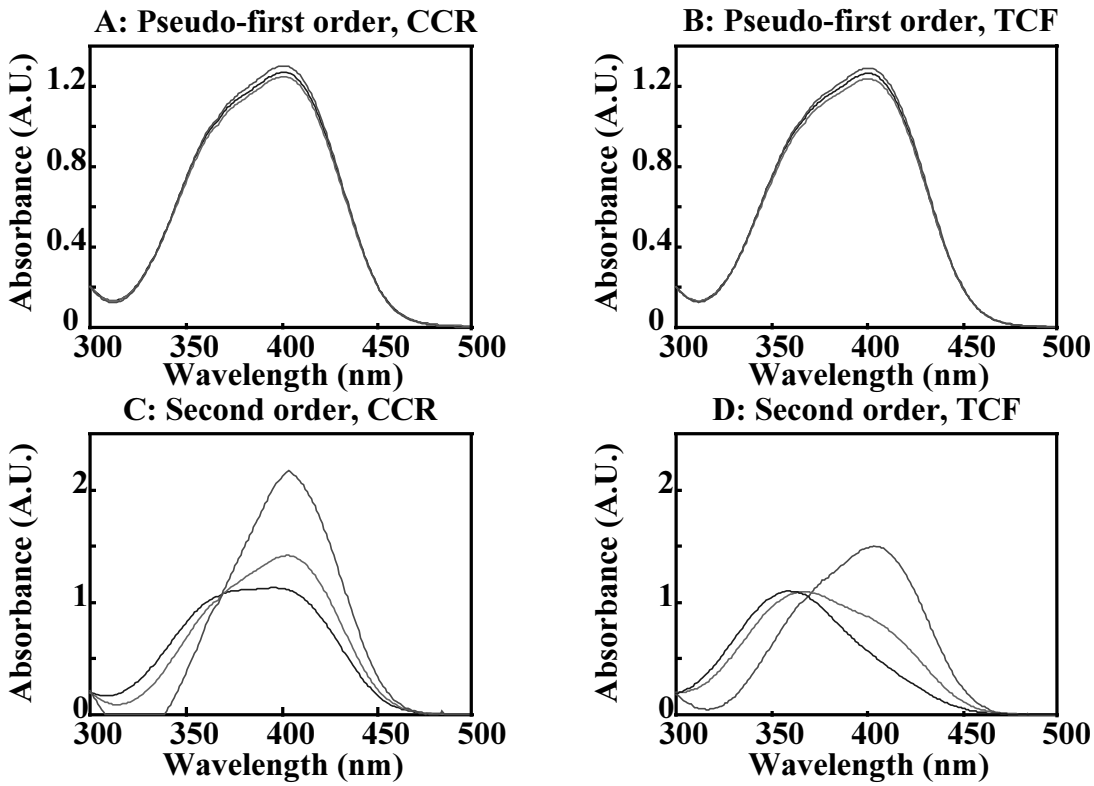

Figure 26. The pure spectra estimates for the intermediate.

OVERALL COMPARISON

Looking at Figure 24 and 25 it can be observed that TCF performed slightly better than CCR for pseudo-first order kinetics according to the precision of the reaction rate constant estimates (compare Figure 24A and 24B). The pure spectra estimates are the same for TCF and CCR (compare Figure 25A and 25B and Figure 26A and 26B). For second order kinetics CCR clearly performed better than TCF with respect to the precision of the reaction rate constant estimates (compare Figure 24C and 24D). The pure spectra estimates are the same for TCF and CCR (compare Figure 25C and 25D) for the reactant and product. However, the pure spectra estimates for the intermediate differ for TCF and CCR (compare Figure 26C and 26D).

6.4.3 Conclusions

In this Section, traditional curve fitting (TCF) and classical curve resolution (CCR) have been compared for estimating reaction rate constants from a two-step consecutive biochemical reaction performed under pseudo-first order (dataset 3) and second order conditions (dataset 4). Fixed-size window evolving factor analysis (FSWEFA) has been used to obtain selective wavelengths for TCF.

For the pseudo-first order dataset, TCF performed the best with respect to the precision of the reaction rate constant estimates. The estimates of the pure spectra are

similar for TCF and CCR. For the second order dataset CCR performed the best with respect to the precision of the reaction rate constant estimates. A possible reason for the relatively poor performance of the TCF algorithm with respect to the precision of the reaction rate constant estimates for the second order dataset, are the small absorbance differences in time in the signal in order to estimate the reaction rate constants. The estimates of the pure spectra differed for TCF and CCR.

In general, it can be concluded that both CCR and TCF perform very well in case of spectral data where the absorbance differences in time are large and a good selective window exists. In that case TCF is preferred because it is simple and fast compared to CCR. These properties make TCF very suitable for on-line monitoring reaction rate constants and process control. In more complicated situations, for example, in case of small absorbance differences in time or severe spectral overlap (no availability of selective wavelengths) CCR performs better. In case of doubt CCR is always preferred.

6.5 General conclusions

In this Chapter, results have been presented using different two-way methods for estimating reaction rate constants. Four different experimental datasets and simulated datasets have been used to test the performance of the algorithms. The following general conclusions can be formulated from the results:

1) WCR leads to a better precision of reaction rate constant estimates compared to CR.
2) If constraint RP is implemented in CCR this leads to a better precision of reaction rate constant estimates compared to WCR.
3) CCR is applicable for *n*-th order kinetics.
4) If there are large absorbance differences in time present (high selectivity in the time direction) in the dataset (in this case this holds for pseudo-first order kinetics), TCF is applicable and is superior to CCR without *a priori* spectral information implemented in the algorithm.
5) If there are small absorbance differences in time present (low selectivity in the time direction) in the dataset (in this case this holds for second order kinetics), TCF leads to a poor precision of reaction rate constant estimates compared to CCR without constraints implemented.

6.6 References

1. Hairfield EM, Moomaw EW, Tamburri RA, Vigil RA. 'The epoxidation of 2,5-di-tert-butyl-1,4-benzoquinone'. *J. Chemical Education*, 1985; **62**: 175-177.
2. Mayes DM, Kelly JJ, Callis JB. 'Non-invasive monitoring of a two-step sequential chemical reaction with shortwave near-infrared spectroscopy', in *Near Infra-Red Spectroscopy: Bridging the Gap between Data Analysis and NIR Applications*, ed. by Hildrum KI, Isaksson T, Naes T, Tandberg A. Ellis Horwood: Chichester, 1992; 377-387.

Chapter 7

Applications of Three-Way Methods

7.1 Introduction

In this Chapter,[i] the results of the application of the generalized rank annihilation method (GRAM) and the generalized rank annihilation method-Levenberg-Marquardt-parallel factor analysis (GRAM-LM-PAR) method to dataset 1 and dataset 2 are presented. Dataset 1 and dataset 2 have been described in Section 5.2 and Section 5.3, respectively, of Chapter 5. The theory of the three-way methods has been described in Section 3.4 and Section 3.5 of Chapter 3. However, in this Chapter the application of the three-way methods the trilinear decomposition method (TLD) and the trilinear decomposition method-Levenberg-Marquardt-parallel factor analysis (TLD-LM-PAR) method are not presented. This is postponed until Chapter 8, where also a comparison is made between the performance of two-way and three-way methods.

7.2 SW-NIR data

7.2.1 Introduction

In this Section, simulations based on a two-step consecutive reaction are used to show that GRAM and GRAM-LM-PAR, described in Section 3.4 and Section 3.5 of Chapter 3, can be applied to estimate reaction rate constants in case of extreme spectral overlap of different species involved in the reacting system. The performance of both algorithms is also tested on the spectra of dataset 1 (SW-NIR data) described in Section 5.2 of Chapter 5. Quality assessment of the estimated reaction rate constants is performed using a jackknife based method (see Section 4.3, Chapter 4).

[i] This Chapter is based on the following papers:

- Bijlsma S, Louwerse DJ, Windig W, Smilde AK. 'Rapid estimation of rate constants using on-line SW-NIR and trilinear models'. *Anal. Chim. Acta*, 1998; **376**: 339-355.
- Bijlsma S, Louwerse DJ, Smilde AK. 'Estimating rate constants and pure UV-Vis spectra of a two-step reaction using trilinear models'. *J. Chemometrics*, 1999; **13**: 311-329.

7.2.2 Simulation set-up

The set-up of the simulations was identical to the set-up described in Section 6.2.2 of Chapter 6. Simulations have been performed using GRAM and GRAM-LM-PAR under different simulated conditions: different amounts of peak overlap and different noise levels. The true values for the reaction rate constants were always 0.30 min^{-1} and 0.05 min^{-1} for k_1 and k_2, respectively. The time shift parameter S was equal to 1 spectrum and the values of the elements in the column with constants, added to datamatrix **X** (soft constraint), were equal to 100000.

7.2.3 Results and discussion

SIMULATIONS

The mean reaction rate constant estimates for k_1 and k_2 using GRAM and GRAM-LM-PAR are listed in Table 11 for two different noise levels (1% and 4%) and four different situations of spectral overlap of the pure spectra of the reacting absorbing species. From Table 11 the following can be observed:

1) A higher noise level results in a poorer precision for both k_1 and k_2 estimates.
2) If the noise level is kept constant and the spectral overlap becomes stronger, a poorer precision is obtained for both reaction rate constants.
3) If GRAM-LM-PAR is used instead of GRAM, the precision of the reaction rate constant estimates is improved for both kinetic parameters. Moreover, the mean estimated values are closer to the true values.

If the noise level is increased to higher values than 4%, many individual k_1 estimates are equal to the corresponding individual k_2 estimates. This is illustrated using the following simulations. For a fixed spectral overlap ($P_{max,U}$ = 900 nm, $P_{max,W}$ = 950 nm and $P_{max,Y}$ = 1000 nm) 100 SW-NIR datasets have been simulated for two different noise levels (10% and 15%). The kinetic parameters have been estimated using GRAM. For a noise level of 10% in five cases k_1 equals k_2. For a noise level of 15% in 27 cases k_1 equals k_2. A possible explanation for this phenomenon is that if the noise level is very high it is very hard to distinguish between the two exponential functions $e^{-k_1 t}$ and $e^{-k_2 t}$. If this noise effect occurs this can easily be detected from the **C** matrix, because the first two columns will be equal and hence k_1 equals k_2.

The choice of the column with constants appeared to be very important. If the constants are equal to 1 the third column of **A** and **C** ($\mathbf{a}_3$ and $\mathbf{c}_3$, respectively) are not always constant. If the column with constants is much larger than the signals present in **X**, $\mathbf{a}_3$ and $\mathbf{c}_3$ are forced to be constant. Therefore the column with constants was

Table 11. Mean estimated k_1 and k_2 with corresponding individual standard deviations (STD's) for 100 simulated sets of SW-NIR spectra using GRAM and GRAM-LM-PAR (values between parentheses). $P_{max,i}$ indicates the spectral position of the maximum of the pure spectrum of species *i*.

$P_{max,U}$ (nm)	$P_{max,W}$ (nm)	$P_{max,Y}$ (nm)	Noise level (%)	Mean k_1 (min^{-1})	STD k_1 (min^{-1})	Mean k_2 (min^{-1})	STD k_2 (min^{-1})
900	950	1000	1	0.2995 (0.2996)	0.0030 (0.0024)	0.0503 (0.0503)	0.0029 (0.0026)
			4	0.2989 (0.2995)	0.0106 (0.0097)	0.0494 (0.0490)	0.0117 (0.0108)
910	950	990	1	0.2998 (0.2996)	0.0030 (0.0023)	0.0504 (0.0504)	0.0030 (0.0028)
			4	0.2946 (0.2951)	0.0122 (0.0096)	0.0528 (0.0519)	0.0124 (0.0111)
920	950	980	1	0.2996 (0.2997)	0.0030 (0.0025)	0.0501 (0.0501)	0.0032 (0.0030)
			4	0.2937 (0.2948)	0.0129 (0.0107)	0.0523 (0.0514)	0.0129 (0.0116)
930	950	970	1	0.2993 (0.2996)	0.0042 (0.0034)	0.0501 (0.0500)	0.0039 (0.0036)
			4	0.2903 (0.2941)	0.0166 (0.0130)	0.0505 (0.0496)	0.0157 (0.0142)

equal to 100000 for the simulated data because the absorbances listed in matrix **X** are approximately between 0 and 0.2 A.U.

EXPERIMENTS

Effect of the time shift on the reaction rate constant estimates

It is very hard to decide, in advance, how large the time shift parameter has to be chosen with respect to the precision of reaction rate constant estimates. If the time shift is very small, the two formed datasets (slabs) from the master dataset (matrix $\mathbf{X}^*$) are nearly the same. Hence, in that case the exponential functions and the shifted exponential functions are almost the same. This will result in a poor precision of reaction rate constant estimates. If the time shift is very large, the two formed datasets will become too small and this will also result in a poor precision of reaction rate constant estimates because of lack of "signals" in the matrices created. Hence, for every specific problem the optimal choice of the time shift parameter has to be determined. In order to investigate the effect of different time shifts, the reaction rate constants have been estimated for the eight repeated individual batch processes of

dataset 1 using GRAM for different time shifts. The results are listed in Table 12. The values of the column with constants added to **X** were equal to 1, because than the third column of loading matrix **C** is constant. In that case, the column with constants will dominate, because of the small values for the second derivative difference SW-NIR spectra shown in Figure 12, Section 5.2.4, Chapter 5. From Table 12 the following can be observed:

1) A small or a large time shift results in k_1 estimates which are equal to k_2. This phenomenon was also present in the simulations if the noise level was increased above the 4%. Probably, it is very hard to distinguish between the two exponentially decaying functions if the noise level is very high or the time shift parameter is large or small.
2) A small or a large time shift can result in k_2 estimates which are negative. Negative reaction rate constants are physically meaningless.
3) A time shift of roughly 30 or 40 spectra gives the best results. This gives the best precision for the k_1 estimates and a compromise in precision for the k_2 estimates.
4) A time shift of 30 spectra is the only situation where for all eight repeated individual batch processes $k_1 \neq k_2$ and $k_2 > 0$ hold. For these reasons a time shift of 30 spectra is used for dataset 1 in the remainder of this Chapter.

Table 12. The mean estimated reaction rate constants and the individual standard deviations (STD's) for eight repeated individual batch processes using GRAM and different time shifts. The values between parentheses indicate how many estimations result in $k_1 = k_2$ or $k_2 < 0$. These values are left out for calculating the mean estimated reaction rate constants.

Time Shift	Mean k_1 (min^{-1})	STD k_1 (min^{-1})	Mean k_2 (min^{-1})	STD k_2 (min^{-1})
10 (3)	0.25	0.05	0.09	0.04
20 (1)	0.28	0.02	0.10	0.07
30 (0)	0.28	0.03	0.10	0.06
40 (1)	0.26	0.02	0.10	0.05
50 (1)	0.25	0.02	0.11	0.05
60 (2)	0.24	0.02	0.09	0.03
70 (4)	0.27	0.03	0.07	0.02
80 (4)	0.26	0.04	0.09	0.05
90 (2)	0.29	0.08	0.12	0.02
100 (3)	0.31	0.10	0.14	0.05

The obtained precision of reaction rate constant estimates has been used as a criterion to select the best value for the time shift. However, it is important to realize that it cannot be checked if biased reaction rate constant estimates have been obtained for a chosen time shift.

Estimation of the upper error bound

The individual reaction rate constant estimates for each repeated individual batch process and the mean batch process of dataset 1 are listed in Table 13 for a time shift of 30 spectra. The mean batch process has been obtained by averaging the eight repeated individual batch processes of dataset 1. GRAM and GRAM-LM-PAR have been both used. The individual standard deviations represent the upper error bound. This is the worst case, because both experimental errors and instrumental noise are involved. Hence, there is no averaging effect.

Table 13. The individual reaction rate constant estimates for eight repeated individual batch processes and the mean batch process using GRAM and GRAM-LM-PAR (values between parentheses).

Number batch run	Estimated k_1 (min^{-1})	Estimated k_2 (min^{-1})
1	0.28 (0.25)	0.11 (0.10)
2	0.33 (0.29)	0.08 (0.08)
3	0.28 (0.28)	0.08 (0.08)
4	0.29 (0.19)	0.17 (0.12)
5	0.26 (0.23)	0.14 (0.13)
6	0.29 (0.27)	0.01 (0.01)
7	0.28 (0.28)	0.06 (0.06)
8	0.22 (0.18)	0.18 (0.15)
	$\bar{k}_1$ = 0.28, STD = 0.03 ($\bar{k}_1$ = 0.25, STD = 0.04)	$\bar{k}_2$ = 0.10, STD = 0.06 ($\bar{k}_2$ = 0.09, STD = 0.04)
Mean batch process	0.28 (0.27)	0.07 (0.07)

From Table 13 the following can be observed:

1) If the individual standard deviations are considered, the precision of the k_2 estimates is better if GRAM-LM-PAR is used instead of GRAM.
2) The precision of the k_2 estimates is poorer than the precision of the k_1 estimates caused by the dominance of k_1 and the high noise level present in the experimental data.

3) The GRAM estimates are nearly always higher for both reaction rate constants compared to the GRAM-LM-PAR estimates.

The precision of reaction rate constant estimates is improved using LM-PAR steps after the GRAM solution obtained, because the LM-PAR part is a least squares algorithm and GRAM is not a least squares algorithm. From the literature,[1] it is known that the application of GRAM can lead to biased estimates and a possible method to correct for the obtained biased estimates has been proposed. There appeared to be a big difference in speed between GRAM and GRAM-LM-PAR: GRAM only took a few seconds, whereas GRAM-LM-PAR took a few hours.

Estimation of the lower error bound

The jackknife based procedure described in Section 4.3 of Chapter 4 has been used to estimate the lower error bound. The jackknife interval has been chosen equal to 26. This resulted in ten jackknife estimations for k_1 and k_2 for the mean batch process of dataset 1. The jackknife procedure has been applied using both algorithms. The time shift was again equal to 30 spectra. The mean estimated kinetic parameters based on ten jackknife estimations and the corresponding individual standard deviations (lower error bounds) obtained with both algorithms are listed in Table 14. The lower error bounds represent mainly instrumental noise. From Table 14, it is observed that the use of GRAM-LM-PAR leads to a decrease of the influence of instrumental noise for the k_1 estimates.

Table 14. The results from the jackknife procedure of the mean batch process using GRAM and GRAM-LM-PAR (values between parentheses).

Mean k_1 (min^{-1})	STD k_1 (min^{-1})	Mean k_2 (min^{-1})	STD k_2 (min^{-1})
0.28 (0.27)	$2.00 \cdot 10^{-3}$ ($1.10 \cdot 10^{-3}$)	0.07 (0.07)	$1.60 \cdot 10^{-3}$ ($1.50 \cdot 10^{-3}$)

Summary results

GRAM-LM-PAR performs better than GRAM. Simulations and experimental data showed that both algorithms can deal with a large spectral overlap. From experimental data, the optimal time shift appears to be roughly 30 or 40 spectra. Experimental data showed, that if the time shift is small or large k_1 and k_2 estimates can be equal.

Simulations showed that these estimates can also be equal if the noise level is increased, because probably no distinction can be made between the two exponentially decaying functions. This problem can easily be detected, because if k_1 equals k_2 the

first two columns of the **C**-matrix (loading matrix obtained by solving a GEP) are identical. If the upper error bound is considered and the performance of GRAM-LM-PAR is compared to the performance of GRAM, the precision of the k_2 estimates is the best if GRAM-LM-PAR is used. The GRAM estimates are always higher than the GRAM-LM-PAR estimates. For the lower error bound the precision of the k_1 estimates is approximately a factor two better using GRAM-LM-PAR instead of GRAM. Despite the fact that the precision of reaction rate constant estimates is poorer if GRAM is used instead of GRAM-LM-PAR, GRAM is very powerful if rapid estimates of reaction rate constants are necessary.

7.2.4 Conclusions

In this Section, GRAM has been used in order to estimate reaction rate constants from on-line SW-NIR measurements (dataset 1) of a reacting system. The interpretation is very easy. The third factor matrix of the three-way array, **C**, gives the reaction rate constants. GRAM-LM-PAR can be used if precise estimates of reaction rate constants are desirable. GRAM can be used to obtain rough estimations of reaction rate constants very fast. Simulations showed that both algorithms can deal with a strong spectral overlap. If the noise level is increased the reaction rate constants estimates can become equal for a simulated dataset. From the simulations it can be concluded, that GRAM-LM-PAR always leads to more precise estimates of reaction rate constants compared to GRAM, because the LM-PAR part of GRAM-LM-PAR is a least squares algorithm.

The results obtained from dataset 1 showed a small difference between GRAM and GRAM-LM-PAR, but GRAM-LM-PAR always leads to more precise estimates for the reaction rate constants compared to GRAM. The optimal time shift appeared to be roughly 30 or 40 spectra in this case. If the time shift parameter is large or small the reaction rate constant estimates can become equal and a poor precision of reaction rate constant estimates is obtained. Probably, it is very hard to distinguish between exponentially decaying functions for these choices of the time shift parameter. Upper and lower error bounds have been estimated also for quality assessment.

GRAM is a very powerful method for estimating reaction rate constants very fast. The speed of the algorithm is known in advance, because of its non-iterative nature. GRAM can be used if rough estimates of kinetic parameters are desirable, for instance if (batch) processes are monitored. GRAM-LM-PAR is in this case not very convenient to use because of the time consuming iterations. In case of GRAM-LM-PAR the speed of the algorithm is not known in advance. If the batch time is elapsed GRAM-LM-PAR can be used to estimate kinetic parameters precisely. Since many measurements are based on exponential functions, GRAM and

GRAM-LM-PAR can have many applications in chemistry.

7.3 UV-Vis data

7.3.1 Introduction

In this Section, GRAM and GRAM-LM-PAR are applied in order to estimate reaction rate constants from the UV-Vis measurements of dataset 2, described in Section 5.3 of Chapter 5. The choice of the time shift parameter has been investigated. The pure spectra of the reacting absorbing species are estimated very easily, without complicated procedures, and compared to their measured pure spectra. If species are unknown, spectrum library search methods can be used to identify the estimated pure spectra of these unknown species. Quality assessment of the estimated reaction rate constants has been performed using a jackknife based method, described in Section 4.3 of Chapter 4.

7.3.2 Results and discussion

EFFECT OF THE TIME SHIFT ON REACTION RATE CONSTANT ESTIMATES

In order to investigate the effect of different time shifts, the kinetic parameters have been estimated for the ten repeated individual batch processes of dataset 2 using GRAM for different time shifts. The results are listed in Table 15. The values of the column with constants added to **X** were equal to 100000. These values will dominate compared to the absorbances differences in time of the UV-Vis spectra (see Figure 14, Section 5.3.3, Chapter 5). From Table 15 the following can be observed:

1) A small time shift results in a poor precision for both k_1 and k_2 estimates.
2) A large time shift results in a poor precision for the k_1 estimates and a good precision for the k_2 estimates.
3) A time shift of 30 spectra is a compromise, because this gives the best precision for k_1 estimates and a compromise in precision for the k_2 estimates. For this reason a time shift of 30 spectra is used for dataset 2 in the remainder of this Chapter.

An important remark is the computation time of reaction rate constants using GRAM or GRAM-LM-PAR. In this case GRAM takes only a few seconds, but GRAM-LM-PAR takes a few hours to perform the necessary iterations, approximately 4000-5000. Hence, GRAM is very fast. The aspects mentioned concerning the computation time were also observed for the SW-NIR dataset investigated in Section 7.2 of this Chapter.

Table 15. The mean estimated reaction rate constants and the individual standard deviations (STD's) obtained using GRAM for different time shifts.

Time Shift	Mean k_1 (min^{-1})	STD k_1 (min^{-1})	Mean k_2 (min^{-1})	STD k_2 (min^{-1})
1	0.3129	0.0239	0.0267	0.0075
2	0.3083	0.0159	0.0280	0.0048
3	0.3062	0.0129	0.0287	0.0036
4	0.3052	0.0112	0.0290	0.0028
5	0.3050	0.0104	0.0291	0.0023
6	0.3048	0.0098	0.0291	0.0020
7	0.3047	0.0094	0.0291	0.0018
8	0.3046	0.0091	0.0291	0.0017
9	0.3047	0.0089	0.0291	0.0015
10	0.3047	0.0087	0.0291	0.0015
20	0.3052	0.0083	0.0286	0.0011
30	0.3040	0.0083	0.0284	0.0010
40	0.3019	0.0091	0.0282	0.0010
50	0.3006	0.0093	0.0280	0.0009
60	0.2995	0.0099	0.0280	0.0008
70	0.2971	0.0096	0.0279	0.0008
80	0.2945	0.0096	0.0279	0.0008

ESTIMATION OF THE UPPER ERROR BOUND

The individual estimates of the kinetic parameters for each repeated individual batch process and the mean batch process of dataset 2 are listed in Table 16 for a time shift of 30 spectra. The mean batch process has been obtained by averaging ten repeated individual batch process runs of dataset 2. The individual standard deviations represent the upper error bound. From Table 16 the following can be observed:

1) If the individual standard deviations are considered, there is no improvement in the precision of reaction rate constant estimates if GRAM-LM-PAR is used instead of GRAM. Both methods perform approximately the same. The mean value for k_1 is higher for GRAM-LM-PAR compared to GRAM. For the k_2 estimates the opposite is valid. Because there is a correlation between the two reaction rate constants, higher k_1 values tend to occur with lower k_2 values.
2) The precision of the k_1 estimates is poorer than the precision of the k_2 estimates.

Table 16. The individual reaction rate constant estimates using GRAM and GRAM-LM-PAR (values between parentheses).

Number batch run	Estimated k_1 (min^{-1})	Estimated k_2 (min^{-1})
1	0.3006 (0.3106)	0.0287 (0.0263)
2	0.3009 (0.3117)	0.0288 (0.0261)
3	0.3040 (0.3117)	0.0285 (0.0264)
4	0.3137 (0.3192)	0.0280 (0.0262)
5	0.3069 (0.3093)	0.0265 (0.0263)
6	0.2932 (0.3070)	0.0298 (0.0262)
7	0.2985 (0.3230)	0.0297 (0.0246)
8	0.3180 (0.3244)	0.0275 (0.0260)
9	0.3109 (0.3304)	0.0277 (0.0232)
10	0.2936 (0.3002)	0.0285 (0.0265)
GRAM: LM-PAR:	$\bar{k}_1$ = 0.3040, STD = 0.0083 $\bar{k}_1$ = 0.3147, STD = 0.0092	$\bar{k}_2$ = 0.0284, STD = 0.0010 $\bar{k}_2$ = 0.0258, STD = 0.0011
Mean batch run	0.3038 (0.3146)	0.0284 (0.0258)

For the reaction rate constant estimates of the mean batch process run of dataset 2 obtained with both GRAM and GRAM-LM-PAR the relative fit error has been estimated as described in Section 3.6 of Chapter 3. The relative fit error is $1.9 \cdot 10^{-3}$ for GRAM and $2.8 \cdot 10^{-4}$ for GRAM-LM-PAR, indicating that the reaction model proposed fits very well. The relative fit error is reduced if GRAM-LM-PAR is used instead of GRAM. Despite the larger relative fit error for GRAM compared to GRAM-LM-PAR, GRAM can be used to estimate reaction rate constants very fast.

ESTIMATION OF THE LOWER ERROR BOUND

The jackknife based procedure has been applied for both algorithms. The jackknife interval has been chosen equal to 25. Finally, this resulted in ten jackknife estimates for k_1 and k_2 for the mean batch process run of dataset 2. The time shift was again equal to 30 spectra. The mean estimated kinetic parameters based on ten jackknife estimations and the corresponding standard deviations (lower error bounds) obtained with both algorithms are listed in Table 17. From this table it is obvious that the use of GRAM-LM-PAR leads to a decrease of the influence of instrumental noise for both k_1 and k_2 estimates.

Table 17. The results from the jackknife procedure of the mean batch process run using GRAM and GRAM-LM-PAR (values between parentheses).

Mean k_1 (min^{-1})	STD k_1 (min^{-1})	Mean k_2 (min^{-1})	STD k_2 (min^{-1})
0.3037 (0.3146)	$1.5425 \cdot 10^{-4}$ ($9.8398 \cdot 10^{-5}$)	0.0284 (0.0258)	$4.1912 \cdot 10^{-5}$ ($1.0852 \cdot 10^{-5}$)

PURE SPECTRA ESTIMATES

For the k_1 and k_2 estimates for both algorithms for the mean batch process run, the pure spectra of the reacting absorbing species have been estimated by means of reconstructing the concentration profiles (matrix **F**) and applying a non-negative least squares step using **F** and **X**. Figure 27 shows difference spectra for the reactant and product using the GRAM and GRAM-LM-PAR results for reconstructing the concentration profiles. The difference spectra have been obtained by subtracting the estimated pure spectrum from the measured pure spectrum. From Figure 27 it is obvious, that GRAM-LM-PAR estimates for the reaction rate constants lead to pure spectra estimates which are closer to the measured pure spectra compared to GRAM results. This is caused by the fact that the LM-PAR part of GRAM-LM-PAR is a least squares algorithm, whereas GRAM is not a least squares algorithm.

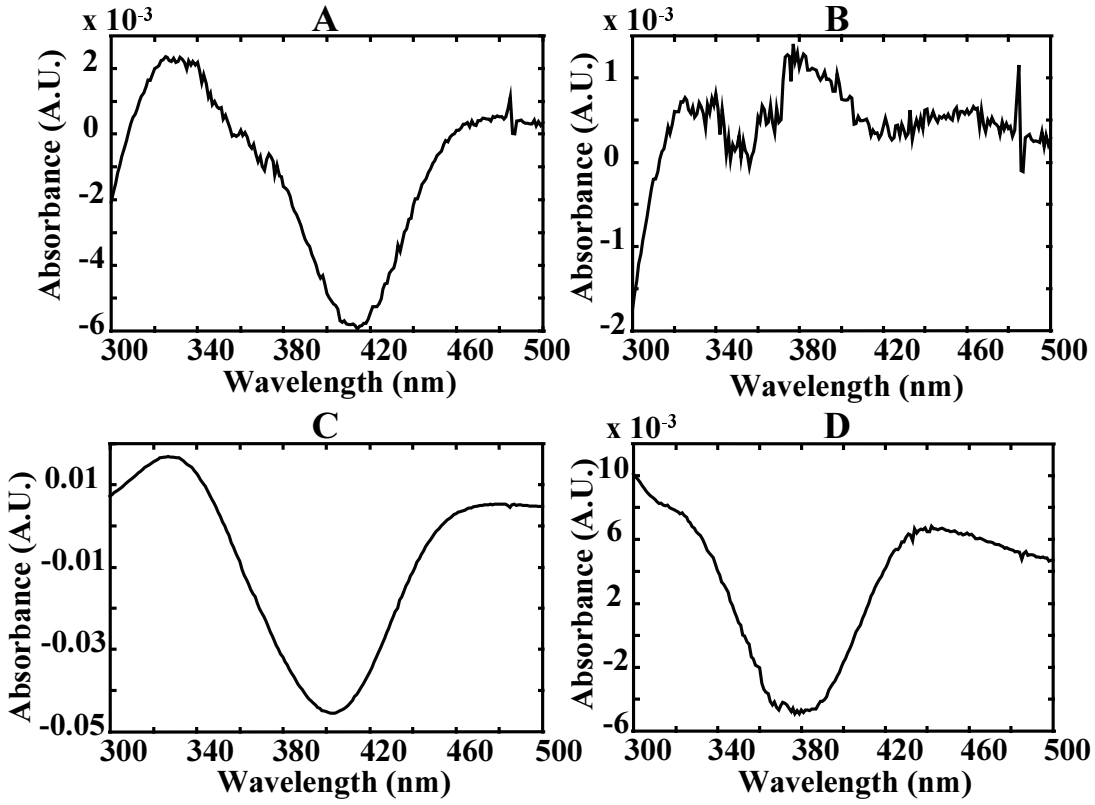

Figure 27. Difference spectra; reactant using GRAM (A), reactant using GRAM-LM-PAR (B), product using GRAM (C) and product using GRAM-LM-PAR (D).

SUMMARY RESULTS

A time shift of 30 spectra appeared to give the best precision for the k_1 estimates and a compromise in precision for the k_2 estimates if GRAM was used. For all the different batch process runs the reaction rate constants have been obtained both with GRAM and GRAM-LM-PAR for this time shift of 30 spectra. The obtained precision for the reaction rate constant estimates showed that there is hardly a difference in performance between GRAM and GRAM-LM-PAR. This is probably caused by the fact that the signal to noise ratio of the dataset is excellent and the absorbance differences in time are very large. For the mean batch process run the reaction rate constants have been estimated using both algorithms. The relative fit errors are $1.9 \cdot 10^{-3}$ and $2.8 \cdot 10^{-4}$ for GRAM and GRAM-LM-PAR, respectively. These values indicate that the kinetic model proposed fitted the best using GRAM-LM-PAR. However, the fit error value for GRAM is still acceptable. The jackknife procedure showed that the influence of the instrumental noise on the precision of both reaction rate constant estimates is smaller using GRAM-LM-PAR compared to GRAM.

Finally, the pure spectra have been estimated for the GRAM-LM-PAR and GRAM results. The pure spectra of reactant and product showed a very good agreement with the measured pure spectra. The difference between the estimated pure spectra and the measured pure spectra is smaller for reaction rate constants which have been obtained by GRAM-LM-PAR compared to the GRAM results.

7.3.3 Conclusions

In this Section, it is shown that GRAM can be used as a very fast non-iterative algorithm in order to estimate reaction rate constants from the UV-Vis spectra of dataset 2. The precision of the reaction rate constant estimates is comparable to the precision obtained with GRAM-LM-PAR. However, GRAM gives a larger fit error. GRAM-LM-PAR can be used in situations where an accurate estimate of reaction rate constants is desirable and there is enough time available to perform the tedious iterations (approximately 4000-5000) which characterizes the GRAM-LM-PAR algorithm. A time shift of 30 spectra appeared to be optimal for this application. This has to be established in practice again for other kinetic model systems.

If the pure spectra estimates of the reacting absorbing species involved in the reaction model are compared with the measured pure spectra the difference is very small. GRAM-LM-PAR gives better pure spectra estimates compared to GRAM.

7.4 General conclusions

From the results described in this Chapter obtained with dataset 1 and dataset 2, some general conclusions can be formulated:

1) For noisy datasets (dataset 1 in this case) GRAM-LM-PAR leads to a better precision of reaction rate constant estimates compared to GRAM, because the LM-PAR part is a least squares algorithm.
2) For datasets with an excellent signal to noise ratio and large absorbance differences in time (dataset 2 in this case) GRAM-LM-PAR and GRAM perform the same with respect to the precision of reaction rate constant estimates. Hence, if the noise level of the data is low a least squares algorithm will hardly improve the precision of parameter estimates. However, a lower fit error is obtained for GRAM-LM-PAR.

7.5 References

1. Faber K, Lorber A, Kowalski BR. 'Generalized rank annihilation method: Standard errors in the estimated eigenvalues of the instrumental errors are heteroscedastic and correlated'. *J. Chemometrics*, 1997; **11**: 95-110.

Chapter 8

Comparison Between Two-Way and Three-Way Methods

8.1 Introduction

In Chapter 6 and 7, applications of two-way and three-way methods to different datasets have been discussed. In this Chapter,[i] the performance of classical curve resolution (CCR) with constraint RP implemented (see Section 2.7, Chapter 2), weighted curve resolution (WCR), the generalized rank annihilation method (GRAM), the generalized rank annihilation-Levenberg-Marquardt-parallel factor analysis (GRAM-LM-PAR) method, the trilinear decomposition method (TLD) and the trilinear decomposition method-Levenberg-Marquardt-parallel factor analysis (TLD-LM-PAR) method are compared. This is the only Chapter of the thesis where results obtained with TLD and TLD-LM-PAR are reported. The theory of TLD and TLD-LM-PAR has been described in Chapter 3. Because of the comparison of two-way and three-way methods, some results described already in Chapter 6 and 7 are repeated in this Chapter, which is unavoidable. The starting values of the reaction rate constants used for the two-way methods have been reported in Section 5.2.4 and Section 5.3.5 of Chapter 5. If other sets of starting values were used, similar results were obtained.

8.2 SW-NIR and UV-Vis data

8.2.1 Introduction

In this Section, the precision and speed of CCR using *a priori* spectral information (constraint RP), WCR, GRAM, GRAM-LM-PAR, TLD and TLD-LM-PAR are compared using dataset 1 and dataset 2. These datasets have been described in

[i] This Chapter is based on the following paper:

- Bijlsma S, Smilde AK. 'Estimating reaction rate constants from a two-step reaction: comparison between two-way and three-way methods'. *J. Chemometrics*, accepted.

Section 5.2 and Section 5.3 of Chapter 5. The theory of the algorithms has been described in Chapter 2 (two-way methods) and Chapter 3 (three-way methods). Important properties of CCR, WCR, GRAM, GRAM-LM-PAR, TLD and TLD-LM-PAR are summarized in Table 18. All methods are least squares methods except GRAM and TLD. Dataset 1 has a moderate signal to noise ratio and dataset 2 has a high signal to noise ratio. Hence, both datasets represent extremes of what can be expected in chemical practice. In case of CCR using *a priori* spectral information, the pure spectra of reactant and product have been explicitly implemented in the algorithm resulting in constraint RP as described in Section 2.7 of Chapter 2. Quality assessment has been performed using a jackknife based method presented in Section 4.3 of Chapter 4.

Table 18. Important properties of CCR, WCR, GRAM, GRAM-LM-PAR, TLD and TLD-LM-PAR. In case of speed ++ means less than ten seconds (fast), + means more than ten seconds (medium) and - means minutes till hours (slow).

Algorithm	A priori information	Time shift	Number of slabs	Iterative	Speed	On-line
CCR	yes	no	1	yes	+	no
WCR	no	no	1	yes	+	no
GRAM	no	yes	2	no	++	yes
GRAM-LM-PAR	no	yes	2	yes	-	no
TLD	no	yes	≥ 3	no	++	yes
TLD-LM-PAR	no	yes	≥ 3	yes	-	no

8.2.2 Results and discussion

REACTION RATE CONSTANT ESTIMATES FROM INDIVIDUAL BATCH PROCESSES

Dataset 1

For eight individual batch process runs of dataset 1, the reaction rate constants have been estimated using WCR, GRAM, GRAM-LM-PAR, TLD (three and four slabs) and TLD-LM-PAR (three slabs). The results are listed in Table 19. The individual standard deviations represent the upper error bounds. The correlation coefficients, r, between the reaction rate constant estimates have been calculated and are also listed in Table 19. The absolute value for r gives an indication about the quality of the algorithm used. A small absolute value of r indicates that the algorithm can distinguish between k_1 and k_2 during the optimization procedure very easily. For GRAM and GRAM-LM-PAR the time shift was equal to 30 spectra. From Chapter 7 it appeared that this time shift led to the best precision of the k_1 and k_2 estimates. For TLD and TLD-LM-PAR the step size was equal to 20 spectra. It appeared that these

Table 19. Results for dataset 1.

Method	Mean k_1 (min^{-1})	STD k_1 (min^{-1})	Mean k_2 (min^{-1})	STD k_2 (min^{-1})	r
WCR	0.26	0.03	0.07	0.03	-0.61
GRAM (Time shift = 30)	0.28	0.03	0.10	0.06	-0.47
GRAM-LM-PAR (Time shift = 30)	0.25	0.04	0.09	0.04	-0.79
TLD, 3 slabs (Step size = 20)	0.25	0.03	0.10	0.06	-0.86
TLD, 4 slabs (Step size = 20)	0.22	0.03	0.11	0.10	-0.93
TLD-LM-PAR, 3 slabs (Step size = 20)	0.24	0.05	0.09	0.04	-0.87

values led to the best precision of reaction rate constant estimates obtained from the results of the individual batches of dataset 1 which are not reported here.

From Table 19 the following can be observed:

1) The best precision of both reaction rate constant estimates is obtained using WCR.
2) All algorithms have led to a similar precision of the k_1 estimates.
3) The precision of the k_2 estimates is very dependent on the algorithm used.
4) There is no improvement in precision of both reaction rate constants if more than two slabs are used. The use of TLD and TLD-LM-PAR have led to no improvement of precision of reaction rate constant estimates compared to the results obtained with GRAM and GRAM-LM-PAR, respectively. Hence, there is no noise reduction if more than two slabs are used. Note, that the same data are used over and over again if slabs are created and therefore the same noise realization of the data is used again and again.
5) GRAM-LM-PAR and TLD-LM-PAR have led to an improvement in precision of the k_2 estimates compared to the results obtained with GRAM and TLD, respectively.
6) With respect to the calculated correlation coefficients GRAM gives the lowest value indicating that GRAM can distinguish between k_1 and k_2 very well.

Because the signal to noise ratio of dataset 1 is moderate and the dominance of k_1, iterative algorithms improve the precision of the k_2 estimates obtained with

non-iterative algorithms.

Dataset 2

For ten individual batch processes of dataset 2, the reaction rate constants have been estimated using CCR with implementation of constraint RP, WCR, GRAM, GRAM-LM-PAR, TLD (three and four slabs) and TLD-LM-PAR (three slabs). The results are listed in Table 20. For GRAM and GRAM-LM-PAR a time shift of 30 spectra has been used. From Chapter 7, it appeared that this time shift led to the best precision for the k_1 and k_2 estimates. For TLD and TLD-LM-PAR the step size was equal to 15 spectra. It appeared that these values led to the best precision of reaction rate constant estimates obtained from the results of the individual batches of dataset 2 which are not reported here. The correlation coefficient, r, between the k_1 and k_2 estimates is also given in Table 20.

Table 20. Results for dataset 2.

Method	Mean k_1 (min^{-1})	STD k_1 ($\cdot 10^{-2}$ min^{-1})	Mean k_2 (min^{-1})	STD k_2 ($\cdot 10^{-2}$ min^{-1})	r
CCR	0.32	0.98	0.03	0.02	-0.54
WCR	0.31	0.98	0.03	0.11	-0.82
GRAM (Time shift = 30)	0.30	0.83	0.03	0.10	-0.71
GRAM-LM-PAR (Time shift = 30)	0.31	0.92	0.03	0.11	-0.79
TLD, 3 slabs (Step size = 15)	0.30	0.82	0.03	0.10	-0.78
TLD, 4 slabs (Step size = 15)	0.30	0.93	0.03	0.09	-0.82
TLD-LM-PAR, 3 slabs (Step size = 15)	0.32	0.91	0.03	0.11	-0.78

From Table 20 the following can be observed:

1) All algorithms led to approximately the same order of magnitude for the precision of the k_1 estimates.
2) Using CCR the best precision for the k_2 estimates is obtained. Hence, using *a priori* spectral information is advantageous.

3) A compromise in precision of both reaction rate constant estimates is obtained with CCR using *a priori* spectral information. Using this method the precision for the k_1 estimates is acceptable.
4) There is hardly an improvement in precision for both reaction rate constant estimates if three-way algorithms with more than two slabs are used. Hence, there is hardly a noise reducing effect.
5) GRAM-LM-PAR and TLD-LM-PAR led to no improvement in precision for both reaction rate constant estimates compared to GRAM and TLD, respectively. This is caused by the very low noise level of the data.
6) With respect to k_1 and k_2 the non-iterative GRAM algorithm gives approximately the same precision of reaction rate constant estimates compared to other algorithms. Only CCR led to a better precision for the k_2 estimates.
7) With respect to the calculated correlation coefficients CCR gives the lowest value indicating that CCR can distinguish between k_1 and k_2 very well because spectral information that is known *a priori* is used in the algorithm.

Because the signal to noise ratio of the data is high, iterative least squares algorithms will hardly improve the precision of reaction rate constant estimates obtained with non-iterative algorithms. Hence, in case of data with a high signal to noise ratio it is not necessary to perform tedious iterations.

JACKKNIFE RESULTS (LOWER ERROR BOUNDS)

Dataset 1

In order to obtain lower error bounds the jackknife based procedure as described in Section 4.3 of Chapter 4 has been applied for the different algorithms considered. Using a certain jackknife interval, a fixed number of spectra has been left out. With the left over spectra the reaction rate constants have been estimated using different algorithms. The jackknife results for dataset 1 are listed in Table 21. Using three-way methods the number of spectra left will be less compared to two-way methods because of the applied time shift or step size. The number of left over spectra must be the same for every algorithm for a fair comparison between lower error bounds obtained with different algorithms. This can be achieved by applying different jackknife intervals as is obvious from Table 21. Hence, each algorithm applied has a specific jackknife interval resulting in the same number of left over spectra. From Table 21 the following aspects can be observed:

1) GRAM-LM-PAR gives a compromise in a lower error bound estimate for both reaction rate constants. Using this method the best precision for the k_2 estimates is

obtained and an acceptable precision for the k_1 estimates. The best precision for the k_1 estimates is obtained with TLD-LM-PAR.

2) The use of GRAM-LM-PAR and TLD-LM-PAR will always lead to an improvement of the precision of reaction rate constant estimates compared to the results obtained with GRAM and TLD, respectively. This is because of the moderate signal to noise ratio of the data. The improvement in precision is approximately a factor two for the k_1 estimates if GRAM-LM-PAR is used instead of GRAM. For the k_2 estimates there is hardly an improvement in precision if GRAM-LM-PAR is used instead of GRAM.

Table 21. The jackknife results for the mean batch process for dataset 1.

Method	Jackknife interval	Mean k_1 (min^{-1})	STD k_1 ($\cdot 10^{-2}$ min^{-1})	Mean k_2 (min^{-1})	STD k_2 ($\cdot 10^{-2}$ min^{-1})
WCR	31	0.26	0.10	0.07	0.18
GRAM (Time shift = 30)	26	0.28	0.20	0.07	0.16
GRAM-LM-PAR (Time shift = 30)	26	0.27	0.11	0.07	0.15
TLD, 3 slabs (Step size = 20)	24	0.25	0.18	0.08	0.22
TLD-LM-PAR, 3 slabs (Step size = 20)	24	0.26	0.08	0.08	0.22

Dataset 2

The jackknife results for dataset 2 are listed in Table 22. Because the number of spectra of dataset 2 is different from dataset 1 the applied jackknife intervals for dataset 2 differ from the jackknife intervals for dataset 1. From Table 22 the following can be observed:

1) CCR gives the best precision for the lower error bound.
2) The use of GRAM-LM-PAR and TLD-LM-PAR result in an improvement in precision of reaction rate constant estimates compared to those obtained with GRAM and TLD, respectively. The gain in precision is approximately a factor two for k_1 and a factor four for k_2 if GRAM-LM-PAR is used instead of GRAM.

Table 22. The jackknife results for the mean batch process for dataset 2.

Method	Jackknife interval	Mean k_1 (min^{-1})	STD k_1 ($\cdot 10^{-3}$ min^{-1})	Mean k_2 (min^{-1})	STD k_2 ($\cdot 10^{-4}$ min^{-1})
CCR	27	0.32	0.03	0.03	0.01
WCR	27	0.32	0.12	0.03	0.13
GRAM (Time shift = 30)	25	0.30	0.15	0.03	0.42
GRAM-LM-PAR (Time shift = 30)	25	0.31	0.10	0.03	0.11
TLD, 3 slabs (Step size = 15)	25	0.30	0.24	0.03	0.39
TLD-LM-PAR, 3 slabs (Step size = 15)	25	0.31	0.09	0.03	0.10

ESTIMATES OF PURE SPECTRA

For the k_1 and k_2 estimates from Table 20 for WCR and GRAM the concentration profiles have been reconstructed. This has not been done for the k_1 and k_2 estimates obtained using TLD, GRAM-LM-PAR and TLD-LM-PAR because these reaction rate constant estimates were very similar to those obtained with GRAM, WCR and CCR, respectively. From the spectra of the mean batch process run and the reconstructed concentration profiles the pure spectra of reactant, intermediate and product have been estimated for dataset 2 by means of a non-negative least squares step. The estimated pure spectra of the reactant and product have been subtracted from the measured spectra of those species. The difference spectra are shown in Figure 28 and Figure 29 for the reactant and product, respectively. From these figures it can be observed that there is some structure present in the difference spectra, but the residuals are quite small. GRAM gives the largest difference spectrum for the reactant and product, because this is no least squares algorithm, whereas WCR is a least squares algorithm.

8.2.3 Conclusions

In this Chapter, two-way methods and three-way methods have been compared using dataset 1 and dataset 2. WCR has led to the best precision of the reaction rate constant estimates for dataset 1. GRAM performed very well, but the precision of the reaction rate constant estimates is improved if iterations are performed after the GRAM solution. This is because of the moderate signal to noise ratio of dataset 1. CCR has led to the best precision of reaction rate constant estimates for dataset 2. Using CCR it is possible to implement spectral information that is known before-hand into the

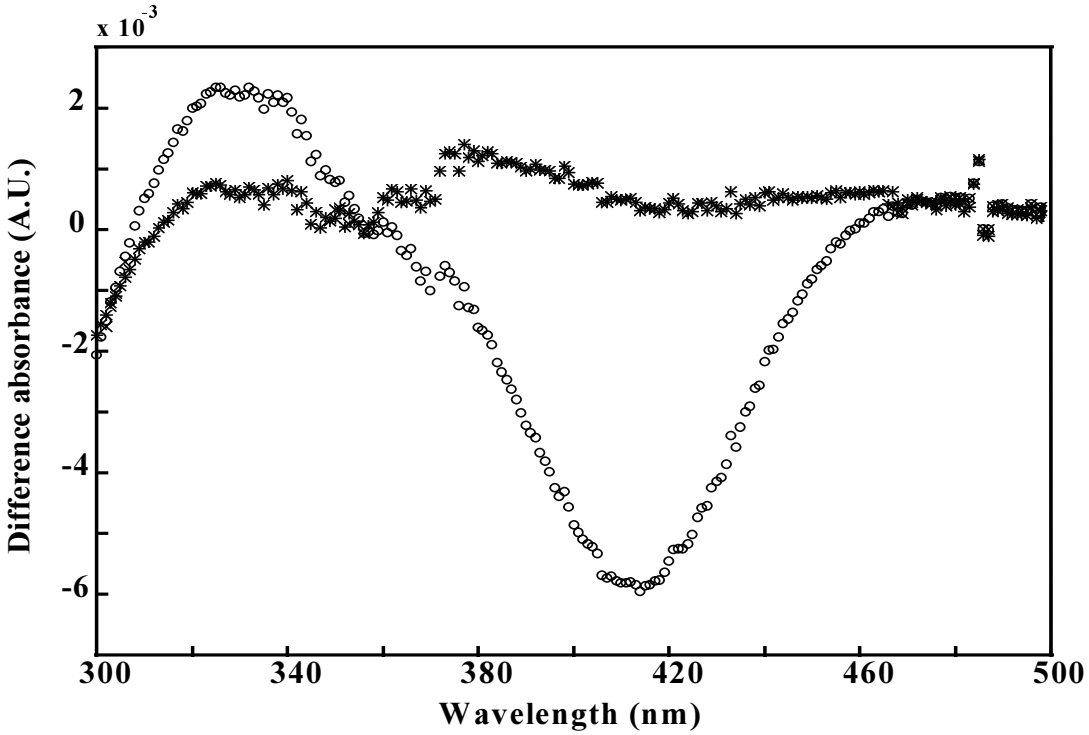

Figure 28. The difference spectra for the reactant obtained with: WCR (*) and GRAM (o).

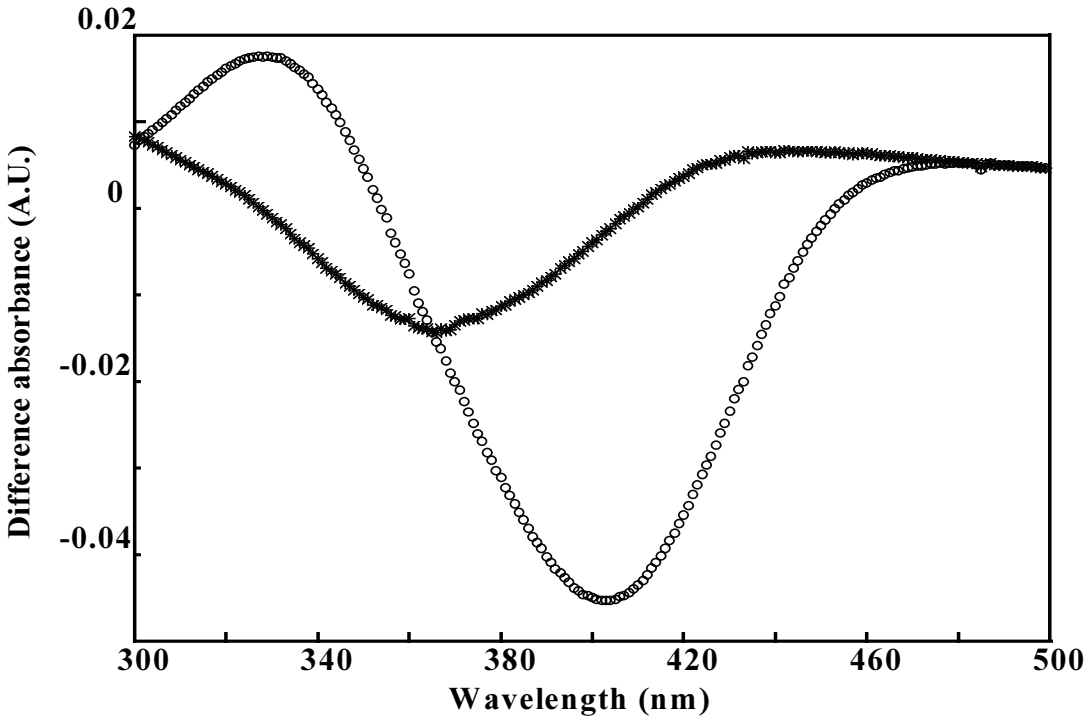

Figure 29. The difference spectra for the product obtained with: WCR (*) and GRAM (o).

algorithm. The WCR algorithm does not use this kind of spectral information. GRAM has led to approximately the same precision of reaction rate constant estimates compared to iterative methods. This is because of the high signal to noise ratio of dataset 2.

In general, two-way methods will lead to a better precision of reaction rate constant estimates compared to three-way methods. For every specific dataset a certain two-way algorithm will perform the best. The two-way methods CCR and WCR are both of medium speed. Because of the iterative nature of both WCR and CCR the exact speed of the algorithm needed to reach the optimal set of parameters is not known beforehand. This is dependent on the choice of the set of starting values. This makes CCR and WCR less suitable for on-line estimating reaction rate constants. In practice it is very often not necessary to know the values of reaction rate constants very precisely. Hence, it is not always necessary to use iterative algorithms. GRAM can be very convenient to use in that case, because the speed of this algorithm is known in advance. This makes GRAM extraordinarily suitable for on-line monitoring reaction rate constants. Both datasets used showed good results using GRAM and hence this method seems to be the best choice for on-line (pseudo) first order kinetic problems. For noisy datasets more reliable estimates of reaction rate constants can be obtained off-line using iterative algorithms.

Chapter 9

The Use of Constraints in Classical Curve Resolution

9.1 Introduction

In this Chapter,[i] the impact of constraints implemented in classical curve resolution (CCR) on the precision of reaction rate constant estimates is investigated using experimental data. Simulated data are used to study the impact of constraints in CCR on the accuracy of reaction rate constant estimates. Simulated data are also used to check if biased estimates are obtained using CCR with and without constraints implemented. The equations used to calculate the precision, the bias, the accuracy and the relative errors of reaction rate constant estimates have been presented in Section 4.2 of Chapter 4. Constraint R, constraint RP and constraint NNLS, which can be implemented in CCR, have already been discussed in Section 2.7 of Chapter 2. The starting values of the reaction rate constants used for the two-way methods have been reported in Section 5.3.5 of Chapter 5. If other sets of starting values were used, similar results were obtained.

9.2 UV-Vis data

9.2.1 Introduction

The goal of this Chapter is to determine the impact of the use of constraints in CCR on the accuracy of the reaction rate constant estimates, to establish whether it is an advantage to use constraints and to define guidelines for the use of constraints. This thesis reports a systematic study on this topic.

From dataset 3, described in Section 5.3 of Chapter 5, reaction rate constants and pure spectra of individual reacting absorbing species have been estimated simultaneously with and without constraints implemented in CCR. For the experimental data only the precision of the reaction rate constant estimates could be

[i] This Chapter is based on the following paper:

- Bijlsma S, Boelens HFM, Hoefsloot HCJ, Smilde AK. 'Constrained least squares methods for estimating reaction rate constants from spectroscopic data'. submitted.

investigated. It was not possible to check whether a bias is present, because the true values for the reaction rate constants are unknown. In order to investigate if biased reaction rate constant estimates can be obtained using CCR, simulations have been performed.

The set-up of the simulations has been chosen so that the simulated spectra are very similar to the spectra of the experimental dataset. The pure spectra and reaction rate constants estimates obtained from the experiments have been used to generate artificial datasets. Two different noise levels have been added.

The use of perfect *a priori* knowledge and imperfect *a priori* knowledge as constraints has been investigated. The results from the experimental dataset and the simulated dataset have been compared in order to define guidelines for the use of constraints.

9.2.2 Simulation set-up

The set-up of the simulations was chosen so that the simulated spectra of the reaction mixture were very similar to the spectra of the experiments. The simulations were performed using the following set-up:

1) The mean k_1 and k_2 from all individual reaction rate constant estimates for the experimental data were calculated. These means were equal to 0.2396 min^{-1} and 0.0266 min^{-1}, respectively (see Section 9.2.3). These values were used as true values in the simulations.
2) These mean k_1 and k_2 were used to reconstruct the concentration profiles assuming an initial concentration of 54 $\mu mol l^{-1}$ of the reactant (species *U*). This resulted in matrix **F**.
3) Matrix **X**, containing the simulated spectra of the reaction mixture in time was generated, using **F** and the pure molar absorbance spectra estimates (matrix **D**) of the reacting absorbing species obtained from one individual batch process run for CCR without constraints implemented. Hence, this individual batch process run chosen, was used to generate the model.
4) Normally distributed white noise was added to **X**. The sigma of the white noise was defined as a certain percentage of the maximum absorbance of the first simulated UV-VIS spectrum (first column) of **X**. Two different noise levels were used, 0.2% and 2%.

Datamatrix **X** containing the fixed noise level was generated 500 times. Each matrix **X** generated can be used for estimating reaction rate constants resulting in 500

reaction rate constant estimates. The starting values for the reaction rate constants were always the same and equal to those chosen for the experimental data discussed.

PERFECT *A PRIORI* KNOWLEDGE

In case of constraint R with perfect *a priori* knowledge, the first column of matrix **D** (pure spectrum of reactant) was fixed in CCR. In case of constraint RP with perfect *a priori* knowledge, the first and third column of **D** (pure spectra of reactant and product, respectively) were fixed and therefore not updated in CCR.

IMPERFECT *A PRIORI* KNOWLEDGE

In case of imperfect *a priori* knowledge two cases can be distinguished: adding noise to the imposed pure spectra or introducing realistic imperfections in the imposed pure spectra by means of shape differences.

In case of adding noise to the pure spectra, white noise was added to the imposed pure spectrum of the reactant (first column of **D**) for constraint R. For constraint RP, white noise was added to the imposed pure spectra of reactant and product (first and third column of **D**, respectively). The noise level added to the imposed pure spectra corresponded to the chosen noise level (0.2% or 2%) added to **X**.

In case of shape differences, realistic imperfections were introduced in the imposed pure spectra. Also large imperfections were introduced in the imposed pure spectra by means of applying large shape differences in these spectra. As already mentioned in Section 5.3.4 of Chapter 5, there are 32 averaged measured pure spectra of the reactant available for dataset 3. Next, difference spectra were calculated between the average pure spectrum of the reactant corresponding to the individual batch process run used to generate the simulation model and the 31 remaining averaged pure spectra of the reactant. The largest difference spectrum obtained was added to the first column of matrix **D** in order to obtain a pure spectrum of the reactant with realistic shape differences in the imposed pure spectrum present. Large shape differences were introduced in the pure spectrum of the reactant by multiplying the difference spectrum that is added to the first column of **D** with a factor ten.

In case of constraint RP, two averaged measured pure spectra of the product were available (see Section 5.3.4, Chapter 5). Next, the difference spectrum was calculated between these two averaged measured spectra of the product. This difference spectrum was added to the third column of matrix **D** in order to obtain a pure spectrum of the product with realistic shape differences present. Large shape differences were introduced in the pure spectrum of both reactant and product by multiplying the difference spectrum that is added to the first and third column of **D**,

respectively, with a factor ten. The imposed pure spectra in case of no shape differences, realistic shape differences and large shape differences present are shown in Figure 30 and Figure 31 for the reactant and product, respectively.

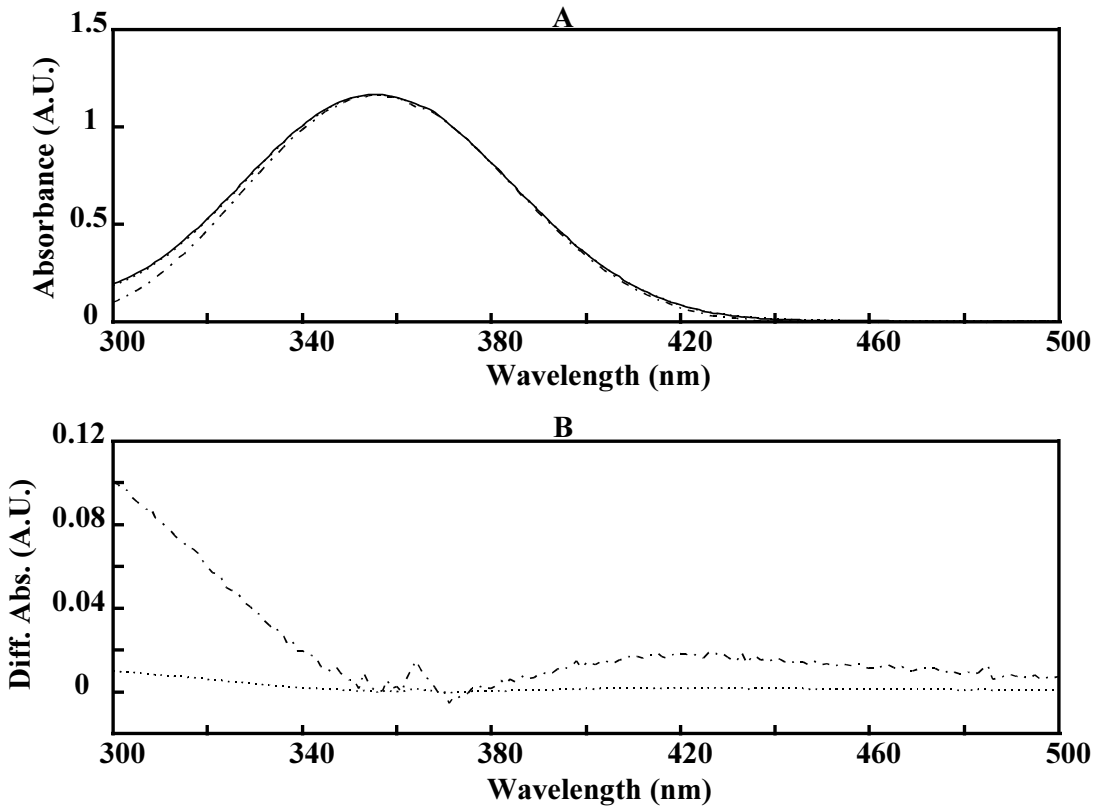

Figure 30. A. The imposed spectrum of the reactant without shape differences (solid line); realistic shape differences (dotted line); large shape differences (solid-dotted line). B. The differences between imposed pure spectrum without shape differences and the imposed pure spectrum with: realistic shape differences (dotted line); large shape differences (solid-dotted line).

9.2.3 Results and discussion

EXPERIMENTS

Precision of reaction rate constant estimates

The CCR algorithm with and without constraints implemented has been used to estimate the reaction rate constants from the pseudo-first order dataset (dataset 3) described. The reaction rate constant estimates from all individual batches are shown in Figure 32.

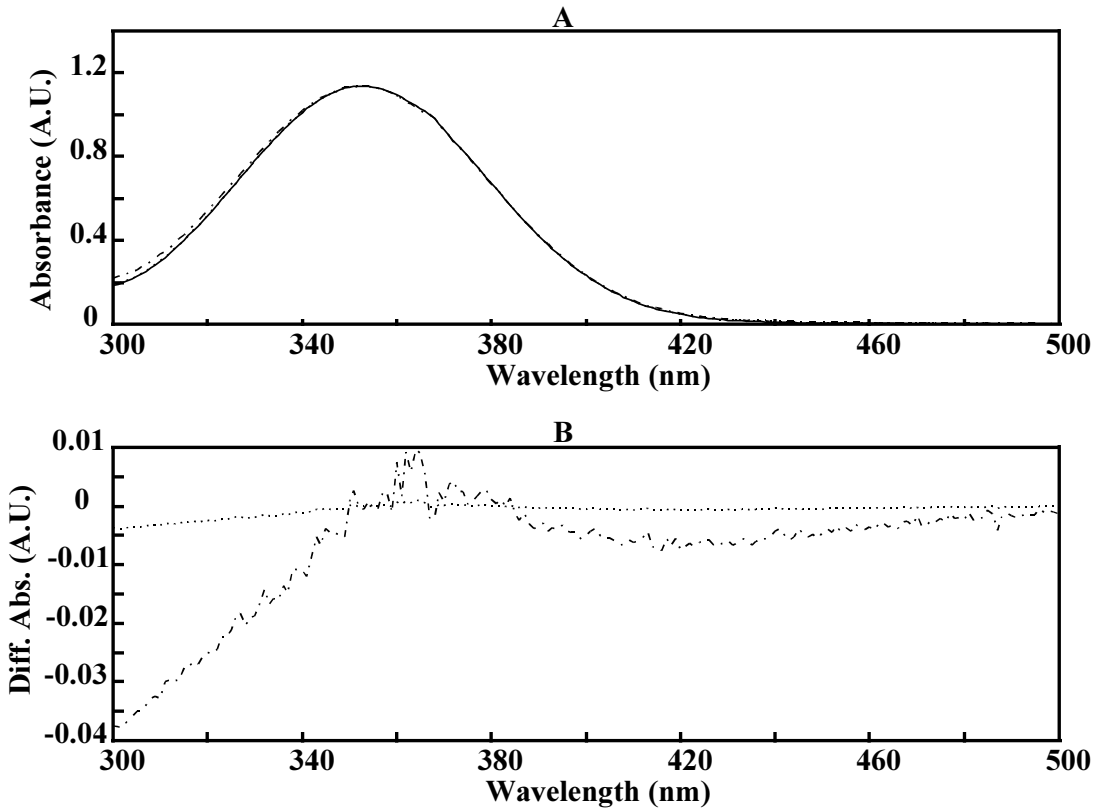

Figure 31. A. The imposed spectrum of the product without shape differences (solid line); realistic shape differences (dotted line); large shape differences (solid-dotted line). B. The differences between imposed pure spectrum without shape differences and the imposed pure spectrum with: realistic shape differences (dotted line); large shape differences (solid-dotted line).

From Figure 32 the following can be observed:

1) The use of constraint R (Figure 32B) has led to a slightly poorer precision of the k_2 estimates compared to the k_2 estimates using no constraints (Figure 32A). The precision of the k_1 estimates is the same.
2) The use of constraint RP (Figure 32C) has led to the best precision of the k_2 estimates compared to the results for no constraints (Figure 32A) and constraint R (Figure 32B). The precision of the k_1 estimates is the same again.

In general, it was expected that the use of constraints would improve the precision of both reaction rate constant estimates. It is possible, that noise and shape differences in the imposed pure spectrum of the reactant are responsible for the poorer precision in case of constraint R. It is not possible to check if biased estimates have been obtained, because the true values for the reaction rate constants are unknown. Both aspects are investigated in detail using the simulated data.

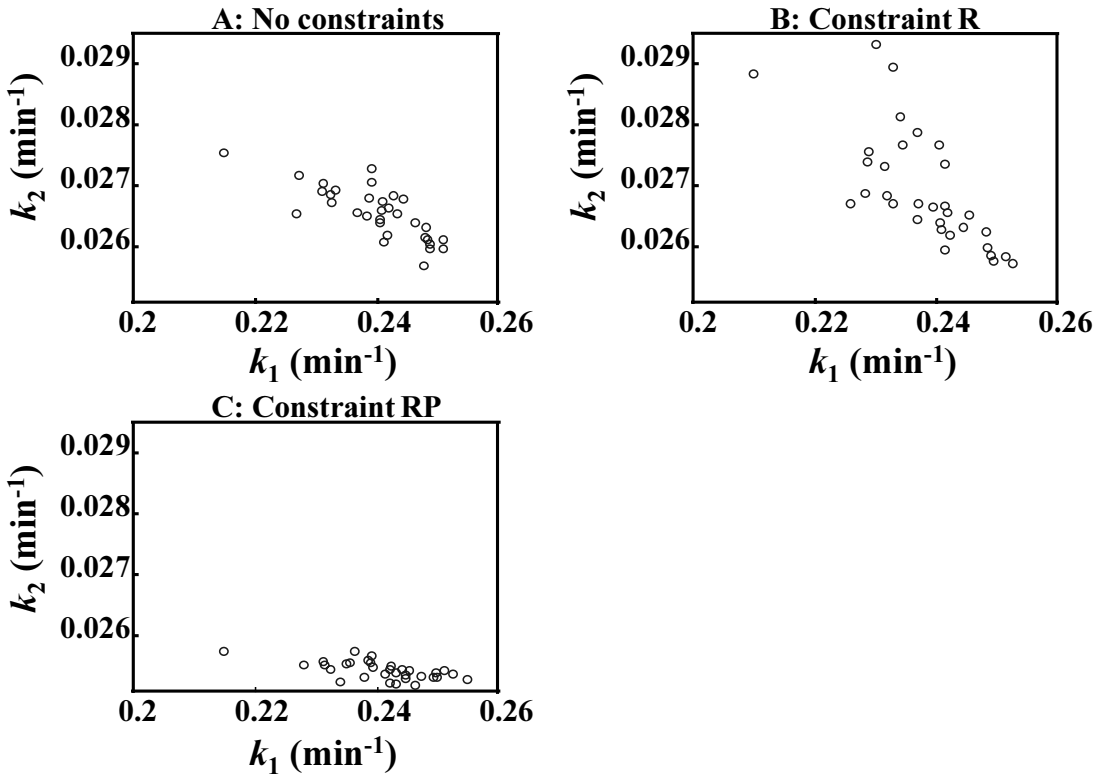

Figure 32. The individual reaction rate constant estimates using CCR.

Imposing constraint NNLS did not improve the precision of the reaction rate constant estimates in this case. In NNLS negative absorbances are not allowed. The noise level of the spectra taken in time of the reacting system is low and hence there are hardly negative absorbances present. Therefore, imposing the NNLS constraint will not improve the precision of reaction rate constant estimates.

Reconstruction error of the pure spectra

The estimated pure spectra of reactant and product using different constraints have been compared to their measured pure spectra. Difference spectra have been calculated by subtracting the measured pure spectrum from the estimated pure spectrum. The difference spectra obtained for one individual batch being representative for all batches are shown in Figure 33. In case of constraint R, only the difference spectrum obtained for the product can be calculated. From Figure 33 the following can be observed:

1) The order of magnitude of all difference spectra is small compared to the original spectra (max. absorbance 1.2 A.U.), see Figure 15, Section 5.3.4, Chapter 5. Yet, structure is still present in the difference spectra of the product (Figure 33A and 33B).

2) The difference spectrum of the reactant is smaller than the difference spectrum of the product (Figure 33A).

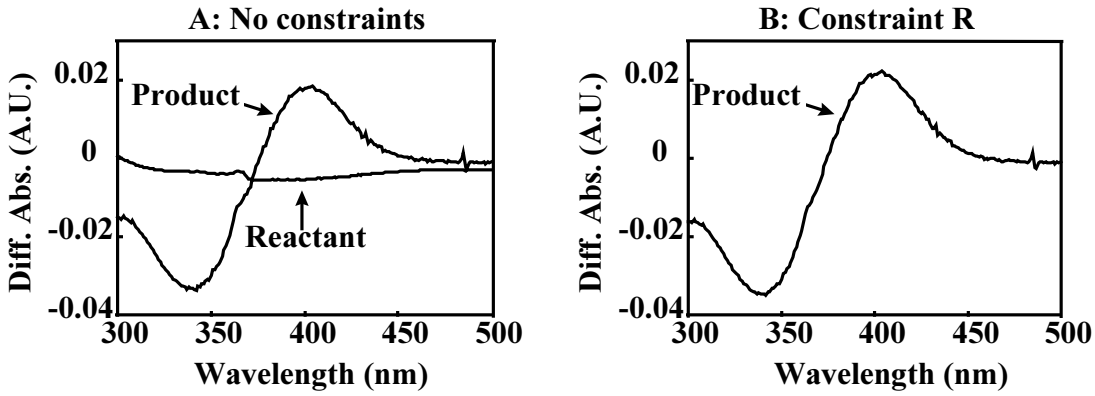

Figure 33. The difference spectra obtained for the reactant and product using one individual batch.

Datamatrix **X** contains a lot of information about the reactant, because of its dominant concentration at the start of the reaction. Therefore, a smaller difference spectrum is obtained for the reactant compared to the difference spectrum obtained for the product (Figure 33A). It was expected that a poorer precision of reaction rate constant estimates would correspond also to a poorer precision of the pure spectra estimates. However, if the precision of the reaction rate constant estimates becomes poorer, in case of CCR using constraint R (Figure 32B) compared to CCR without constraints (Figure 32A), this does not correspond to a larger difference spectrum of the product (compare Figure 33A and 33B).

The individual estimates of the intermediate spectrum show very small shape differences. If the precision of the k_2 estimates becomes poorer this is compensated by shape differences in the intermediate pure spectra estimates. A similar pure spectrum estimate of the product is obtained in case of a good and poor precision of the k_2 estimates, because the product is more dominantly present compared to the intermediate.

For all individual batches, the correlation coefficient between estimated and measured pure spectrum for the reactant and product has been calculated in case of CCR using no constraints. For the pure spectra estimates obtained with CCR using constraint R only the correlation coefficient between estimated and measured pure spectrum for the product has been calculated for all batches. If the correlation coefficient is equal to 1 this indicates a perfect match of estimated and measured pure spectrum. The correlation coefficients calculated were in all cases equal to 0.99 or higher.

Spectral residuals

The root mean sum of squares of residuals was equal to $1.6 \cdot 10^{-4}$ A.U. (no constraints), $2.9 \cdot 10^{-4}$ A.U. (constraint R) and $32 \cdot 10^{-4}$ A.U. (constraint RP). The root mean sum of squares of the spectral noise level is equal to $1.9 \cdot 10^{-4}$ A.U. From these values it can be concluded that hardly any overfitting occurs.

SIMULATIONS

Table 23 shows the simulation results in case of two different noise levels. Perfect *a priori* knowledge has been used. Hence, no noise or shape differences have been added to the imposed pure spectra. From Table 23 the following can be observed:

Precision

1) For both noise levels, the best precision of both reaction rate constant estimates is obtained using constraint RP.
2) For both noise levels, the precision of the k_1 estimates obtained using constraint R is slightly better than the results obtained in case of no constraints. The precision of the k_2 estimates is similar for constraint R and no constraints.
3) Imposing the NNLS constraint leads to a slight improvement of the precision of both reaction rate constant estimates only for a noise level of 2%.

Bias

Imposing the NNLS constraint leads to a large bias (approximately a factor 1000 for k_1 and a factor 160 for k_2) of reaction rate constant estimates for a noise level of 2%.

Accuracy

1) The best accuracy of both reaction rate constant estimates is obtained using constraint RP. This holds for both noise levels used.
2) For both noise levels, the accuracy of the k_1 estimates obtained using constraint R is better than the results obtained in case of no constraints. The accuracy of the k_2 estimates is similar for constraint R and no constraints.
3) For a noise level of 2% imposing the NNLS constraint leads to a poorer accuracy of reaction rate constant estimates compared to the results obtained in case of no constraints.

Using perfect *a priori* spectral knowledge is always useful with respect to the precisions and accuracies of reaction rate constant estimates with the exception of constraint NNLS. The best precision/accuracy of reaction rate constant estimates is obtained if constraint RP is implemented in CCR. If constraint R is used a better

Table 23. Simulation results for different constraints (constr.) in case of perfect *a priori* knowledge and two different noise levels. The relative error is indicated between parentheses in the columns of the accuracies.

Constr.	Noise level (%)	Precision $k_1 \cdot 10^{-9}$ $(min^{-1})^2$	Precision $k_2 \cdot 10^{-9}$ $(min^{-1})^2$	Bias $k_1 \cdot 10^{-9}$ $(min^{-1})^2$	Bias $k_2 \cdot 10^{-9}$ $(min^{-1})^2$	Accuracy $k_1 \cdot 10^{-9}$ $(min^{-1})^2$	Accuracy $k_2 \cdot 10^{-9}$ $(min^{-1})^2$
none	0.2	20	3	< 1	< 1	20 (<1%)	3 (<1%)
R	0.2	12	3	< 1	< 1	12 (<1%)	3 (<1%)
RP	0.2	4	< 1	< 1	< 1	4 (<1%)	< 1 (<1%)
NNLS	0.2	20	3	< 1	< 1	20 (<1%)	3 (<1%)
none	2	1973	257	1	< 1	1974 (<1%)	257 (<1%)
R	2	1169	227	7	1	1176 (<1%)	228 (<1%)
RP	2	345	3	2	< 1	347 (<1%)	3 (<1%)
NNLS	2	1383	150	1030	162	2413 (<1%)	312 (2%)

precision/accuracy for k_1 is obtained compared to the results in case of no constraints and a poorer precision/accuracy is obtained compared to the results for constraint RP. Datamatrix **X** contains less information about the product (low selectivity) compared to the reactant and there is a large spectral overlap present between the pure spectrum of the reactant and product. Hence, imposing constraint RP will result in a large gain in precision/accuracy of reaction rate constant estimates.

A higher noise level of the spectral data results in a large bias if constraint NNLS is imposed. An explanation for this is the existence of negative absorbances in the spectra taken in time of the reaction mixture. In NNLS negative absorbances are not allowed. This means that an offset is introduced in the data which may result in a bias dependent on the order of magnitude of the offset.

Table 24 shows the simulation results using imperfect *a priori* knowledge and two different noise levels. Noise has been added to the imposed pure spectra of the reacting absorbing species. From Table 24, the following can be observed:

Precision

1) For both noise levels, the use of constraint R or constraint RP leads to a poorer precision of reaction rate constant estimates compared to the precision in case of unconstrained CCR. However, there is one exception. For a noise level of 2%, the use of constraint RP leads to a better precision for k_2 compared to unconstrained CCR.
2) Again, for both noise levels, the use of constraint RP gives a better precision of reaction rate constant estimates compared to the precision obtained for constraint R (approximately a factor two for k_1 and a factor eight for k_2).

Bias

1) In all cases a large bias (≥1%) is obtained compared to unconstrained CCR.
2) For both noise levels, the use of constraint R has led to a smaller bias for k_1 compared to the bias for k_1 in case of constraint RP. However, the opposite is observed for k_2.
3) For the two noise levels used the bias of reaction rate constant estimates is almost independent of these noise levels.

Accuracy

1) For both noise levels, the use of constraint RP only gives a better accuracy of k_2 compared to the accuracy obtained for constraint R.
2) For both noise levels, the use of constraint R has led to a dramatic poor accuracy of the reaction rate constant estimates compared to the accuracy in case of unconstrained CCR.
3) For a noise level of 2%, the accuracy is improved for k_2 if constraint RP is used compared to unconstrained CCR.

The use of constraint RP gives only a better accuracy of k_2, because this reaction rate constant is directly connected to the product. Hence, imposing product information will influence mainly the k_2 estimates.

It is obvious that imposing constraints based on the use of imperfect *a prior* knowledge (noise added to pure spectra) must be avoided. The accuracy of reaction rate constant estimates obtained is independent of both noise levels used. In all cases imposing noisy pure spectra results in biased reaction rate constant estimates.

Table 24. Simulation results for different constraints (constr.) in case of imperfect *a priori* knowledge and two different noise levels. Noise has been added to the pure spectra in case of the

use of constraints. The relative error is indicated between parentheses in the columns of the accuracies.

Constr.	Noise level (%)	Precision $k_1 \cdot 10^{-9}$ $(min^{-1})^2$	Precision $k_2 \cdot 10^{-9}$ $(min^{-1})^2$	Bias $k_1 \cdot 10^{-9}$ $(min^{-1})^2$	Bias $k_2 \cdot 10^{-9}$ $(min^{-1})^2$	Accuracy $k_1 \cdot 10^{-9}$ $(min^{-1})^2$	Accuracy $k_2 \cdot 10^{-9}$ $(min^{-1})^2$
none	0.2	20	3	< 1	< 1	20 (<1%)	3 (<1%)
R	0.2	3830	186	6090	760	9920 (1%)	946 (3%)
RP	0.2	1630	26	10052	105	11682 (1%)	131 (1%)
none	2	1973	257	1	< 1	1974 (<1%)	257 (<1%)
R	2	4657	382	6484	768	11141 (1%)	1150 (3%)
RP	2	2316	27	10182	109	12498 (1%)	136 (1%)

Table 25 shows the simulation results using imperfect *a priori* knowledge with realistic or large shape differences in the pure imposed spectra of the reacting absorbing species. From Table 25, the following can be observed:

Precision

1) For both noise levels, the use of constraint RP gives the best precision of reaction rate constant estimates compared to the precision using constraint R or no constraints.
2) If for both noise levels the precision of reaction rate constant estimates for constraints R and RP (Table 25) are compared to those obtained for these constraints in Table 23 (perfect *a priori* knowledge), it is obvious that these are similar.

Bias

1) In case of large shape differences a large bias (≥1%) is obtained for both noise levels.
2) The order of magnitude of the bias of reaction rate constant estimates is independent of the two noise levels used.

Accuracy

1) In case of large shape differences a poor accuracy of reaction rate constants is obtained.
2) The order of magnitude of the accuracy of reaction rate constant estimates is independent of the two noise levels used.

Table 25. Simulation results for different constraints (constr.) in case of imperfect *a priori* knowledge and two different noise levels. Realistic (r) or large (l) shape differences have been introduced in the pure spectra in case of the use of constraints. The relative error is indicated between parentheses in the columns of the accuracies.

Constr.	Noise level (%)	Precision $k_1 \cdot 10^{-9}$ $(min^{-1})^2$	Precision $k_2 \cdot 10^{-9}$ $(min^{-1})^2$	Bias $k_1 \cdot 10^{-9}$ $(min^{-1})^2$	Bias $k_2 \cdot 10^{-9}$ $(min^{-1})^2$	Accuracy $k_1 \cdot 10^{-9}$ $(min^{-1})^2$	Accuracy $k_2 \cdot 10^{-9}$ $(min^{-1})^2$
none	0.2	20	3	< 1	< 1	20 (<1%)	3 (<1%)
R (r)	0.2	13	3	1	< 1	14 (<1%)	4 (<1%)
R (l)	0.2	12	2	20134	1541	20146 (2%)	1543 (5%)
RP (r)	0.2	4	< 1	< 1	< 1	4 (< 1%)	< 1 (< 1%)
RP (l)	0.2	3	< 1	16118	83	16121 (2%)	83 (1%)
none	2	1973	257	1	< 1	1974 (<1%)	257 (2%)
R (r)	2	1299	256	10	< 1	1309 (< 1%)	256 (2%)
R (l)	2	1253	239	19865	1479	21118 (<1%)	1718 (5%)
RP (r)	2	398	3	2	< 1	400 (< 1%)	3 (< 1%)
RP (l)	2	404	3	16148	84	16552 (2%)	87 (1%)

It is obvious that imperfect *a priori* knowledge by means of introducing large shape differences in the pure spectra has no effect on the precision of the reaction rate constant estimates. However, independent of the noise levels used a large bias and a poor accuracy of reaction rate constant estimates are obtained. If realistic shape

differences are introduced, which are representative for the experiments performed, the precision, bias and accuracy are not affected.

Summary of the simulation results

In case of perfect *a priori* knowledge applying constraints leads to better precisions and accuracies of reaction rate constant estimates. If noise is added to the imposed pure spectra, which results in imperfect *a priori* knowledge, the precisions and accuracies of reaction rate constant estimates become poorer. However, there is one exception. For a noise level of 2%, the precision and accuracy of the k_2 estimates is improved if constraint RP is used compared to unconstrained CCR. If imperfect knowledge is present in the form of realistic or large shape differences in the pure spectra, the precisions of reaction rate constant estimates are similar compared to those obtained in case of perfect *a priori* knowledge. Hence, the precision is mainly affected by the presence of noise on the imposed pure spectra.

In case of a high noise level and perfect *a priori* knowledge, imposing the NNLS constraint gives a large bias for both reaction rate constant estimates due to negative absorbances present in the spectral data. If imperfect *a priori* knowledge is used (noise or large shape differences added to the imposed pure spectra), a large bias of reaction rate constant estimates can be obtained. The order of magnitude of the bias of reaction rate constant estimates is independent of the two noise levels used in this study. No bias is obtained in case of realistic shape differences introduced in the imposed pure spectra.

Spectral residuals

For the results of the simulations, spectral residuals have been inspected. In all cases (perfect and imperfect *a priori* knowledge) the spectral residuals represented white noise except for imperfect *a priori* knowledge where large shape differences have been introduced in the pure spectra. Hence, it might be claimed that structure in the residuals is an indication of the quality of the *a priori* incorporated spectra.

In Figure 34, the spectral residuals are shown for one batch process of the experimental dataset (dataset 3) in case of unconstrained CCR. The two largest spectral residual spectra are the first two spectral residual spectra of the batch process. The spectral residuals for other batches were similar. The residuals show some structure, which can be caused by spectral characteristics like drift, non-uniform errors and coloured noise. Hence, spectral residuals are not good indicators for the quality of the *a priori* imposed pure spectra, because in the residuals of unconstrained CCR there is already structure present. In case of unconstrained CCR, a comparison of pure spectra estimates and measured pure spectra can serve as a diagnostic tool.

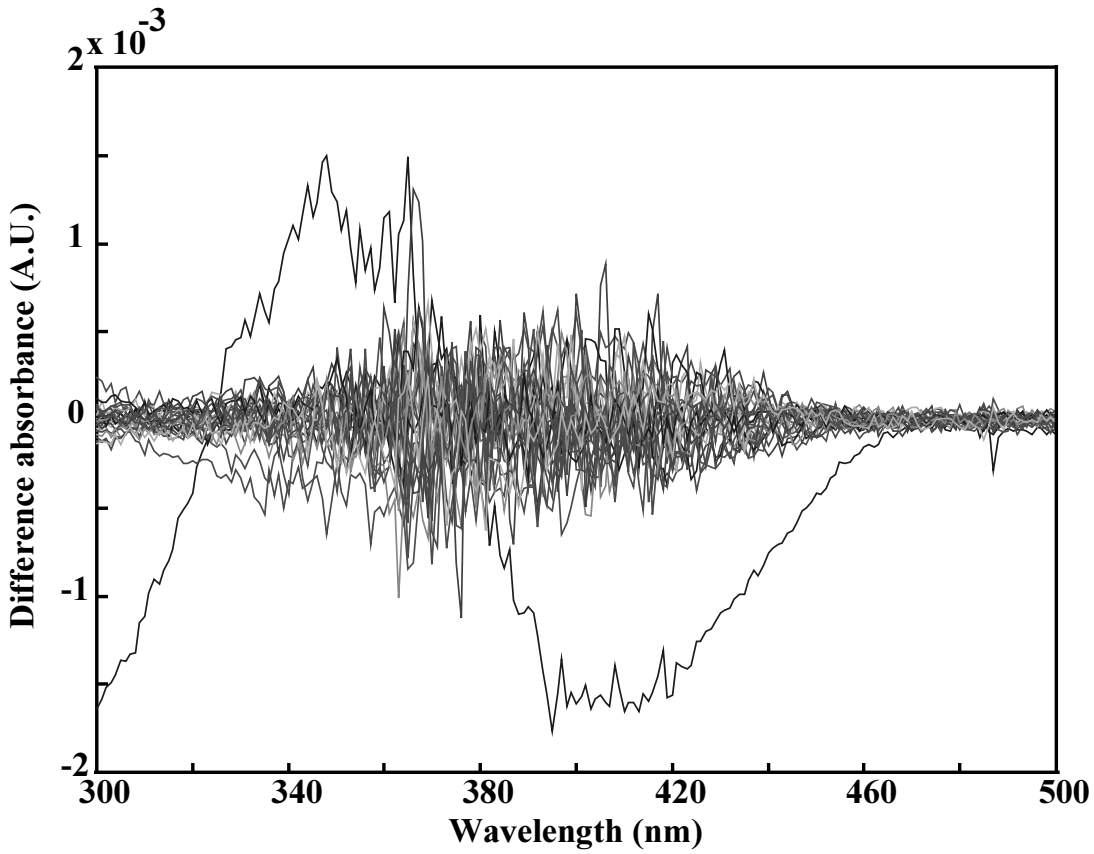

Figure 34. The spectral residuals of one individual batch process using unconstrained CCR. The spectral residuals have been plotted using an interval of 10 residual spectra.

Bias of NNLS

For a noise level of 2%, k_1 and k_2 have been estimated using no constraints and constraint NNLS for one particular simulated UV-Vis dataset. Next, a grid of k_1 and k_2 values has been chosen around the optimal values found. For every combination of k_1 and k_2 grid values, the concentration profiles have been reconstructed and the pure spectra involved have been estimated. Finally, the sum of squares of the spectral residuals has been calculated for every combination of k_1 and k_2 grid values. Now, it is possible to make contourplots which show lines of constant sums of squares. In Figure 35 contourplots are shown obtained in case of no constraint and in case of constraint NNLS. The optimal values found for the reaction rate constants are also plotted in the same figure indicated by '*'. It is obvious that approximately the real minimum has been found in both cases. The contourlines in Figure 35A and 35B are different because in case of constraint NNLS parts of the cross section of the total error surface are not accessible. This can lead to a large bias of reaction rate constant estimates if negative absorbances are present in the spectral data. This issue will play a more dominant role if the noise level of the spectral data is increased.

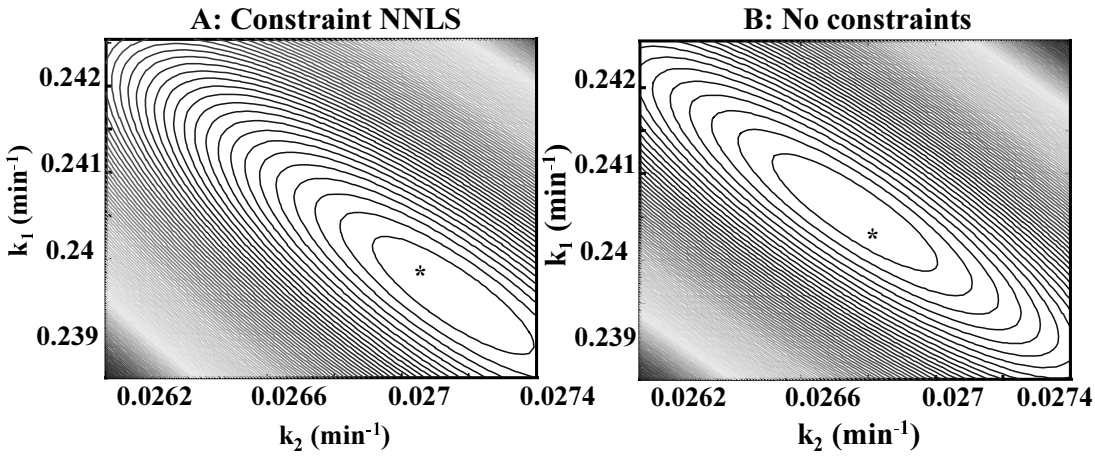

Figure 35. Contourplots of sum of squares of spectral residuals obtained using a simulated dataset and a grid of k_1 and k_2 values. The reaction rate constant estimates found in these particular cases are indicated by *.

GUIDELINES FOR USING CONSTRAINTS

From the experiments and simulations guidelines can be formulated for using constraints with respect to the accuracy of reaction rate constant estimates valid for the kinetic system discussed in this paper. If the measured spectra contain no local regions in the time direction where only one species is dominantly present (no selectivity in the time direction) and the quality of the constraints is high, it is recommended to use these constraints. Also in case of a large spectral overlap (low selectivity in the wavelength direction) constraints are recommended. If the measured spectra contain local regions in the time direction where only one species is dominantly present (selectivity in the time direction) it is better to use unconstrained models. If the quality of constraints is poor (imperfect *a priori* knowledge) unconstrained models are also preferred.

COMPARISON BETWEEN EXPERIMENTAL AND SIMULATION RESULTS

A noise level of 0.2% in the simulated data is approximately comparable to the level of instrumental noise present in the experiments. If the simulations results for this noise level and the precision of the reaction rate constant estimates for the experimental data are considered the following can be observed. Imposing constraint R on the experimental data leads to a poorer precision of reaction rate constant estimates compared to the results obtained for no constraints. The opposite is observed for the simulations. However, small changes in the noise level of the datamatrix may lead to another trend.

The use of constraint RP gives a gain in precision of reaction rate constant estimates for the simulated and experimental data. This is probably caused by the fact that the spectral data measured in time contains less information of the product (low

selectivity) and a large spectral overlap of the pure spectrum of the reactant and the product is present.

9.2.4 Conclusions

In this Chapter, the usefulness of constraints in CCR for improving the accuracy of rate constant estimates from kinetic data has been investigated. From the results obtained from dataset 3 it can be concluded that the precision of the reaction rate constant estimates is the best if the *a priori* known pure spectra of both reactant and product are implemented as constraints in CCR. The presence of biased estimates of reaction rate constants could not be checked.

In order to investigate if biased reaction rate constant estimates are obtained using CCR with and without constraints implemented, simulations have been set up so that the simulated UV-Vis spectra looked very similar to the experimental spectra. Using perfect *a priori* knowledge improved the precisions and accuracies of reaction rate constant estimates. However, imposing noisy pure spectra (imperfect *a priori* knowledge) resulted in a poor precisions and accuracies of reaction rate constant estimates. Moreover, a large bias of reaction rate constant estimates is obtained. In case of imposing imperfect *a priori* knowledge by means of introducing large shape differences in the pure spectra a large bias of reaction rate constants is obtained, but the precision is not affected.

From the results of the simulated data, guidelines have been formulated for the use of constraints with respect to the accuracy of reaction rate constants valid for the kinetic system discussed in this paper. If the measured spectra contain no local regions in the time direction where only one species is dominantly present (low selectivity) and the quality of the constraints is high it is useful to impose the constraints. Also in case of a large spectral overlap it is useful to apply constraints. If the measured spectra contain local regions in the time direction where only one species is dominantly present (high selectivity) it is better to use unconstrained models. It is also better to use unconstrained models if the quality of constraints is poor (imperfect *a priori* knowledge). In practice, a better precision obtained for experimental data is no good reason to use constraints. The true values of the reaction rate constants of interest are always unknown. This makes it difficult to check if biased reaction rate constant estimates have been obtained.

Chapter 10

General Conclusions and Future Work

10.1 General conclusions

In this thesis, modified curve resolution based methods (two-way methods) and three-way methods are presented to estimate reaction rate constants from chemical reactions. Applications of the two-way and three-way methods described in this thesis, show the applicability of these methods for estimating reaction rate constants from spectroscopic data of time evolving chemical systems. Attention is paid to the use of constraints implemented in two-way and three-way methods. *The main conclusion of the work presented in this thesis is that in principle two-way and three-way methods are all applicable to estimate reaction rate constants from spectroscopic data obtained in time of chemical reactions. However, because of the different properties of the two-way and three-way methods, in every situation a different method is preferred.* From the work reported, some conclusions can be summarized.

Two-way methods

- A combination of fixed-size window evolving factor analysis (FSWEFA) and traditional curve fitting (TCF) has resulted in a method for estimating reaction rate constants from spectroscopic data based on wavelength selection (**Section 2.3** and **2.4**, **Chapter 2**). This approach is superior to full wavelength two-way methods in case of spectral data where the absorbance differences in time of the species of interest, from which the reaction rate constants are estimated, are large and a good selective window exists (**Section 6.4**, **Chapter 6**).
- The two-way methods are suitable for *n*-th order kinetics (**Chapter 2** and **6**).
- If two-way methods are considered, the use of *a priori* spectral information is only possible in case of classical curve resolution (CCR) (**Chapter 2**).
- CCR with *a priori* spectral information implemented gives the best precision of reaction rate constant estimates compared to other two-way methods (**Chapter 6** and **8**).

Three-way methods

- The precision of reaction rate constant estimates is affected by the choice of the applied time shift or step-size (**Chapter 7** and **8**).
- The generalized rank annihilation method (GRAM) and the trilinear decomposition method (TLD) can both have many future applications in the field of process monitoring and control because of the fast and non-iterative nature of the algorithms (**Chapter 7** and **8**).
- Three-way methods are only applicable for (pseudo-) first order kinetics (**Chapter 3**, **7** and **8**).

Comparison of two-way and three-way methods

- In case of spectroscopic data with a moderate signal to noise ratio present, two-way methods are preferred instead of three-way methods. Two-way methods give an acceptable precision of reaction rate constant estimates (**Chapter 8**).
- In case of spectroscopic data with a high signal to noise ratio present, two-way methods and three-way methods perform the same. These methods give similar precisions of reaction rate constant estimates (**Chapter 8**). The three-way methods GRAM and TLD are preferred, because of their fast performance and non-iterative nature. However, it is unkown if biased estimates are obtained in this case using two-way and three-way methods.

Constraints in two-way methods

- For experimental data, the best precision of reaction rate constant estimates is obtained if *a priori* spectral information is implemented in CCR (**Chapter 6**, **8** and **9**). However, it is never possible in practice to check if biased estimates have been obtained.
- Simulations proved that an improvement of the precision of reaction rate constant estimates can be associated with the presence of biased estimates. Hence, the use of constraints within CCR is not always recommended (**Chapter 9**). If a high selectivity of species is present in time it is better to use unconstrained models. In case of a low selectivity of species in time or a large spectral overlap of some of the pure spectra of the reacting absorbing species, it is useful to apply constrained models if the quality of the constraints is high.

Constraints in three-way methods

- For the application of three-way methods in practice, the choice of the order of magnitude of the column with constants that has to be added to the spectral datamatrix is a very important constraint that has to be implemented in the

non-least squares methods GRAM and TLD (**Chapter 3**, **7** and **8**).

10.2 Future work

From the results reported in this thesis, it is obvious that some aspects have to be investigated further in detail.

Constrained and unconstrained models

In **Chapter 2** and **Chapter 6**, the theory and applications of two-way methods have been discussed, respectively. In **Chapter 9**, the use of constraints within the two-way method CCR has been discussed very extensively. However, further research is necessary to investigate the impact of the use of constraint P and penalty functions[1] on the precision of reaction rate constant estimates. With the aid of simulated data imposing perfect and imperfect *a priori* knowledge it is worthwhile to investigate if this may lead to biased estimates. The use of *a priori* known pure spectra within iterative three-way methods and the effect on the precision, bias and accuracy of reaction rate constant estimates must be investigated in the future. Attention should be payed to the comparison between constrained and unconstrained three-way models.

GRAM

In general, it is very interesting to investigate GRAM (**Chapter 3**, **7** and **8**) in more detail. This method is based on the principle that the reaction rate constant of interest can be extracted immediately from the ratio of the equation of the concentration profile and the equation of the time shifted concentration profile. The manner in which two slabs are created from one spectral dataset using GRAM can also be done in another way. For example, the first slab can be created from the spectra measured at odd time points and the second slab can be created from the spectra measured at even time points. It may be worthwhile, to find a procedure to split the spectral dataset in such a way that the precision of the reaction rate constant estimates is the best and no biased estimates are obtained. Faber *et al*.[2] wrote a paper about the derivation of expressions for predicting the bias and the variance in the eigenvalues obtained with GRAM. Maybe it is possible to correct for biased estimates.

Multivariate curve resolution (MCR)

In multivariate curve resolution (MCR) the spectral data of several experiments are analyzed simultaneously. This can be an advantage with respect to noise reduction and improving the accuracy of reaction rate constant estimates. Hence, MCR is an interesting approach which is also possible in multiway analysis. In this way it is also

feasible to analyze pseudo-first order and second order spectral kinetic data simultaneously by means of stacking multiple two-way datasets.

New research area

A whole new area in the field of kinetics could be the on-line monitoring of reaction rate constants combined with process control. Using tools from multivariate statistical process control may help to achieve this goal.

10.3 References

1. Lee S-Y. 'Estimation of covariance structure models with parameters subject to functional restraints'. *Psychometrika*, 1980; **45**: 309-324.
2. Faber K, Lorber A, Kowalski BR. 'Generalized rank annihilation method: Standard errors in the estimated eigenvalues of the instrumental errors are heteroscedastic and correlated'. *J. Chemometrics*, 1997; **11**: 95-110.

Appendix

A. Short summary of the datasets

Dataset 1

Dataset 1 contains SW-NIR spectra taken in time of the two-step consecutive epoxidation of 2,5-di-*tert*-butyl-1,4-benzoquinone using *tert*-butyl hydroperoxide and Triton B catalyst. The reaction consists of the following two steps:

$$U + V \xrightarrow{k_a} W + Z$$
$$W + V \xrightarrow{k_b} Y + Z$$

with second order reaction rate constants k_a and k_b both in $M^{-1}min^{-1}$. If species V is present in large excess, the first and second reaction step become both pseudo-first order reactions with pseudo-first order reaction rate constants k_1 (min^{-1}) and k_2 (min^{-1}), respectively. Species U, W, and Y are spectroscopically active. The experiment was repeated eight times under identical pseudo-first order conditions.

Dataset 2

Dataset 2 contains UV-Vis spectra of the two-step consecutive reaction of 3-chlorophenylhydrazonopropane dinitrile with 2-mercaptoethanol. The reaction consists of the following two steps:

$$U + V \xrightarrow{k_a} W$$
$$W \xrightarrow{k_2} Y + Z$$

with second order reaction rate constant k_a ($M^{-1}min^{-1}$) and first order reaction rate constant k_2 (min^{-1}). If species V is present in large excess the first step of the reaction becomes pseudo-first order with pseudo-first order reaction rate constant k_1 (min^{-1}). Species U, W, and Y are spectroscopically active. The experiment was repeated ten times under identical pseudo-first order conditions at a pH of 5.4.

Dataset 3

Dataset 3 contains spectra taken in time of the same reaction as in case of dataset 2. However, in case of dataset 3 the experiment was repeated 32 times under identical pseudo-first order conditions at a pH of 5.2.

Dataset 4

Dataset 4 contains spectra taken in time of the same reaction as in case of dataset 2. However, in case of dataset 4, the first reaction is performed under second order conditions. A pH of 5.2 was used, the same pH that is valid for dataset 3. In case of dataset 4, the second order experiment was repeated six times for three different initial concentrations of both reactants (species U and species V). The ratio's $C_{U,0}$:$C_{V,0}$ were chosen equal to 1:4, 1:5 and 1:6. Hence, for a ratio of $C_{U,0}$:$C_{V,0}$ equal to 1:4, six experiments were fulfilled. In total 18 second order experiments were performed.

B. The proof for a unique solution of the curve resolution model

Imposing a kinetic model on the data

In this Section,[i] a proof is given that a unique solution of the curve resolution model is obtained in case of imposing a kinetic model in the curve resolution algorithm. Consider matrix **F** from Equation (1), Section 2.2, Chapter 2. Consider also Equation (6)-(8) from the same Section which describe the concentration profiles of species U, W and Y of the chemical reaction from Section 2.2 of Chapter 2. Matrix **F** has a fixed structure, given the kinetic model, and depends only on k_1 and k_2. This will be indicated as **F**(k_1, k_2). A simple basis **B** for the concentration profiles **F** in Equation (1) can be found by defining **B** (Equation (51)) and **C** (Equation (52)):

$$\mathbf{B} = [\mathbf{1} \;\; \mathbf{e}^{-k_1\mathbf{t}} \;\; \mathbf{e}^{-k_2\mathbf{t}}] \tag{51}$$

$$\mathbf{C} = \begin{bmatrix} 0 & 0 & 1 \\ 1 & \dfrac{k_1}{k_2 - k_1} & -\left(\dfrac{k_1}{k_2 - k_1} + 1\right) \\ 0 & \dfrac{-k_1}{k_2 - k_1} & \dfrac{k_1}{k_2 - k_1} \end{bmatrix} \tag{52}$$

where it can be checked that **F** = **BC**. The notation $\mathbf{e}^{-k_r\mathbf{t}}$ is shorthand for the vector $[e^{-k_r t_1} \;\; . \;\; . \;\; e^{-k_r t_N}]^T$ where the time points t_1, ..., t_N are the sampling points. The structure of **B** and **C** are fixed. The elements of these matrices depend only on k_1 and

[i] This Section is based on the following paper:

- Smilde AK, Hoefsloot HCJ, Bijlsma S, Boelens HFM. 'Sufficient conditions for unique solutions within a certain class of curve resolution models'. submitted.

k_2. This will be indicated by **B** (k_1, k_2) and **C** (k_1, k_2). **B** is of full rank three (see later), **C** is also of full rank (see Equation (52)), hence **F** is of full rank three.[ii] Therefore, the columns of **B** are a basis for the column space of **F**.

If rotational freedom is present, then a (3x3) nonsingular **Q** exists such that **FQ** = **F*** still has the structure of the kinetic model. This means that a k_1* and k_2* should exist such that **F*** = **F** (k_1*, k_2*). Hence, **FQ** = **F*** = **F** (k_1*, k_2*). Also, **F*** = **B*C***, where **B*** = **B** (k_1*, k_2*) and **C*** = **C** (k_1*, k_2*).

The transformation **FQ** leaves the column-space of **F** intact, because **Q** is nonsingular. Now, **B** is a basis for the column-space of **F**, and likewise, **B*** is a basis for the column-space of **F*** = **FQ**. Therefore, **B** should also be a basis for the column-space of **F***. Hence, it should be possible to write all columns of **B*** as linear combinations of the columns of **B**. Consider the columns $\mathbf{e}^{k_1^*\mathbf{t}}$ and $\mathbf{e}^{k_2^*\mathbf{t}}$ of **B***. Later it is shown that $[\mathbf{1} \quad \mathbf{e}^{-k_1\mathbf{t}} \quad . \quad . \quad \mathbf{e}^{-k_J\mathbf{t}}]$ forms a linear independent set for $k_1 \neq k_2 \neq ... \neq k_J$ and all $k_j > 0$. Hence, the only solutions are: $k_1 = k_1^*$, $k_2 = k_2^*$ or $k_1 = k_2^*$, $k_2 = k_1^*$. The first solution means that there is no rotation possible, and the second solution is simply a relabeling of the reaction constants. The latter can always be checked by associating the constant related to the first profile in **F** to the first reaction. Hence, in essence, rotational ambiguity is not present anymore.

The proof given above can be used for any kinetic model imposed on the data where the matrix **F** is of full column-rank and each column of **F** can be written as a linear combination of a basis $[\mathbf{e}^{-k_1\mathbf{t}} \quad \mathbf{e}^{-k_2\mathbf{t}} \quad . \quad . \quad \mathbf{e}^{-k_J\mathbf{t}}]$. Of course, by extending **F** with more columns, there are more labeling permutations possible, but these can be resolved as commented above.

The intensity problem is trivially solved by imposing the kinetic model, because all relative concentrations are imposed by the kinetic model. Providing the algorithm with the correct starting concentrations gives then the unique intensities.

A linear independent set of exponential functions

It is shown that the exponential functions $e^{-k_j t}$ (j = 1, ..., J; $t \geq 0$) form a linear independent set provided that $k_1 \neq k_2 \neq ... \neq k_J$ and $k_j \geq 0$ for all j. In the following the k_1, ... k_J will be ordered, without loss of generality, such that $k_J > k_{J-1} > ... > k_1 \geq 0$. Consider the linear combination:

$$a_1 \cdot e^{-k_1 t} + a_2 \cdot e^{-k_2 t} + ... + a_J \cdot e^{-k_J t} = 0; t \geq 0 \qquad (53)$$

[ii] Schott JR. *Matrix Analysis for Statistics*, John Wiley & Sons: New York, 1997.

then it should follow that necessarily $a_1 = a_2 = .. = a_J = 0$. From Equation (54) follows

$$\int_0^\infty (a_1 e^{-k_1 t} + a_2 e^{-k_2 t} + ... + a_J e^{-k_J t}) f(t) dt = 0 \qquad (54)$$

which should hold for all functions f(t). By using $f(t) = e^{k_1 t}\delta(t-\infty)$, where $\delta(t-\infty)$ is the Dirac delta function,[iii] it holds that

$$\begin{aligned}
&\int_0^\infty (a_1 e^{-k_1 t} + a_2 e^{-k_2 t} + ... + a_J e^{-k_J t}) e^{k_1 t}\delta(t-\infty) dt = 0 \Rightarrow \\
&\int_0^\infty (a_1 e^{-k_1 t} e^{k_1 t} + a_2 e^{-k_2 t} e^{k_1 t} + ... + a_J e^{-k_J t} e^{k_1 t})\delta(t-\infty) dt = 0 \Rightarrow \\
&\int_0^\infty (a_1 + a_2 e^{(k_1-k_2)t} + ... + a_J e^{(k_1-k_J)t})\delta(t-\infty) dt = 0 \Rightarrow \\
&a_1 = 0
\end{aligned} \qquad (55)$$

where the last step is true because if t approaches infinity, all terms in the summation within the integral sign disappear except a_1, which is a constant. Multiplied by $\delta(t-\infty)$ the integral can only be zero if $a_1 = 0$.

After having found that $a_1 = 0$, the whole procedure can be repeated with $f(t) = e^{k_2 t}\delta(t-\infty)$ and following the same reasoning as in Equation (55). This results in $a_2 = 0$. This procedure can be repeated for all terms in the linear combination of Equation (53). Hence, all a_j are necessarily zero and thus the functions powers of $e^{-k_j t}$ are linearly independent.

If the functions $e^{-k_j t}$ are sampled in time, this will result in vectors $[e^{-k_j t_1} \quad . \quad . \quad e^{-k_j t_N}]^T$, with shorthand notation $\mathbf{e}^{-k_j \mathbf{t}}$. If the number of time points N is large enough (that is, $N \geq J$), then the resulting vectors $\mathbf{e}^{-k_j \mathbf{t}}$ (j = 1, ..., J) are linearly independent.

[iii] The Dirac delta function $\delta(t-a)$ is defined as ∞ for $t = a$, and 0 otherwise. Moreover,

$$\int_0^\infty \delta(t-a) = 1.$$

Summary

In this thesis, new two-way and three-way methods for estimating reaction rate constants from spectroscopic measurements of chemical reactions are presented. Applications of these methods to simulated and experimental data are reported.

In **Chapter 1**, a historical overview of chemical kinetics is given. Experimental techniques, spectroscopy, multivariate analysis tools and the use of constraints in kinetics are discussed. In **Chapter 1**, the goal and structure of the thesis are also described.

In **Chapter 2**, the theory of the two-way methods traditional curve fitting (TCF), classical curve resolution (CCR) and weighted curve resolution (WCR) is described. In TCF reaction rate constants are estimated from the absorbance differences in time (this is a concentration profile) of a certain species obtained from one (or more) selective wavelength(s), that is (are) specific for mainly this species. The unknown reaction rate constants are obtained by means of fitting the rate equation of the specific species to the obtained concentration profile. It is important to stress that TCF is an univariate method in case of one selective wavelength. Selective wavelengths for the species of interest are obtained using fixed-size window evolving factor analysis (FSWEFA), a local rank selection method.

Curve resolution is a set of techniques based on the determination of qualitative information and the recovery of response profiles, for example time profiles. If parameters of interest, for example reaction rate constants, are incorporated as unknowns in curve resolution this results in modifications of curve resolution techniques, because specific kinetic information is used explicitly. One of these modifications is the CCR algorithm. In CCR, reaction rate constants and pure spectra of reacting absorbing species are estimated simultaneously. It is possible to implement specific constraints in CCR. For example, if pure spectra of reacting absorbing species are known *a priori*, this can be implemented in the CCR algorithm. The implementation of constraints can be advantageous with respect to improving the accuracy of reaction rate constant estimates.

In WCR only reaction rate constant estimates are obtained. No pure spectra are estimated by the algorithm. Hence, it is not possible to implement *a priori* spectral information. In WCR, the concentration space and spectral space are separated firstly. Next, only the concentration space is used to find the optimal reaction rate constants. WCR can be seen as a target testing method. In WCR, certain matrices are weighted by certain factors. In case that these matrices are not weighted the algorithm is labeled

curve resolution (CR), which should not be confused with traditional curve resolution techniques, because specific kinetic information is used in CR.

In **Chapter 3**, the theory of non-iterative and iterative three-way methods is described. Three-way methods can be applied in cases where the contributions of the different species in the mixture spectra are of exponential character. From a single two-dimensional dataset two two-way datasets are formed by splitting the original dataset such that there is a constant time lag between the two two-way datasets. Next, a trilinear structure is formed by stacking these two two-way datasets into a three-way array. In the generalized rank annihilation method (GRAM), the trilinear structure is decomposed by solving a generalized eigenvalue problem (GEP). Because GRAM is sensitive to noise it may lead to rough reaction rate constant estimates. In these cases the iterative algorithm GRAM-Levenberg-Marquardt-parallel factor analysis (GRAM-LM-PAR) can be used to refine the estimates obtained with GRAM. GRAM-LM-PAR consists of a combination of the Levenberg-Marquardt algorithm and alternating least squares steps of the PARAFAC algorithm using the GRAM results as initial values.

In case of GRAM or GRAM-LM-PAR two datasets are created by splitting one dataset. If more than two datasets are created from one dataset a trilinear decomposition (TLD) method, which is also non-iterative, is used to decompose the trilinear structure built by means of stacking multiple datamatrices. Analogous to GRAM, the TLD results can be refined, resulting in the iterative TLD-LM-PAR algorithm. GRAM and TLD are both no least squares methods whereas the LM-PAR parts of GRAM-LM-PAR and TLD-LM-PAR are least squares methods. The implementation of constraints is possible for non-iterative and iterative three-way methods. However, the use of constraints in the non-iterative three-way methods is limited.

In **Chapter 4**, quality assessment of reaction rate constant estimates is described. The accuracy of these estimates can be divided into the precision of the estimates and the bias of the estimates. The accuracy of reaction rate constant estimates is influenced by model errors, experimental errors and instrumental noise. The precision of the reaction rate constant estimates represents the upper error bound which is a worst case situation, because both experimental errors and instrumental noise are involved if it is assumed that model errors are negligible. A lower error bound of mainly instrumental noise is estimated by means of a jackknife based method.

In **Chapter 5**, the four datasets used for the applications presented in **Chapter 6, 7, 8** and **9** are described. Dataset 1 consists of short-wavelength

near-infrared (SW-NIR) spectra taken in time of the two-step consecutive epoxidation of 2,5-di-*tert*-butyl-1,4-benzoquinone using *tert*-butyl hydroperoxide and Triton B catalyst performed under pseudo-first order conditions. Dataset 2 consists of UV-Vis spectra taken in time of the two-step consecutive reaction of 3-chlorophenylhydrazonopropane dinitrile with 2-mercaptoethanol performed under pseudo-first order conditions at a pH of 5.4. Dataset 3 consists of UV-Vis spectra taken in time of the same reaction as in case of dataset 2. However, for dataset 3 a pH of 5.2 was used. Dataset 4 consists of spectra of the same reaction as in case of dataset 2 or dataset 3. However, for dataset 4 the reaction was performed under second order conditions at a pH of 5.2.

In **Chapter 6**, the two-way methods presented in **Chapter 2** are used to estimate the reaction rate constants from dataset 1 and dataset 2, which were described in **Chapter 5**. Dataset 1 was used to test the performance of CR and WCR in case of data with a moderate signal to noise ratio. Simulations showed that CR and WCR can be both applied successfully in case of an extreme overlap of the pure spectra of the reacting absorbing species involved in the considered process. From the reaction rate constant estimates obtained from experimental and simulated data it can be concluded that WCR performed the best with respect to the precision of reaction rate constant estimates.

Dataset 2 was used to test the performance of CCR using *a priori* spectral information and WCR in case of data with a high signal to noise ratio. Hence, in case of CCR a constraint is implemented in the algorithm. From the upper and lower error bounds obtained it can be concluded that there is a gain in precision of the reaction rate constant estimates if CCR with *a priori* spectral information implemented is used instead of WCR. If the pure spectra estimates obtained with both algorithms are compared it can be concluded that the difference is quite small. Hence, using information about pure spectra that is known in advance is very useful since it will result in more precise results.

The performance of TCF and CCR without *a priori* spectral information implemented was tested using dataset 3 and dataset 4. In general, it was concluded that both CCR and TCF performed very well in case of spectral data where the absorbance differences in time were large and a good selective window existed. In that case TCF was preferred because it is simple and fast compared to CCR. In more complicated situations, for example, in case of small absorbance differences in time or severe spectral overlap (no availability of selective wavelengths) CCR performed better.

In **Chapter 7**, GRAM and GRAM-LM-PAR were both applied to dataset 1 and dataset 2. Simulations showed that both algorithms were able to deal with a strong

spectral overlap. For simulated data, it was concluded, that GRAM-LM-PAR always led to more precise estimates of reaction rate constants compared to GRAM. Dataset 1 showed a small difference in performance between GRAM and GRAM-LM-PAR, but GRAM-LM-PAR always led to more precise estimates for the reaction rate constants compared to GRAM. For dataset 2, the precision of the reaction rate constant estimates for GRAM was comparable to the precision obtained with GRAM-LM-PAR. However, GRAM gave a larger fit error. If the pure spectra estimates of the reacting absorbing species involved in the reaction model were compared with the measured pure spectra the difference was very small. GRAM-LM-PAR gave better pure spectra estimates compared to GRAM.

In **Chapter 8**, the performance of the two-way methods CCR using *a priori* spectral information and WCR and the three-way methods GRAM, TLD, GRAM-LM-PAR and TLD-LM-PAR were compared using dataset 1 and dataset 2. WCR has led to the best precision of the reaction rate constant estimates for dataset 1. GRAM performed very well, but the precision of the reaction rate constant estimates is improved if iterations are performed after the GRAM solution. This is because of the moderate signal to noise ratio of dataset 1. CCR using *a priori* spectral information has led to the best precision of reaction rate constant estimates for dataset 2. GRAM has led to approximately the same precision of reaction rate constant estimates compared to iterative methods. This is because of the high signal to noise ratio of dataset 2.

In **Chapter 9**, the impact of different constraints on the accuracy of reaction rate constant estimates was investigated using CCR. Different types of constraints were used in CCR. From dataset 3 reaction rate constants and pure spectra were estimated simultaneously with and without implementation of constraints in CCR. Because only the precision of reaction rate constant estimates could be investigated using the experimental data obtained, simulations were set-up with data that were very similar to the experimental data in order to additionally investigate the bias of reaction rate constant estimates. From the results of the simulated data it can be concluded that the use of constraints does not always improve the accuracy of rate constant estimates. Guidelines for using constraints are given.

In **Chapter 10**, general conclusions are formulated and suggestions for further research are discussed.

Samenvatting

In dit proefschrift worden nieuwe twee-weg en drie-weg methoden beschreven voor het schatten van reactiesnelheidsconstanten uit spectroscopische metingen van chemische reacties. Deze methoden zijn toegepast op gesimuleerde en experimentele datasets.

In **hoofdstuk 1**, wordt een historisch overzicht gegeven van de chemische kinetiek. Experimentele technieken, spectroscopie, multivariate analyse methoden en het gebruik van specifieke voorkennis in kinetiek worden beschreven. In **hoofdstuk 1**, worden ook het doel en de opzet van het proefschrift beschreven.

In **hoofdstuk 2**, wordt de theorie van de twee-weg methoden *traditional curve fitting* (TCF), *classical curve resolution* (CCR) and *weighted curve resolution* (WCR) beschreven. In TCF worden de reactiesnelheidsconstanten geschat uit de absorptieverschillen in de tijd (dit is een concentratieprofiel) van een bepaalde chemische component verkregen met behulp van één (of meer) selectieve golflengte(n), die specifiek is (zijn) voor deze chemische component. Vervolgens worden de reactiesnelheidsconstanten verkregen door middel van het *fitten* van de snelheidsvergelijking van de chemische component aan het verkregen concentratieprofiel. Het is belangrijk om te benadrukken dat TCF een univariate methode is voor het geval van één selectieve golflengte. Selectieve golflengten voor een chemische component zijn verkregen met behulp van *fixed-size window evolving factor analysis* (FSWEFA), dat een lokale rang selectie methode is.

Curve resolutie bestaat uit een set van technieken gebaseerd op de bepaling van kwalitatieve informatie en het verkrijgen van responsprofielen, bijvoorbeeld tijdsprofielen. Wanneer reactiesnelheidsconstanten in curve resolutie technieken geïmplementeerd worden als onbekenden resulteert dit in modificaties van bestaande curve resolutie technieken, omdat specifiek bepaalde kinetische informatie gebruikt wordt. Een voorbeeld van zo'n modificatie is CCR. In CCR worden reactiesnelheidsconstanten en zuivere spectra van reagerende absorberende chemische componenten gelijktijdig geschat. Het is mogelijk om specifieke voorkennis te implementeren in CCR. Wanneer bijvoorbeeld zuivere spectra van chemische componenten van tevoren bekend zijn kunnen deze geïmplementeerd worden in het CCR algoritme. Dit kan voordelig zijn met het oog op het verbeteren van de nauwkeurigheid van de schattingen van reactiesnelheidsconstanten.

In WCR worden alleen schattingen voor de reactiesnelheidsconstanten verkregen. Er worden geen zuivere spectra van reagerende absorberende componenten geschat. Het is dus ook niet mogelijk om spectrale voorkennis te implementeren in het

WCR algoritme, omdat de concentratie ruimte en de spectrale ruimte volledig van elkaar gescheiden zijn. WCR kan gezien worden als een *target testing* methode. In WCR worden bepaalde matrices gewogen door bepaalde factoren. In het geval dat dit niet plaatsvindt, wordt het algoritme *curve resolution* (CR) genoemd, dat niet verward moet worden met traditionele curve resolutie technieken omdat in CR specifieke kinetische informatie wordt gebruikt.

In **hoofdstuk 3**, wordt de theorie van niet iteratieve en iteratieve drie-weg methoden beschreven. Drie-weg methoden kunnen worden toegepast in gevallen waar de bijdrage van verschillende chemische componenten van exponentiële aard is. Uit één enkele tweedimensionale dataset worden twee tweedimensionale datasets gevormd door de originele dataset op te splitsen zodat het tijdsverschil tussen de twee gevormde datasets gelijk is. Vervolgens wordt er een drie-weg structuur gevormd door de twee tweedimensionale datasets die gevormd zijn op elkaar te stapelen. In *the generalized rank annihilation method* (GRAM) wordt een decompositie van de drie-weg structuur uitgevoerd door het *generalized eigenvalue problem* (GEP) op te lossen. Aangezien GRAM gevoelig is voor ruis kan het gebruik hiervan tot grove schattingen van reactiesnelheidsconstanten leiden. In dit soort gevallen kan het iteratieve GRAM-Levenberg-Marquardt-*parallel factor analysis* (GRAM-LM-PAR) uitkomst bieden waarbij de GRAM schattingen verfijnd worden. Het GRAM-LM-PAR algoritme bestaat uit een combinatie van het Levenberg-Marquardt algoritme en alternerende stappen van het PARAFAC algoritme waarbij de GRAM schattingen als startwaarden voor de reactiesnelheidsconstanten gebruikt worden.

In geval van GRAM of GRAM-LM-PAR worden er twee datasets geconstrueerd uit één dataset. Als er meer dan twee datasets geconstrueerd worden uit één dataset wordt de trilineaire decompositie (TLD) methode, dat overigens ook een niet-iteratieve methode is, gebruikt om een decompositie van de trilineaire structuur uit te voeren, die ontstaan is na het op elkaar stapelen van de datasets. Op dezelfde wijze als het geval is voor GRAM kunnen de TLD resultaten verfijnd worden dat resulteert in het iteratieve TLD-LM-PAR algoritme.

GRAM en TLD zijn allebei geen kleinste kwadraten methoden, terwijl de LM-PAR gedeelten van GRAM-LM-PAR en TLD-LM-PAR dat wel zijn. Implementatie van specifieke voorkennis is mogelijk voor de zowel de niet-iteratieve als de iteratieve drie-weg methoden. Echter, het implementeren van specifieke voorkennis in niet-iteratieve drie-weg methoden is beperkt.

In **hoofdstuk 4**, wordt beschreven op welke wijze de kwaliteit van verkregen schattingen voor de reactiesnelheidsconstanten bepaald kan worden. De nauwkeurigheid van schattingen kan onderverdeeld worden in de precisie en bias. De nauwkeurigheid van schattingen wordt beïnvloed door modelfouten, experimentele

fouten en instrumentele ruis. De precisie van de schattingen van reactiesnelheidsconstanten geeft de bovenste foutengrens weer. Deze grens wordt voornamelijk bepaalt door de experimentele fouten en de instrumentele ruis als mag worden aangenomen, dat de modelfouten verwaarloosbaar klein zijn. Een onderste foutengrens kan geschat worden met behulp van een op de *jackknife* gebaseerde methode.

In **hoofdstuk 5**, worden de vier datasets beschreven die voor de applicaties van verschillende technieken gebruikt zijn in de **hoofdstukken 6, 7, 8** en **9**. Dataset 1 bestaat uit *short-wavelength near-infrared* (SW-NIR) spectra opgenomen in de tijd van de twee-staps vervolg epoxidatie van 2,5-di-*tert*-butyl-1,4-benzoquinone met *tert*-butyl hydroperoxide onder invloed van de Triton B katalysator. Deze reactie werd uitgevoerd onder pseudo-eerste orde condities. Dataset 2 bestaat uit *ultraviolet-visible* (UV-Vis) spectra opgenomen in de tijd van de twee-staps vervolg reactie van 3-chlorophenylhydrazonopropane dinitrile met 2-mercaptoethanol. Deze reactie werd eveneens uitgevoerd onder pseudo-eerste orde condities en een pH van 5.4. Dataset 3 bestaat ook uit UV-Vis opgenomen spectra van dezelfde reactie als voor dataset 2, alleen voor dataset 3 werd een pH van 5.2 gebruikt. Dataset 4 bestaat uit spectra opgenomen van dezelfde reactie als voor dataset 2 en dataset 3, alleen werd voor dataset 4 een pH van 5.2 gebruikt en tweede orde condities.

In **hoofdstuk 6**, worden de twee-weg methoden die beschreven zijn in **hoofdstuk 2** toegepast op dataset 1 en dataset 2. Dataset 1 werd gebruikt om de werking van CR en WCR te testen voor het geval van een dataset met een matige signaal ruis verhouding. Simulaties toonden aan dat CR en WCR beide succesvol toegepast kunnen worden wanneer er sprake is van een zeer grote spectrale overlap van de zuivere spectra van de reagerende absorberende chemische componenten van het beschouwde proces. Op basis van de verkregen schattingen voor de reactiesnelheidsconstanten voor zowel gesimuleerde data als experimentele data kon geconcludeerd worden dat WCR het beste resultaat opleverde in termen van de precisie van de geschatte reactiesnelheidsconstanten.

Dataset 2 werd gebruikt om de werking van CCR met gebruik van voorinformatie en WCR te testen voor het geval van een goede signaal ruis verhouding. In dit geval is bepaalde voorkennis geïmplementeerd in het CCR algoritme, wat niet mogelijk is voor het WCR algoritme. Op basis van de verkregen bovenste en onderste foutengrenzen kon geconcludeerd worden dat er een winst is in precisie van de geschatte reactiesnelheidsconstanten wanneer CCR met voorkennis werd toegepast. Het verschil tussen de schattingen van de verkregen zuivere spectra met behulp van CCR met voorkennis en WCR is klein. Het gebruik van voorkennis is nuttig, omdat de precisie van de geschatte reactiesnelheidsconstanten verbetert.

De werking van TCF en CCR zonder voorkennis werd getest door gebruik te maken van dataset 3 en dataset 4. In het algemeen kon er geconcludeerd worden dat zowel CCR als TCF beide goede resultaten opleveren wanneer spectrale data gebruikt wordt, die grote absorptieverschillen in de tijden hebben en een goed selectief *window* aanwezig is. TCF verdient dan de voorkeur, omdat het een stuk sneller is dan CCR. In gecompliceerde situaties, bijvoorbeeld wanneer de spectrale verschillen in de tijd klein zijn of geen selectief *window* aanwezig is, verdient CCR de voorkeur.

In **hoofdstuk 7**, werden GRAM en GRAM-LM-PAR beide toegepast op dataset 1 en dataset 2. Simulaties toonden aan dat beide algoritmen toegepast kunnen worden bij een grote spectrale overlap. Op basis van de gesimuleerde data en dataset 1 werd geconcludeerd dat GRAM-LM-PAR altijd leidt tot een betere precisie van de geschatte reactiesnelheidsconstanten vergeleken met GRAM. Voor dataset 2 was echter de precisie van de geschatte reactiesnelheidsconstanten verkregen met zowel GRAM als GRAM-LM-PAR gelijk. De verschillen tussen de geschatte spectra met beide algoritmen waren erg klein.

In **hoofdstuk 8**, werd de werking van de twee-weg methoden CCR met voorkennis en WCR en de drieweg-methoden GRAM, TLD, GRAM-LM-PAR en TLD-LM-PAR getest met behulp van dataset 1 en dataset 2. WCR leidde tot de beste precisie van de geschatte reactiesnelheidsconstanten voor dataset 1. GRAM is echter wel toepasbaar. CCR met voorkennis leidde voor dataset 2 tot de beste precisie van de geschatte reactiesnelheidsconstanten, hoewel de precisie verkregen met behulp van GRAM niet veel slechter was. Dit kan verklaard worden uit het feit dat de signaal ruis verhouding voor dataset 2 erg goed is.

In **hoofdstuk 9**, werd de invloed bestudeerd van het implementeren van voorkennis in CCR op de nauwkeurigheid van de verkregen schattingen voor de reactiesnelheidsconstanten. Verschillende typen voorkennis werden geïmplementeerd in CCR. Voor dataset 3 werden de reactiesnelheidsconstanten en de zuivere spectra geschat zonder en met implementatie van voorkennis in CCR. Voor de experimentele data kon alleen de precisie onderzocht worden. Daarom werd data gesimuleerd die veel leken op de experimentele data om de bias en uiteindelijk de nauwkeurigheid van schattingen te onderzoeken. Er kon geconcludeerd worden dat het gebruik van voorkennis niet altijd leidt tot een verbetering van de nauwkeurigheid van de schattingen van de reactiesnelheidsconstanten. Richtlijnen voor het gebruik van voorkennis worden in het hoofdstuk gegeven.

In **hoofdstuk 10**, worden de algemene conclusies weergegeven en aanbevelingen gedaan voor verder onderzoek.

List of Publications

1. Bijlsma S, Louwerse DJ, Smilde AK. 'Rapid estimation of rate constants of batch processes using on-line SW-NIR'. *AIChE J.*, 1998; **44**: 2713-2723.
2. Bijlsma S, Louwerse DJ, Windig W, Smilde AK. 'Rapid estimation of rate constants using on-line SW-NIR and trilinear models'. *Anal. Chim. Acta*, 1998; **376**: 339-355.
3. Bijlsma S, Louwerse DJ, Smilde AK. 'Estimating rate constants and pure UV-Vis spectra of a two-step reaction using trilinear models'. *J. Chemometrics*, 1999; **13**: 311-329.
4. Windig W, Antalek B, Sorriero LJ, Bijlsma S, Louwerse DJ, Smilde AK. 'Applications and new developments of the direct exponential curve resolution algorithm (DECRA). Examples of spectra and magnetic resonance images'. *J. Chemometrics*, 1999; **13**: 95-110.
5. Bijlsma S, Smilde AK. 'Application of curve resolution based methods to kinetic data'. *Anal. Chim. Acta*, 1999; **396**: 231-240.
6. Bijlsma S, Smilde AK. 'Estimating reaction rate constants from a two-step reaction: comparison between two-way and three-way methods'. *J. Chemometrics*, accepted.
7. Bijlsma S, Boelens HFM, Smilde AK. 'Rapid determination of rate constants in second order kinetics'. submitted.
8. Bijlsma S, Boelens HFM, Hoefsloot HCJ, Smilde AK. 'Estimating reaction rate constants: comparison between traditional curve fitting and curve resolution'. submitted.
9. Bijlsma S, Boelens HFM, Hoefsloot HCJ, Smilde AK. 'Constrained least squares methods for estimating reaction rate constants from spectroscopic data'. submitted.
10. Gurden SP, Westerhuis JA, Bijlsma S, Smilde AK. 'Modelling of spectroscopic batch process data using grey models to incorporate external information'. *J. Chemometrics*, accepted.
11. Smilde AK, Hoefsloot HCJ, Bijlsma S, Boelens HFM. 'Sufficient conditions for unique solutions within a certain class of curve resolution models'. submitted.

Dankwoord

Op deze bladzijde wil ik iedereen die aan de totstandkoming van dit proefschrift heeft bijgedragen hartelijk bedanken.

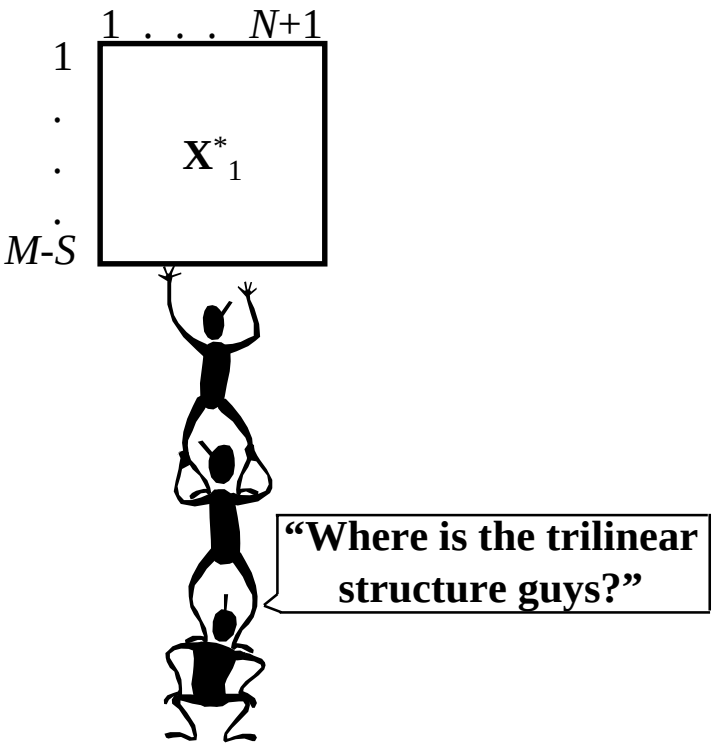
1 . . . N+1
1
.
.
.
M-S
$\mathbf{X}^*_1$
"Where is the trilinear structure guys?"